



An analysis of the global atmospheric methane budget under different climates

Abhijit Basu

Forschungszentrum Jülich GmbH
Institute for Energy and Climate Research (IEK)
Troposphere (IEK-8)

An analysis of the global atmospheric methane budget under different climates

Abhijit Basu

Schriften des Forschungszentrums Jülich
Reihe Energie & Umwelt / Energy & Environment

Band / Volume 168

ISSN 1866-1793

ISBN 978-3-89336-859-4

Bibliographic information published by the Deutsche Nationalbibliothek.
The Deutsche Nationalbibliothek lists this publication in the Deutsche
Nationalbibliografie; detailed bibliographic data are available in the
Internet at <http://dnb.d-nb.de>.

Publisher and
Distributor: Forschungszentrum Jülich GmbH
Zentralbibliothek
52425 Jülich
Phone +49 (0) 24 61 61-53 68 · Fax +49 (0) 24 61 61-61 03
e-mail: zb-publikation@fz-juelich.de
Internet: <http://www.fz-juelich.de/zb>

Cover Design: Grafische Medien, Forschungszentrum Jülich GmbH

Printer: Grafische Medien, Forschungszentrum Jülich GmbH

Copyright: Forschungszentrum Jülich 2013

Schriften des Forschungszentrums Jülich
Reihe Energie & Umwelt / Energy & Environment Band / Volume 168

D 38 (Diss., Köln, Univ., 2012)

ISSN 1866-1793

ISBN 978-3-89336-859-4

The complete volume is freely available on the Internet on the Jülicher Open Access Server (JUWEL) at
<http://www.fz-juelich.de/zb/juwel>

Neither this book nor any part of it may be reproduced or transmitted in any form or by any
means, electronic or mechanical, including photocopying, microfilming, and recording, or by any
information storage and retrieval system, without permission in writing from the publisher.

Abstract

Methane is the second most important gas after CO₂ in the atmosphere in terms of radiative forcing. It also plays an important role in tropospheric chemistry and influences the oxidation capacity of atmosphere and amount of CO, O₃ and water vapour. Various biogenic and anthropogenic sectors including gas and oil extraction, wetlands, animal ruminants emit methane in the atmosphere while it is mainly OH which displaces it. At present, the mean global methane concentration is balanced approximately at 1780 ppb after undergoing several changes over the past decades. The sources and sinks currently contribute between 450 and 510 Tg per year although the strength of each source components suffers from uncertainty. Methane is also assumed to be a key player in past climatic changes and its global abundance underwent several transitions which were recorded in the ice cores. One of the drastic changes in methane mixing ratio is observed during the last glacial-interglacial transition, as it shows an increasing trend from 350 ppb till it reaches 700 ppb at the pre-industrial Holocene. The post industrial increase in global methane concentration is also unprecedented.

In this study, methane distribution at present climate as well as at Last Glacial Maximum (LGM) and pre-industrial era is simulated with a simplified global tropospheric model ECHAM MOZ. For this simulation, methane emissions from various inventories have been used. A new parameterisation method is developed to estimate wetland methane emission for present day which is later adapted for LGM and pre-industrial time. Wetlands are the largest natural source of methane, still suffers from huge uncertainties. Contrary to the other hydrological models, the present wetland parameterisation follows a simplified approach based on a handful of soil parameters from CARAIB vegetation model. This method is easily adaptable to past climate simulations. The model result for present day from ECHAM MOZ chemistry simulation has been validated with station observation data across the globe and a set of sensitivity analysis with the modified sources are carried out to optimize the global methane budget. One of the major findings from this study is the optimized wetland methane strength which falls in the lower range of IPCC AR4 report. The ECHAM MOZ transient simulation could produce the recent methane trend and inter annual variability between 1990 and 2006 reasonably well although shows an underestimation in a range of 20-40 ppb for the first eight years. This is perhaps caused due to the underestimation of the oil and gas extracted methane source used in the model. For LGM and pre-industrial period, the model, using my wetland methane source successfully reproduces the ice core methane records. Compared to previous studies, the present LGM model source strength is weaker which raises the possibility of a less deviated sink than present. This is supported by some recent studies on the tropospheric oxidative chemistry which found less OH variability than previously assumed. The important aspect of the present study is that contrary to previous studies where sinks are often hold responsible to explain atmospheric methane variability, here the emphasis has been given to the role of changing source based on these recent findings.

Zusammenfassung

Methan ist das zweitwichtigste Treibhausgas nach Kohlendioxid. Es spielt eine wichtige Rolle in der troposphärischen Chemie und beeinflusst die Oxidationskapazität der Atmosphäre sowie die Konzentrationen von Kohlenmonoxid, Ozon und Wasserdampf. Methan stammt aus verschiedenen biogenen und anthropogenen Quellen, unter anderem Feuchtgebiete, Wiederkäuer, aber auch die Gas- und Ölgewinnung. Methan wird in der Atmosphäre hauptsächlich durch die Reaktion mit dem OH-Radikal abgebaut. Derzeit liegt die daraus resultierende mittlere globale Methankonzentration bei etwa 1780 ppb; dieser Wert unterlag größeren Schwankungen in den letzten Jahrzehnten. Die Quellen und Senken liegen zwischen 450 und 510 Tg / Jahr, wobei die Quellstärken der einzelnen Sektoren relativ unsicher sind. Man nimmt auch an, dass Methan einen wichtigen Beitrag zu vergangenen Klimaänderungen geleistet hat, was sich an den in Eisbohrkernen enthaltenen Spuren der Änderungen im atmosphärischen Methan ablesen lässt. Eine der drastischsten Änderungen der Methankonzentration fand während der letzten glazial-interglazialen Übergangsphase statt, während der die Konzentration von 350 ppb auf 700 ppb anstieg. Dieser positive Trend wurde nur noch übertroffen vom Anstieg auf das derzeitige Methan-Level während der letzten 150 Jahre.

In dieser Arbeit wird der globale Methanhaushalt im derzeitigen Klima sowie für das letzte glaziäre Maximum (Last Glacial Maximum, LGM) und das Klima des vorindustriellen Zeitalters mit Hilfe des vereinfachten globalen troposphärischen Chemie-Klimamodells ECHAM-MOZ berechnet. Für die Simulationen wurden Methanemissionen verschiedener Emissionsinventare benutzt. Es wurde eine neue Parametrisierung für die heutigen Emissionen aus Feuchtgebieten entwickelt, die dann auch für die LGM und vorindustriellen Simulationen angepasst wurden. Die Emissionen der Feuchtgebiete stellen die stärkste Methanquelle dar, sind gleichzeitig aber auch mit großen Unsicherheiten behaftet. Im Gegensatz zu anderen hydrologischen Modellen folgt die hier vorgestellte Parametrisierung einem vereinfachten Ansatz, der auf mehreren Boden-Parametern des Vegetationsmodells CARAIB beruht. Diese Methode kann leicht für vergangene Klimaperioden angepasst werden. Sensitivitätsstudien mit ECHAM-MOZ wurden für das heutige Klima mit modifizierten Quellen durchgeführt und die Ergebnisse wurden mit globalen Beobachtungsdaten von weltweiten Stationen validiert.

Als ein wesentliches Ergebnis dieser Arbeit konnten optimierte Methanemissionen bestimmt werden, die im unteren Bereich der im IPCC AR4 Report angegebenen Emissionsstärken liegen. Eine transiente Simulation mit ECHAM-MOZ für die Jahre 1990 bis 2006 konnte den beobachteten Methan-Trend und die interannuelle Variabilität zufriedenstellend simulieren, allerdings mit einer Unterschätzung der Konzentrationen für die ersten acht Jahre um 20 – 40 ppb. Dies könnte an einer Unterschätzung der Emissionen aus der Öl- und Gasgewinnung liegen. Für LGM und das vorindustrielle Zeitalter kann das Modell mit meiner Parametrisierung der Emissionen von Feuchtgebieten die aus den Eisbohrkernen bestimmten Methankonzentrationen erfolgreich simulieren. Verglichen mit bisherigen Studien sind die hier präsentierten Quellen für LGM schwächer, was auch auf schwächere Senken hindeutet. Diese Annahme wird unterstützt

durch einige neuere Studien zur Oxidation in der Troposphäre, die eine geringere OH-Variabilität fanden als bisher vermutet. Im Gegensatz zu jenen Arbeiten wird hier versucht, den globalen Methanhaushalt über die Anpassung der Quellen, nicht der Senken, zu erklären.

Table of Contents

Abstract	i
Zusammenfassung	ii
1. Introduction	1
1.1 Methane and its role on climate	1
1.2 Present methane concentration and its history	1
1.3 The global methane cycle.....	3
1.4 Methane modeling: Aim of the study	4
2. Methane sources and sinks	6
2.1 Literature survey: Modeling of methane sources	6
2.2 Isotopic composition of methane	9
2.3 Methane sources	11
2.3.1 Natural sources	11
2.3.2 Anthropogenic sources	12
2.4 Methane sinks.....	15
3. Methane emission from wetlands.....	18
3.1 Wetlands: Definition and characteristics.....	18
3.2 Methanogenesis and methane emissions	22
3.3 Global wetlands and methane emissions estimates (literature survey)	24
3.4 Model parameterisation of wetland methane emission	26
3.4.1 Parameterisation of wetland area	26
3.4.2 Parameterisation of methane emission	34
3.4.3. Results	37
3.5 Conclusion.....	41
4. Present day methane simulation	43
4.1Methane sources and sinks	43
4.1.1 Sources for ECHAM simulation	43
4.1.2 Sinks for present day simulation	46
4.2 Model description for methane simulation.....	47
4.3 Model results	48

4.3.1 Present day methane distribution	48
4.3.2 Comparison between model output and methane surface observations	50
4.4. The sensitivity analysis of model with changes in source strengths	58
4.5 Conclusion.....	60
5. Methane trend at present.....	62
5.1 Simulation set-up.....	63
5.2 Results	67
5.2.1 Simulations with different model set ups	71
5.3 Conclusion.....	72
6. Methane at past climate: LGM, Pre-industrial.....	74
6.1 Methane budget during LGM: Role of sources and sinks.....	74
6.1.1 Modeling of LGM wetlands	76
6.1.2 Modeling methane emissions from LGM wetlands	79
6.1.3 Methane sources for LGM	81
6.1.4 Methane sinks for LGM	82
6.1.5 Model Simulation for LGM methane.....	83
6.2 Methane budget during pre-industrial (PI).....	85
6.2.1 Transition of methane from LGM to PI	85
6.2.2 Atmospheric methane in PI: In perspective to present day	86
6.2.3 Methane sources in pre-industrial epoch.....	87
6.2.4 Methane sinks.....	88
6.2.5 Results from PI ECHAM model simulation.....	89
6.2.6 Conclusion.....	90
7. Summary and conclusion.....	91
Bibliography.....	95
Acknowledgments.....	109
Erklärung.....	110
Lebenslauf	111

1. Introduction

1.1 Methane and its role on climate

Methane (CH_4) is one of the most abundant organic trace gases in the atmosphere emitted both from anthropogenic and biogenic sources across the globe. Its strong global warming potential, along with its role in atmospheric chemistry makes it a key player in the earth-atmosphere feedback. Although the atmospheric abundance of methane is less than 0.02% of that of carbon dioxide (CO_2), methane shows a 30 times greater radiative potential per molecule than carbon dioxide. A study by Donner and Ramanathan (1980) found that the presence of methane at current levels causes the globally averaged surface temperature to be about 1.3K higher than it would be without methane. In addition to the direct radiative forcing of the climate, methane also influences climate through chemical interactions affecting other important greenhouse gases. The oxidation of CH_4 by the hydroxyl (OH) radical in the troposphere in the presence of sufficiently high levels of nitrogen oxides (NO_x) leads to the formation of formaldehyde (CH_2O). The oxidative process influences the concentration of carbon monoxide (CO) and Ozone (O_3) in troposphere. Along with CO and other volatile organic compounds (VOCs), methane helps to control the amount of OH in the troposphere. Methane also affects the concentration of water vapour and ozone in the stratosphere and plays a key role in the conversion of reactive chlorine to less reactive HCl .

1.2 Present methane concentration and its history

Atmospheric methane concentrations have been observed over the past few decades at several stations spread across the globe (Dlugokencky et al., 1998, Cunnold et al., 2002, Morimoto et al., 2006). Information about methane concentrations in earlier periods (up to 650 kyr before present) can be obtained from ice cores (Chappellaz et al., 1990, Etheridge et al., 1998, Sphani et al., 2005) Furthermore CH_4 measurements from satellites became available since March 2002 (Bergamaschi et al., 2007, 2009). The observations found the present global mean concentration to lie around 1800 ppb. The spatial distribution of methane mixing ratio is characterized by the strong hemispherical gradient in the range of 150 ppb. Due to dominance of large sources like energy, wetlands and rice emission, the mean methane mixing ratio in the northern hemisphere is higher by 150 ppb than the southern hemisphere. The seasonal cycle in the northern hemisphere is also more complex than in the south due to larger interactions between the sources and sinks. Amplitude of seasonality in high northern latitudes is twice as much compared to southern latitudes where methane is very well mixed (Law et al., 1992). Methane attained the present mixing ratio after undergoing several changes over the past

millennium. Methane transitions in past are attributed to the changes in its natural sources dominated by wetlands, changes in OH concentration due to shift in vegetation covers or even some debated hypothesis like clathrate decomposition from ocean. The most drastic change of methane in recent past is observed with the advent of global industrialization during when it increased from 900 ppb during the 1850s to 1750 ppb in the late 1990s (Etheridge et al., 1998, Chappellaz et al., 1997). Since the 1990s surface methane concentrations show a continued rise and are now between 1770 and 1790 ppb (Dlugokencky et al., 2011). The post industrial increase is primarily sourced driven, concomitant with an unprecedented rise in anthropogenic emission (Khalil and Rasmussen, 1985, Crutzen et al., 1991, Wang et al., 1994). The inter hemispherical gradient also increased from 30-60 ppb to 150 ppb during the last century, mainly due to growing emission in the Northern hemisphere attributed to the expansion of industrial and agricultural activities, biomass burning due to land cover changes and emission from domestic animals (Wuebbles et al., 2002). Pre-industrial methane also underwent several changes which are recorded in carbon isotopes trapped in ice cores. The isotope records reveal that during the glacial-interglacial transitions, methane concentrations rose from 320-350 ppb up to a maximum of 650-780 ppb (Chappellaz et al., 1990, Stauffer et al., 1988). This rise has been interpreted as an effect of changing sources, primarily the wetlands, and reduced oxidizing capacity due to changes in global vegetation pattern (Cao et al., 1995, Valdes et al., 2005, Webber et al., 2010). The more recent trend of atmospheric methane over the last few decades is also characterised by strong inter annual variability caused due to changes in sources and sinks which are related to global climatic events such as volcanic eruptions of mount Pinatubo in 1991, El Nino during 1997-98 or wetlands shift during 1991-93 with widespread northern hemisphere cooling (Bousquet et al., 2006). A steady slowdown of the methane growth rate was observed since the 1970s, from 20 ppb/year in 1970s to 10 ppb/year in the 1980s. Since the early nineties, although methane concentration continues to increase, the inter-annual growth rates were small and even reached zero at the beginning of 2000. However a renewed growth in global methane concentration is observed after 2006 with a rate between 5 and 8 ppb per year.

1.3 The global methane cycle

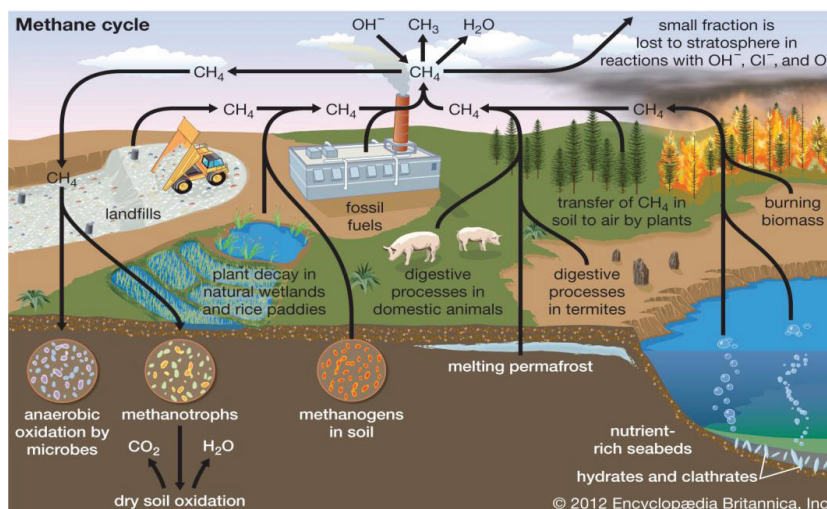


Figure 1.1 Schematic representation of the global methane cycle with various sources and sinks. Taken from Encyclopædia Britannica, 2012

Methane is released into the atmosphere by a wide variety of sources, both natural and anthropogenic. Almost 60% of the methane in the atmosphere is emitted from human related sectors, while the rest is from natural sectors. A large fraction of the anthropogenic emissions are related to biological processes such as agriculture and waste disposal, including animal waste, enteric fermentation, rice paddies and biomass burning. Non biogenic methane sources are mainly from the extraction of fossil fuels, natural gas and coal mining. Natural emissions of methane come mainly from wetland with minor contributions from termites, wild ruminants, ocean and hydrates. Other sources that have been suggested in the literature include emission from plant leaves (Keppler et al. 2006) and geological seepage (Etiope et al., 2002). However, recent studies by Nisbet et al., (2010) and Kirschbaum et al., (2008) rule out any possible plant emissions while Methane emissions from seepage needs further substantiation.

Due to the variety of methane sources, the global amount of emissions is affected by numerous factors, including energy use, human population distribution, agriculture practices and climate. Methane emission from biogenic sources result primarily from anaerobic decomposition and reduction of organic material by bacteria in flooded soils, in landfills or other waste disposal sites, and in the digestive tracts of domestic ruminants. In rice fields, emissions are dependent on conditions and agriculture practices employed during cultivation, water management etc. Wetland emissions, on the other hand, are more dependent on soil porosity, temperature and water table depth. Fossil fuel related methane emissions occur from the leaks during natural gas processing and are estimated between 1% and 2% of natural gas production in the developed countries (Beck et al., 1993). At present, although major methane sources and their combined

strength have been identified, there remains massive disagreement among existing inventories on the individual source strengths and their geographic locations. According to various studies summarized in the IPCC AR4 report (IPCC, 2007), the global methane emission ranges between 503 and 610 Tg per year with huge uncertainty in wetland and rice emission.

In contrast to diverse sources of methane, its sinks are limited and well constrained. Methane is primarily removed from the atmosphere due to its reaction with OH. The OH radical is produced in the troposphere from the reaction of singlet excited atomic oxygen produced by photolysis of ozone with water vapour. The rest of the methane sink is due to uptake by dry soils, reaction with Cl in the marine boundary layer (Platt et al., 2004) and transportation to the stratosphere. Together the budget of its source and sink influence the global methane abundance and its lifetime in the atmosphere. Compared to other trace gases in the troposphere, methane is sufficiently long lived with an average life time of 9 years.

1.4 Methane modeling: Aim of the study

Climate models with prescribed methane emissions and comprehensive chemistry have been used to reproduce the atmospheric methane concentrations at different times. These models have used either the “bottom up” (forward) or “top down” (inverse) approaches for methane simulation. The forward method (Wuebbles et al., 2001, Fiore et al., 2006, Patra et al., 2009) depends on the quality of emission data for individual sources at the regional scale. The performance of the inverse modeling (Houweling et al., 2000, Wang et al., 2004, Chenn and Prinn et al., 2005, Bosquet et al., 2006) also depends on a priori surface fluxes. Satellite retrievals are then used to optimize the source strengths in an adjoint chemical transport model (CTM) (Bergamaschi et al., 2009).

Several model studies investigated also the methane trend over past climatic periods (Dällenbach et al., 2000, Valdes et al., 2005, Kaplan et al., 2006, Weber et al., 2010). However, there remains large uncertainty in exact quantification of methane sources and sink strength over past climates which lead to disagreement among the studies.

The present study aims to develop a global methane model to produce the evolution of atmospheric methane from past to present climate. The roles of individual source and sink processes are evaluated. Based on a detailed evaluation with surface observations an attempt has been made to better constrain the present methane budget. A particular attention was given to develop a parameterization for wetland methane sources which can be used in present-day as well as paleo-climate methane studies with global climate models and reproduces the present-day wetland distribution rather well.

The thesis is structured as follows:

In the second chapter the existing methane inventories are reviewed and the strengths of individual methane sources and sinks with their global distribution are discussed. The third

chapter focuses on wetlands, the strongest natural source of methane. Here, the parameterisation of global wetland methane emissions is described which is subsequently used in the chemistry climate model simulations. The fourth chapter describes a present day methane simulation with the ECHAM MOZ chemistry climate model. The model results are evaluated in comparison to observational data with a specific focus on the seasonal variability. Chapter five discusses the trend of methane between 1990 and 2006 based on comparing long-term measurements with a transient ECHAM MOZ simulation.

In the sixth chapter, the methane model is applied to the simulation of two past climatic periods, the pre-industrial epoch and Last Glacial Maximum (LGM). The methane budget during these two periods and the changes thereafter has been discussed.

The concluding chapter provides a summary of the main results and outlook for future studies.

2. Methane sources and sinks

Methane is released into the atmosphere by a wide variety of sources, which consist of emissions from several natural and anthropogenic sectors. According to IPCC AR4 report, the annual methane emission from anthropogenic sources figures around approximately 340Tg where as the natural sources contribute 200 Tg (1 Tg = 10^{12} g).

Anthropogenic emissions arise from biogenic sources related to agriculture, waste disposal, and animal ruminants as well as from non biogenic sources such as extraction of fossil fuels, coal mining etc. Among the natural sources of methane, wetlands are the major ones along with minor contributions from ocean and termites and geological seepages. Methane is removed from the atmosphere mainly due to its chemical reaction with hydroxyl radical. Soil oxidation and stratospheric transport constitute 10% of the total loss rate. Together, the strength of the sources and sinks determine the methane abundance in the atmosphere which measures around 1800 ppb at present day. Compared to pre-industrial time, when methane mass mixing ratio lay around 700 ppb, there is a drastic elevation in methane concentration. During pre-industrial time, the global emission is estimated around 200 Tg which was contributed from the natural sources of wetlands, ocean, termites and ruminants of wild animals. These sources are unlikely to go major transformation with the industrialization even if land use change could decrease their strength by 8 to 10% (Houweling et al., 2000). The OH level in the atmosphere is also not assumed to change much over this transition (Law et al., 1993). So the sudden rise is attributed to fossil fuel sources of methane from natural gas extraction, processing, and transmission coupled with coal and oil extraction, gas flaring etc. Total emissions from this sector are estimated at approximately 130 Tg per year.

Agricultural emission was raised due to increasing population over the last century, at the expense of land use changes which initiated additional methane emission from anthropogenic biomass burning. Methane emission from rice paddies grew large and dominant over South Asian countries of China, India, and Thailand etc. Due to increase in domestic animals, methane emission from ruminants also contributed largely to the biogenic emission and is counted as one of the major sources.

2.1 Literature survey: Modeling of methane sources

Even if the global methane budget is well constrained, large uncertainties exist about the relative contribution of various sources to the global budget and their spatial distribution.

A variety of methods have been used to estimate the surface methane emission which could be classified into two categories, the “bottom up ” and “ top down” approaches. For estimating natural emission, bottom up estimates use local measurements to assess the emission factors

that are extrapolated into biogeochemical models to estimate global emission for a given process (Fung et al., 1991, Walter et al., 2001). For estimating anthropogenic emission, various statistical activity data including economic and demographic data as well as industrial data is needed. Fung et al., (1991) computed seasonal distribution of the major sources using flux measurements from several places and energy and agricultural statistics in conjunction with global digital data bases of land surface characteristics and anthropogenic activities. The major limitation with the bottom-up approaches is that they demand information on regional scale, which is not always available. More recently, combination of satellite measurements and biogeochemical models have been used to improve the estimates of the location and strength of individual sources such as biomass burning (Van der Werff et al., 2003, 2006) and wetland emissions (Ringeval et al., 2010). The isotopic measurement of methane is also used to distinguish between the biogenic and non biogenic sources (Fletcher et al., 2004).

Top down estimates are based on optimizing a priori surface emission estimates with atmospheric measurements using a chemical transport model (CTM). This approach is called a Bayesian inverse model and increasingly used for trace gases like methane (Bergamaschi et al., 2005, Dlugokencky et al., 1995, Hein et al., 1997, Houweling et al., 1999, Wang et al., 2004). Sometimes the inverse models use measurements of isotopic composition along with atmospheric CH₄ mixing ratio for better constraining of the sources (Fletcher et al., 2004).

Methane trend has been observed over the past few decades at several stations spread across the globe. Mixing ratios of atmospheric CH₄ have been directly monitored since 1983 by National Oceanic and Atmospheric Administration (NOAA). There are other research organization all over the world such as Commonwealth Scientific and Industrial Research Organization (CSIRO) and Advanced Global Atmospheric Gases Experiment (AGAGE) which provides valuable record of current methane trend. Furthermore CH₄ measurements from satellites became available from the SCIAMACHY instrument onboard ENVISAT from March 2002 to March 2012.

The suitability of the inversion models is largely influenced by the density and quality of atmospheric observations, quality of CTM and the accuracy of prior information. Most of the inverse studies optimize emissions from larger global regions or from different source categories and focused on shorter time scale or climatological averages. Recent studies by Frankenberg et al., (2005, 2006) focused on refinement of spatial resolution of inversions with the continuous in situ observation or satellite data.

In the IPCC AR4 report, methane inventories from various modeling studies have been compiled to assess the present day budget of methane (shown in Table 2.1).

Table 2.1: Global methane budget derived from modeling studies reported in IPCC AR4 and the estimates from EDGAR 4.2 for the present day model simulation in this study

Study	Approach	CTM/Process based models	Surface observation	Annual methane sources (in Tg)	
				Natural	Anthropogenic
Hein et al., 1997	Top-down	TM2 3D transport model	a)NOAA CMDL observation b) $\delta^{13}\text{C}/^{12}\text{C}$ at point Barrow Alaska(Quay et al., 1991)	231	361
Houweling et al., 2000	Top-down	TM3 3D transport model	a) Global view CH_4 b) $\delta^{13}\text{C}/^{12}\text{C}$ at Greenland ice cores (Cranget et al., 1998)	222	-----
Wuebbles et al., 2001	Bottom-up	Source specific estimates by multiplying average emission rate (Fung et al., 1991, Khalil, 1993b, Crutzen et al., 1986. Levine et al., 2000) with extrapolent		145	358
Wang et al., 2004	Combination of top-down and bottom – up	GEOS CTM using Baysian approach	a)Surface emission from Fung et al., 1991, b) NOAA CMDL observation data	200	307
Fletcher et al., 2004	Top-down	Time dependent assimilation and source retrieval technique (Bruhwiler et al., 2000)	a) Global view CH_4 , b) NOAA CMDL	260	350
Chenn and Prinn 2006	Top down	MATCH CTM	CMDL (1996-2001)	168	428
EDGAR 4.2				215	325

It is evident from Table 2.1 that there remains considerable disagreement among the modeling studies in determining the methane budget from natural sectors as well as anthropogenic sectors. Among the studies reported in IPCC AR4, the strength of natural emission lies in a range between 145 to 260 Tg. The lowest estimate from natural sources is reported in Wuebbles et al., (2002). Wuebbles et al., (2002) had used the bottom up method and made source specific estimates by multiplying average emission rate by an extrapolant applied over the globe. In general, this type of method contains numerous uncertainties which often subjects to over or underestimation of various sources as shown by Sass et al., (1999), Johnson et al., (2000), and Levin et al., (2002). The highest natural emission is reported in IPCC AR4 from the inverse modeling study by Fletcher et al., (2004) who used observed spatiotemporal distribution of $\delta^{13}\text{C}/\delta^{12}\text{C}$ ratio for constraining the individual methane source strengths. For most of the other inverse studies the natural emission ranges within 200 to 230 Tg which includes study by Bergamaschi et al., (2009) whose source estimates are used in the model simulation in Chapter 4. The 4DVAR inverse method used by Bergamaschi et al. (2009) for source estimation is based on SCIAMACHY retrievals of columnar methane. For the anthropogenic methane emission the range of estimates lies between 307 and 428 Tg. The largest emission reported by Chenn and Prinn (2006) is between 50 and 100 Tg higher than the rest of estimates and indicates an overestimation for few of the sectors. Indeed, Chenn and Prinn (2006) list values of 189 and 112 Tg for ruminants and rice agriculture respectively. Although ruminants include waste emission in their budget, still it is significantly high compared to other studies. The rice emission is in fact double than the other estimates. However, the budget of natural emission by Chenn and Prinn (2006) is estimated 168 Tg which is remarkably low than the other inventories. It is exactly opposite to Fletcher et al., (2004) which estimated a low rice emission but a high wetland emission of 231 Tg. It appears that the source segmentation by Chenn and Prinn (2006) is inconsistent and contradicts the other studies. Bergamaschi et al., (2009) estimate anthropogenic emission to be 325 Tg which lies within the range of 310 to 350 Tg as reported by rest of the modeling studies as in IPCC AR4.

2.2 Isotopic composition of methane

The isotopic combination of atmospheric methane is determined by specific chemical and physical processes which yield valuable information on the strength of methane sources, sinks and their contribution to atmospheric methane changes. The most commonly measured isotope is of atmospheric methane is $\delta^{13}\text{C}$ which is known as the ratio of ^{13}C to ^{12}C . The isotope measurements from the ice cores are often used as constraints to estimate the global budget. Isotopic measurements carry strong signatures about methane sources and its high precision monitoring provide useful constraints on the regional and latitudinal methane distributions and strength of individual sources. There are many examples of modeling studies where the

isotopic measurements are coupled with top-down approaches for estimating individual methane source strength and their spatial distribution (Fletcher et al., 2004). Isotopes of methane sources are enriched or depleted in $\delta^{13}\text{C}$ or D relative to ambient background air, which typically has $\delta^{13}\text{C}$ -47‰ and δD -85‰. Methane formed at high temperatures, generally from combustion process such as biomass burning, are enriched in the heavier isotope where methane from biogenic origin is depleted. Wetlands have signature that vary between -70 and 60‰ at high northern latitudes and between -60‰ to -50‰ at tropics (see Figure 2.1). Because of different photosynthetic pathways, C_3 and C_4 plants have very different carbon isotope signature, so the CH_4 released from forest burning have distinct isotope signature as well. Therefore methane emitted from boreal and savannah forest burning can be distinguished. The natural gas industry produces methane of variable isotopic signature depending on formation temperature of the gas reservoir. The recent gas distribution network contains gas at close to -50‰ in the Russian pipelines and around -25 to 25‰ for North Sea.

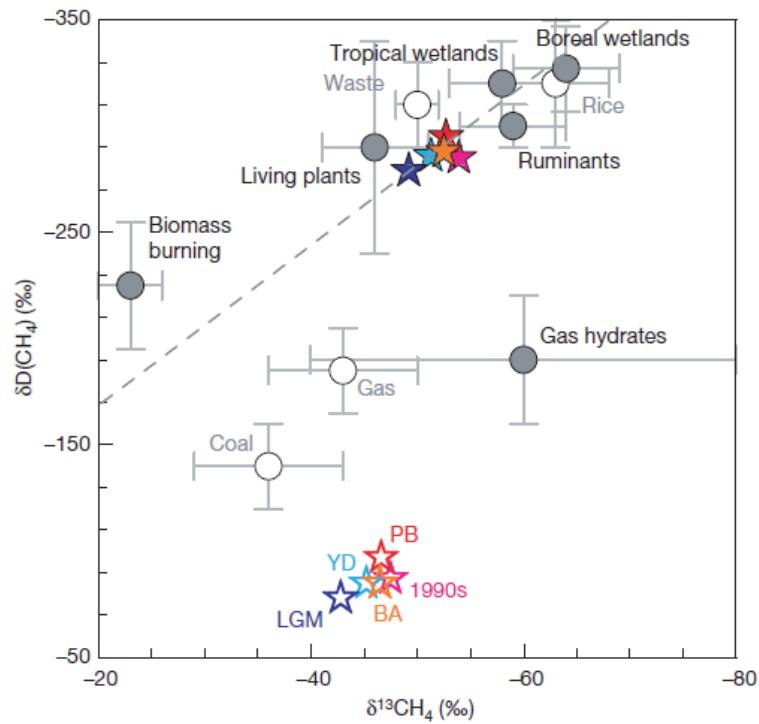


Figure 2.1: Carbon and Hydrogen isotopic signatures of different methane sources. Taken from Fischer et al., 2008.

2.3 Methane sources

2.3.1 Natural sources

Wetlands

Wetlands are the largest natural source of atmospheric methane contributing approximately 30% to its present global budget. Wetlands are also perceived to be one of the major factors in changes of methane level during past climatic transitions. Wetlands provide anaerobic condition which is ideal for microbes to decompose the complex organic compounds within the soil into simple ones and eventually to produce methane. Methane is transported from deep down of the soil to surface by means of different pathways such as plant mediated transport, diffusion and ebullition.

According to IPCC AR4 report, wetland contribution to global methane budget lies in a range between 100 and 237 Tg per year. The uncertainty in the wetland budget occurs due to lack of agreements on global wetland distribution among the available databases and differences in methodologies in estimation of methane emission (see Chapter 3 of this thesis). Over the past years, a number of modeling studies concerning wetland methane emission were carried out (Cao et al., 1995, Walter and Heimann, 2000, Granberg 2001, Segers and Leffelaar, 2001, Kaplan et al., 2002, Valdes et al., 2005, Gedney et al., 2004). A number of field observations using box chamber and eddy co-variance techniques were also done, for various wetland sites (Wilson et al., 1989, Phelps et al., 1998, Rinne et al., 2007). Often they are used in conjunction to make an estimate on global wetland methane emission. Wetlands show a strong seasonality in their areal extent and methane emissivity since the dependence on various ecological and climatic factors such as soil temperature, organics and precipitation pattern. The presence of wetlands at boreal uplands and tropics has a significant influence on the methane mixing ratio at these latitudes. The highest of wetland emissions are reported by Hein et al., (1997) and Fletcher et al., (2004) while the lowest is by Wuebbles et al., (2002). For the rest of the studies, which include Houweling et al., (2000), Wang et al., (2004), Chen and Prinn (2006) and Bergamaschi et al., (2009), the annual wetland methane budget lies between 145 to 176 Tg. In this study, a new estimate of wetland emissions is derived from potential wetlands using soil temperature and soil carbon as control parameters (Chapter 3). Average annual emissions are estimated to be 153 Tg which falls near the lower end of literature estimates.

Termites

Methane is also emitted from termites, generally located in the grasslands and forests of tropics and subtropics. The global strength of termites methane budget is fairly well constrained with a figure lying between 20 and 29 Tg which is confirmed by various modeling studies such as Houweling et al., (2000), Wuebbles et al., (2002) and Fletcher et al., (2004).

Ocean

Ocean is a weak emitter and contributes between 5 to 15 Tg of methane per year according to the studies reported in IPCC AR4.

Geological seepage

Geological seepage is also found to be a source of methane by Etiope et al., (2009). According to them, considerable amount of methane in the range of 40 to 60 Tg is released into the atmosphere annually from Earth's crust through faults and fractured rocks.

In 2005, Frankenberg et al., speculated about the alternative missing sources of methane in their comparative study of SCIAMACHY retrievals and a transport model. Keppler et al., (2006) in their study using stable carbon isotopes found methane emission both from plant leaves and litters which could bridge the reported gap. According to Keppler et al., (2006) the global methane emission strength from plants could contribute 62 to 236 Tg per year. It is supported by Ferreti et al., (2007), although they claim it to be less than that. This finding, although has the potential to alter the existing knowledge on methane budget, is refuted by many studies following. In fact, Nisbet et al., (2010) in further experiments on plant related methane emission show that plants do not contain any biochemical mechanism for methanogenesis and thus denies any possible plant emission which is supported by Kirschbaum et al., (2008) and Dueck et al., (2007). However Nisbet et al., (2010) has found that a small amount of methane release from litters under high UV radiation. Their source is too small to have any significant impact on the present day CH₄ budget.

2.3.2 Anthropogenic sources

Rice paddies

Flooded rice fields, like natural wetlands, are anaerobic environments favorable for methane production. Methane emission from rice paddies mainly occurs from the Asia. India, China, Indonesia and Thailand are the major rice producing countries in the world. In rice fields, emissions are dependent on the ambient conditions such as climate, soil characteristics, and on cultivation practices including water management, fertilizers and different varieties of rice plants. Emissions over the rice producing regions have individual seasonal patterns which influence the local methane signature as well. In most of the modeling studies, emissions from rice fields are determined by multiplying the total area under cultivation with the emission factors which are derived from the number of crops and the irrigation practice at individual regions. Matthews et al., (1991) have compiled the global rice methane emission with seasonal characteristics combining regional databases. Among the emission inventories as described in the IPCC AR4 report, the rice budget varies between 40 to 60 Tg per year. The only exception

is Chenn and Prinn, (2006) which estimated more than 100 Tg of methane emission from rice by using inversion approach which seems unreasonable in comparison to other top-down studies from by Hein et al., 1997, Houweling et al., (2000) and Fletcher et al., (2004) and bottom up approaches such as Wuebbles et al., (2002). Chen and Prinn (2006) suggested that the high estimate may be partially due to wetlands since wetlands and rice paddies have similar methane signatures. However, Chenn and Prinn (2006) have estimated emission strength separately for wetlands which lies in the lower range of IPCC report. If one considers the total strength of rice and wetlands, it lies in the highest range of IPCC table similar to Fletcher et al., (2004) and Wang et al., (2004).

Enteric fermentation and ruminants

Methane is produced by enteric fermentation in animals, mainly ruminants as a byproduct of incomplete digestion. Direct emission from ruminants including cattle, sheep, buffalo and other domestic animals are affected by diet. A higher quality of diet allows animals to digest their food completely thereby reducing methane emission which is seen in developing countries. Europe and South Asia have high densities of cattle and dairy cows which show a strong effect in surface methane level. Methane mixing ratio over central plains of North America and South East Brazil is also influenced by emissions from domestic animals (Fung et al., 1991). Animal manure is another source of methane, if pooled and stored, could amount a rise in methane emission by a factor of 10 (Bogner et al., 1995) than allowed to dry quickly. They together contribute between 75 to 90 Tg methane emission per year as described in IPCC AR4 and are well constrained compared to the other anthropogenic methane sources.

Landfills

Methane is emitted by the decomposition of biogenic waste in the anaerobic environment found in the landfills and waste water pools. Emissions from landfills are affected by factors such as temperature, amount of organic composition and the age of the waste. Most of the methane emissions from landfills are found in North America where the per capita production of municipal solid waste is high and the rate of waste burning is comparably low. It is to be mentioned here that waste incineration or waste burning is observed in several regions, particularly in North America, Europe and UK. However, the amount of methane emission from incineration is insignificant compared to other gases like CO₂, N₂O and NO_x. According to IPCC report the annual methane emission from landfills both from soil and liquid waste range between 35 to 70 Tg. Although Houweling et al., (2000) and Fletcher et al., (2004) estimate emissions in the lower range, studies by Schelle et al. (2002), Wuebbles et al., (2002) and Olivier et al. (2005), estimated close to 70 Tg of emission from this sector.

Fossil fuel sources

The main sources of fossil fuel related methane emission are the leaks that occur during natural gas processing, transmission and distribution. With the global annual natural gas consumption equivalent to 1200 Tg methane per year, the emission from the leakage of natural gas is a significant source of atmospheric methane which according to IPCC AR4 contributes between 30 and 68 Tg of methane annually. According to Fung et al., (1991), who mapped the global distribution of natural gas consumption using database on political units, human population densities and natural gas consumption data by all countries, atmospheric methane response is influenced by the gas leakages even at regional scale. According to them, the surface methane concentration at Eastern USA and Central Europe is elevated by 30 ppb and 40 ppb respectively where natural gas is commonly used. Fossil fuel sources are also seen as a major contributor to the slowdown of methane increase during the early 1990s (Bousquet et al., 2006), and the apparent rise since late 2000s. If the breakdown of USSR in the early 90s resulted in reduced usage of fossil fuels and a drop in methane growth rate, the booming Chinese industrialization and consequent rise in fossil fuel extraction in late 2000s causes the methane rise.

Coal

Methane is also emitted from the coal mines when the gas, trapped between the layers during the formation is released as the coal is mined. Global and regional estimates of methane emission from coal mines depend on type of coal, depth of mine, mining practices, the methane content of the coal seam and whether methane is flared or released. According to the emission inventories adopted by IPCC AR4, the methane budget from coal mines ranges between 30 and 50 Tg per year.

Biomass burning

Methane emission from biomass burning is a result of incomplete combustion during large scale burning of woodlands, savanna and agricultural waste. Wood burning as a domestic fuel source releases significant amounts of methane on a global scale. The rate of methane emission depends on the stage of combustion as well as the carbon content of the biomass and the amount of biomass burned (Levine et al., 2000). The recent studies described in the IPCC AR4 using both the bottom up and top down approaches, give a range of annual budget between 40 and 50 Tg. However, the inverse modeling study by Fletcher et al., (2004) from the methane isotope data estimates an emission of 90 Tg of methane which is high compared to Hein et al., (2007) and Bergamaschi et al., (2009). Fletcher et al., (2004) however found limitations in those studies since they have used few $\delta^{13}\text{CH}_4$ observations, that too in different observational time periods. The inverse methodologies adapted in those studies also varied a lot. However, the methane budget from biomass burning as reported in “Reanalysis of the tropospheric composition over the past 40 years” (RETRO) project (Schultz et al., 2008) is quite low

compared to Fletcher et al. (2004). RETRO is a 41 year inventory which is produced based on literature review, satellite products and numerical model and assumed to be most realistic among the contemporaries. It is to be mentioned that biomass burning also shows a strong inter annual variability and could be related to the global climatic events such as El Nino which is seen in the year 1994. During this year, the biomass burning events increased with overall high soil dryness, eventually resulting to an enhancement in methane emission and elevated atmospheric methane mixing ratio.

2.4 Methane sinks

In contrast to the manifold sources there are only three major sink processes of atmospheric methane among which its oxidation due to reaction with OH is the major one and accounts for 90% of methane removal. The rest is shared among the soil oxidation process and transportation to the stratosphere. Oxidation of methane occurs in aerated soils by methanotrophic bacteria. Methane also reacts with atomic chlorine and atomic oxygen, but these reactions are of no importance in the troposphere. The strengths of these sinks are quantified by various studies and adopted in IPCC AR4 report which is shown in Table 2.2

Table 2.2: *Methane sinks (in Tg per year) as described by various studies and adopted by IPCC AR4*

Sinks (in Tg/yr)	Hein et al. 1997	Wuebbles et al., 2002	Wang et al., 2004	Fletcher et al., 2004
Tropospheric loss	488	445	428	507
Soil oxidation	26	30	34	30
Stratospheric loss	45	40	30	40
Total	559	515	492	577

The oxidation of atmospheric CH₄ is initiated by its reaction with OH, especially in the strong sunlight in the tropics. OH is formed from disassociation of ozone in the troposphere at the presence of water vapour. Apart from methane there are any other pollutant tracers in the atmosphere which are also gets oxidized and removed from the atmosphere after reacting with OH. OH is involved in a chain of chemical reactions in the troposphere, where OH is converted to HO₂ as a result of the reaction with CH₄, CO or volatile organic compounds (VOCs). HO₂ can be transformed back to OH via the reaction of HO₂ and NO. This is a critical step in tropospheric ozone formation. OH and these tracers are involved in a chemical feedback cycle. This set of reactions and the chemical loop is shown in Figure 2.2.

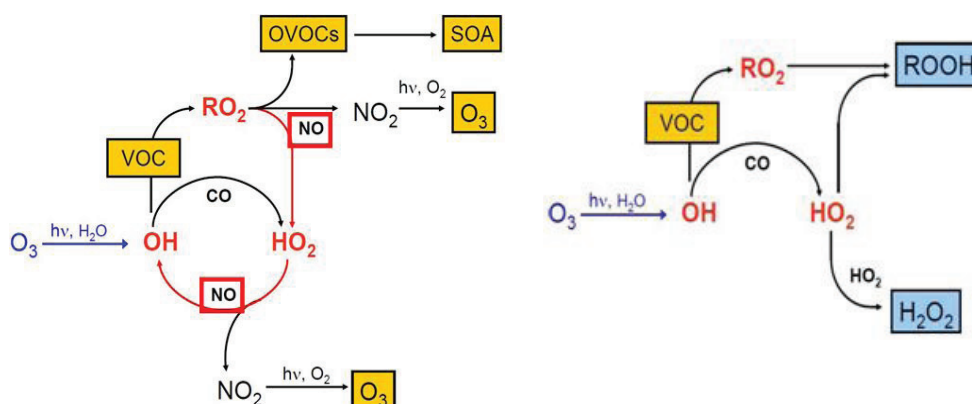


Figure 2.2: Atmospheric OH radical and the pathway of its oxidative chemistry in high NO_x (left) and low NO_x (right) condition.

At global scale, the mean OH concentration is estimated to be around 10×10^5 molecules cm^{-3} , ranging from 8×10^5 molecules cm^{-3} to 12×10^5 molecules cm^{-3} (IPCC 2001) with strong spatial and temporal variability, depending on available radiation, ozone content and water vapour concentration (see Table 2.3). The short lifetime of OH in the troposphere makes it difficult to determine the actual concentration of OH at regional to global scale. Thus proxy methods are used to estimate its global average. Among the proxies used, most of the estimates of OH concentration have been obtained through measurement of methyl chloroform (CH_3CCl_3). Using a chemical transport model and the chloroform measurements the atmospheric OH concentration is estimated (Prinn et al., 1995, Krol et al., 1998, Bosquet et al., 2005, Montzka et al., 2011).

Table 2.3: Mean OH concentration (in $\times 10^5$ molecules cm^{-3}) for four latitudinal bands, for the two hemispheres and the global scale. Prior values are calculated from MOZART OH field (Hauglustaine et al., 1998) and optimized values come from the mean inversion

OH concentration	Prior	Optimized	Prinn et al., (2001)	Krol and Leileveld (2003)	Present model study
Global	12.1	9.8 ± 0.9	9.4 ± 1.3	10	11
Northern Hemisphere	13.5	9.0 ± 1.2	8.9 ± 2.0	9.8	13.2
30°N-90°N	9.1	6.9 ± 1.4	---	---	8.6
0°-30°N	17.3	10.7 ± 1.8	---	---	17.6
Southern Hemisphere	10.7	10.6 ± 1.4	10.0 ± 2.0	10.2	8.9
0°-30°S	15.5	14.4 ± 2.1	---	---	13.7
30°S-90°S	4.7	6.3 ± 1.5	---	---	3.9

Table 2.3 shows that there is a clear agreement between the modeling studies used to derive the global OH concentration which is well constrained compared to methane sources. It is also evident that for the present model study (discussed in detail in Chapter 4), mean OH concentration is higher than Prinn et al., (2001) and Krol et al., (2003) in Northern Hemisphere where it is a bit low in Southern Hemisphere. Compared to other latitudinal bands, OH is always high in the tropics due to availability of water vapour and sunlight which accelerates the OH formation from ozone photolysis.

3. Methane emission from wetlands

Wetlands play an important role in the global methane budget and contribute 30% of the global methane emission per year. However, this is perhaps the least well constrained methane source with considerable uncertainty which is already discussed in Chapter 2. Given the strong climatic influence on them, wetlands are not only important to understand the present day methane budget, but to study the evolution of methane from past climate as well as to project its future trend. In this chapter, wetlands are discussed separately in order to reduce the uncertainty and find its contribution to atmospheric methane abundance.

3.1 Wetlands: Definition and characteristics

The term “wetland” refers to an area covered partially or completely by shallow pools of water over whole or part of the year. Wetlands, possessing both the land and aquatic characteristics, happen to be one of the most diverse and productive ecosystems in the world. In fact, wetlands are habitat of numerous biological species and play an integral role in the ecological food chain. They are involved intimately in a number of hydrologic and biogeochemical processes and significantly affect water quality, soil nutrients and aquatic chemistry. Wetlands are found across the globe under a wide spectrum of vegetation covers and hydrological regimes. In general, the wetland areas have the water table at or near to the soil surface.

It is difficult to define wetlands from a common perspective, particularly due to their varying characteristics. Over the past, wetlands have been defined and classified in various ways on the basis of hydrology, geomorphology, and vegetation. The most reliable definition is given by U.S. Fish and Wildlife Service (1979). According to them, wetlands are “land transitional between terrestrial and aquatic systems where the water table is usually at or near the surface or the land is covered by shallow water with one or more of the following three attributes: i) at least periodically, the land supports predominantly hydrophytes, ii) the substrate is predominantly undrained hydric soil, iii) the substrate is non soil and is saturated with water at some time during the growing season of each year”. The other well accepted definition is provided by the Ramsar convention (1971) that identifies wetlands as “areas of marsh, fen, peat land or water, whether natural or artificial, permanent or temporary, with water that is static or flowing, fresh, brackish or salt, including areas of marine water the depth of which at low tide does not exceed six meters”. However, these detailed definitions are impractical for using in global modeling studies, because the information needed to map and characterize a wetland in the model is not available. Therefore on the global scale, wetlands are often identified by the associated vegetation, soil properties or inundation pattern (Matthews et al., 1987). Matthews et al., (1987) have listed 28 vegetation types which are identified as wetlands in the UNESCO

(1973) classification system under major wetland groups such as forested and non-forested bogs at northern latitudes, swamps and alluvial wetlands while at tropical regions.



Bogs



Swamps



Marsh



Fens

Figure 3.1: *Various types of wetlands and associated habitats*

For the purpose of this study we define wetlands as semi-permanent water bodies with strong seasonal dynamics that are created either by precipitation or from ground water resources. In this definition, we have also considered those terrains as wetlands which are covered by snow in winter months, but eventually inundated by snowmelt water over rest of the year. The existence, shape and size of wetlands depend largely on regional climatic features, land characteristics and their water holding capacities.

Formation of wetlands

Wetlands are formed due to various hydrological factors, pre-dominantly driven by the precipitation cycle. Precipitation in the form of rain, sleet and snow reaches the ground, flows down-slope across the land, moves laterally within the soil layers and forms wetlands. The whole process depends on a number of hydrological and surface parameters. As of the primary

criteria to initiate the process of wetland formation, precipitation must exceed evaporation for a considerable period. The other important criterion is the favourable structure of the soil layers which would force water table to remain near to the surface and soil water stagnant. The precipitation cycle over a region is the key factor for wetland formation. The amount of precipitation along with its seasonality has high impact on wetlands and its seasonal behavior. Tropical wetlands are a good example of it as the excess rainfall leads to flooding of adjacent river flood plains and subsequent formation of wetlands. However, apart from rainfall, large water source due to snowmelt also provides the necessary hydrological input for wetlands particularly across northern latitudes. In these regions, along with the snowfall pattern, the soil temperature pattern also affects the wetland formation to a great extent. With the termination of winter, the soil temperature shows a steady increase which instigates thawing and melting of accumulated snow. They subsequently provide large source of water for wetlands formation. Apart from the precipitation cycle, the terrain pattern and landscape position play a major role in wetland formation. In fact, wetlands could be ground water or run off dominated as well. Wetlands form in landscape positions at which the water table actively discharges. Such wetlands have a steady supply of water from and to groundwater. Similarly wetlands in low points are dominated by overland flow although might get recharged with the ground water. Flat terrain slows down the runoff process of surface water and eventually supports wetland formation. Wetlands also maintain the level of water table and exert control on the hydraulic head (O'Brian 1988). Soil type is another key parameter which largely affects the hydraulic activity. Soil types with high water holding capacity is a good indicator for potential wetland formation (Matthews et al., 1987). According to them, wetlands are commonly associated with histosols, humic gleysols and fluvisols are the other often found for tropical wetlands.

Different processes within wetlands

Under the anaerobic condition, wetlands produce CO₂ and methane by heterotrophic respiration. Methanogenesis or methane production results from microbial activities within the wetland soils and is of great importance in the biogeochemical cycle. Soil respiration within the anaerobic zone of wetlands involves nitrate, sulfate, iron and organic matters. There are various microbes found in the form of methanogens and the methanotrophs in the soil anaerobic zone to produce and oxidize methane.

Wetlands store carbon within peat and soil. Storing carbon is an important function within the carbon cycle. When wetlands are drained, the oxidizing conditions increase organic matter decomposition, thus increasing the release of carbon dioxide. When wetlands are preserved or restored, the wetlands act as a sink for carbon since organic matter decomposition is stable or slowed.

Major global wetlands

Major wetland areas are found in the temperate-boreal region between 50° and 70°N, and in the tropics between 10°N and 15°S. 50% of the total wetland area is located at the high northern latitudes and around 35% in the tropics. The rest are distributed in the extra tropics of both the hemispheres and the southern latitudes. Global lake and wetland database (GLWD) by Lehner et al., (2004) is the most reliable wetland database available, constructed from integrating local information from various sources on GIS platform. In the following, the GLWD wetland distribution is compared to the wetland map from Matthews et al., (1987) which is one of the earliest wetland maps and modeled using biome, soil and inundation characteristics.

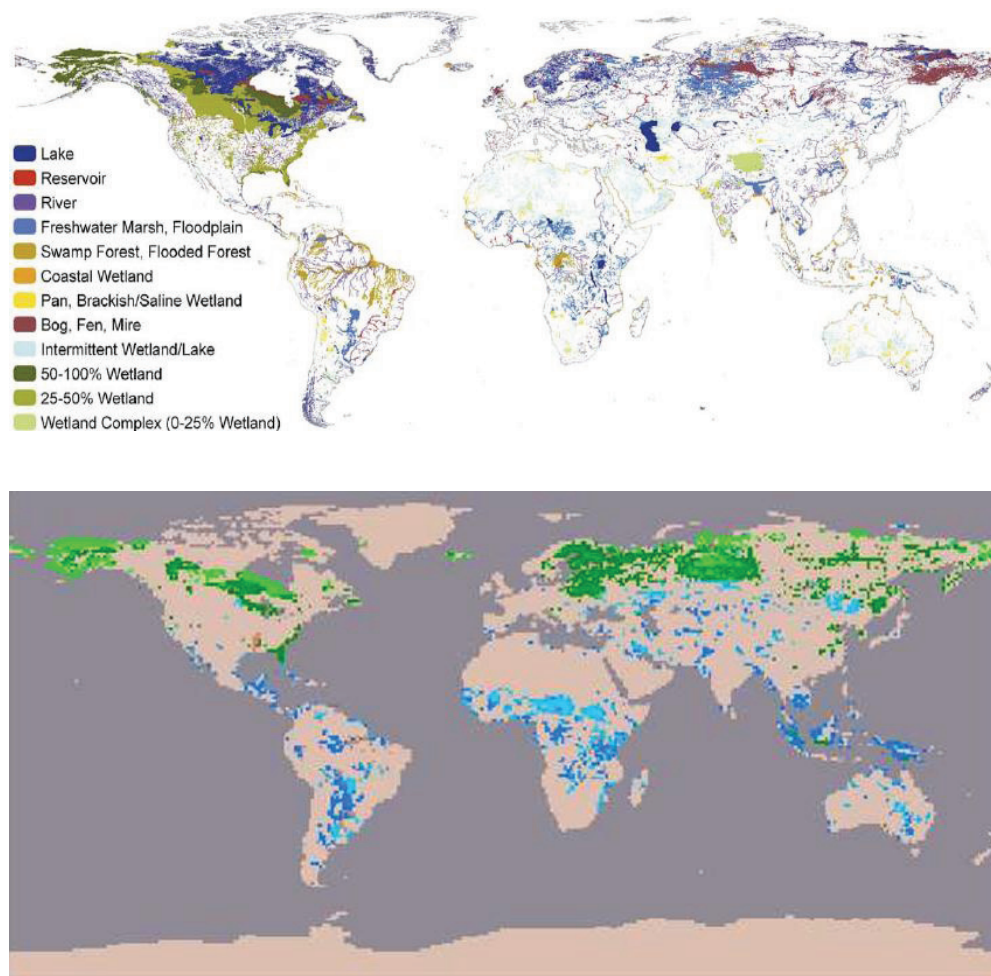


Figure 3.2: Comparison of wetland map derived from Lehner et al., (2004) at the top and Matthews et al., (1987) at the bottom. Lehner et al., shows the wetland distribution in eight different classes, while Matthews et al., (1987) shows it in classes like bogs (in green) and swamps (in blue).

GLWD map has classes like freshwater Marsh, floodplains, swamps, bogs which are assumed to be good indicator of wetlands. Apart from them GLWD classifies wetlands in 0-25%, 25-50% and 50-100% sub classes. According to both of the datasets, most of the wetlands in northern latitude exist in Northern America, Alaska and Canada. Similarly large wetland areas are found over Western Europe, Scandinavia, Siberia and Central Asia. Tropics also hold quite a few well known wetlands over South American floodplain, African plain land and Indonesia. Some differences on wetland locations are visible between the databases. GLWD shows large extent of wetlands over North America which are less pronounced in Matthwes et al., (1987) map. Similarly Matthwes et al., (1987) shows large wetland extent in South America below 40°S which are missing in GLWD map. Australian continent holds some wetlands in Matthwes et al., (1987) map which is not there in GLWD map.

3.2 Methanogenesis and methane emissions

Process of CH₄ formation within wetland soil

Methanogenesis or the process of methane formation within wetland soil layers is an integral part of wetland ecology. In fact, wetlands are the strongest natural contributor of methane in the atmosphere and constitute around 70% of natural emissions. The whole process of wetland methane emission to adjacent atmosphere comprises of several intermediate steps. At first Methane is produced at the soil root zone through a chain of chemical reactions which is transported to atmosphere via different pathways.

To begin with, methanogenesis occurs in an anaerobic ambience condition in the presence of microbes and methanogenic substrate specific bacteria. They decompose the available complex organic compounds into simple ones through different chains of chemical reactions.

From a kinetic viewpoint, this anaerobic treatment is described by three processes involved. In the first step complex organics are converted to less complex soluble organic compounds by enzymatic hydrolysis. In the second step, these hydrolytic products are fermented to simple organic compounds, predominantly volatile fatty acids by a group of anaerobic fermentative bacteria. Finally, simple organic compounds are fermented to methane and CO₂ by methanogenic bacteria.

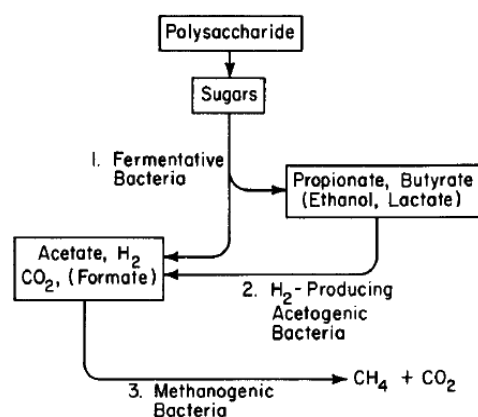


Figure 3.3: *The chemical pathway of methanogenesis. Taken from Bryant, 1979*

There are several studies on methanogenesis, investigating the methanogenesis process chain and the nature and extent of individual control. Soil temperature and substrate properties are the major control factors.

Soil temperature, influences the methane production rate. The optimum lies within the range of 30 to 40°C. Q_{10} known as the temperature co-efficient is often used to assess microbial sensitivity to temperature change. The Q_{10} value varies over different wetland habitat with a range from 3-16. The rate of methane production holds a strong relation with Q_{10} . On the other hand, methanogenesis also depends largely on content and nature of soil organic matter. The redox potential (Eh) of the organic matter strongly influences methane production which varies over different soil types from bogs to fen.

Among other factors, water table position at wetland sites is also important as water table near to the surface provides anaerobic condition which is a pre-requisite for methanogenesis. A reduction in water table decreases the zone of methanogenesis and at the same time increases the zone of methane oxidation.

Transport and loss processes

In the wetland ecosystems, methane is transported to surface by means of different mechanisms. They are dominated by plant mediated transport, followed by diffusion (due to pressure gradient) and ebullition (due to bubble formation).

Wetland plants serve as a gas conduit in order to transport methane from wetland soil to the atmosphere. They transport CH_4 from the depth of the root zone to the peat surface, thus bypassing the unsaturated, oxygen rich zone of CH_4 consumption. In the former process, respiratory consumption paves the way for outward diffusion of O_2 and subsequent influx of CH_4 which diffuses upwards along a concentration gradient to the atmosphere. The later process is mainly thermo-osmosis where a temperature difference between plant interior and exterior results in the methane out gassing.

On the other hand, water table depth plays the decisive role in ebullition of methane. Sometimes, methane escapes to the atmosphere in the form of bubble mainly due to water table elevation or changes in temperature and pressure. However Moore et al., (1989) and Windsor et al., (1992) note that this ebullitive methane flux has a highly discontinuous spatiotemporal distribution and globally represents only 1-10% of total wetland emission.

Methane oxidation within soil

During the diffusive transport to soil layers, methane passes through oxygen rich layers where it can be oxidized by single class of micro organisms known as methanotrophs.

In general, methanotroph bacteria possesses both dissimilatory and assimilatory pathways of methane oxidation. In dissimilatory pathways, methane is oxidized completely to CO₂, thereby produces cellular energy, and none of the carbons become cellular material or biomass. The produced CO₂ is then gassed out to the surrounding environment. On the other hand, in assimilatory pathways, oxidized methane is converted to cellular biomass. In both pathways, methane is first oxidized to methanol, which is then oxidized to formaldehyde. The formaldehyde can be used as a reducing power in electron transport chain, oxidised to formate, or assimilated by the cell. The cell then oxidizes the formate to CO₂.

3.3 Global wetlands and methane emissions estimates (literature survey)

According to the IPCC AR4 report, wetlands comprise of approximately 70% of natural methane sources and 30% of all the methane sources taken together. Previous studies estimated the global wetland methane emission in the range from 150-325 Tg per year. The large uncertainty among these studies is attributed mainly to differences in total wetland area estimations as well as disagreements on regional wetlands identification (Aselmann et al., 1989, Chappellaz et al., 1993, Kaplan 2002). Further uncertainty also arises from various emission schemes adapted in these approaches.

Over the past two decades, there were a number of attempts to map global wetlands, either from global modeling studies or from integrating regional databases (see Table 3.1). Among the modeling studies, Matthews et al., (1987) is the first where wetlands are mapped using regional soil types, biome patterns and inundation characteristics. Aselmann et al., (1989) compiled global wetland distribution by digitizing the available regional wetland maps as well as integrating land-use classifications from various sources. Other global wetland inventories were published by Finlayson et al., (1995), Cogley et al., (1994), Stilwell-Soller et al., (1995), Sanderson et al. (2001) and more recently a wetland intercomparison project (WETCHIMP-<http://arve.epfl.ch/research/wetchimp/>) compiled different wetland inventories. Among the current inventories, most robust is the one prepared by Lehner et al., (2004), integrating

existing regional data, maps and records on GIS platform. Some groups have explored the use of satellite data as well to map wetlands. For example, Pringent et al., (2001) used microwave reflection changes detected by Special Sensor Microwave/Imager (SSM/I). However until now, these attempts did not yield satisfactory results. Among the observational studies Pringent et al., (2001) is the solitary attempt to map wetland dynamics globally with passive and active microwave along with visible and infrared measurements from SSM/I. The published inventories disagree both in total area estimation and identification of local wetlands. While the Matthews et al.1989 wetland map amounts to 5.2 million km² of area, Cogley et al., (1994) and Stillwe-Soller et al., (1995) estimate 4.7 million. GLWD by Lehner et al., (2004) measures wetland of around 9.1 million km². Similarly modeling study by Kaplan 2002 even outreaches GLWD to estimate wetland area of 11 million km². Kaplan (2002) estimated potential wetlands using FAO soil map, with BIOME4 derived soil wetness and a digital elevation model (DEM).

Table 3.1: *Global wetland inventories and corresponding methods*

Reference	Method	Global Wetland area (in 10 ⁶ km ²)
Matthews et al. (1987)	Integration of independent global. digital sources (vegetation, soil and inundation pattern)	5.2
Aslemann et al., (1989)	Compiling regional wetland maps, land-use classifications from various sources	5.7
Cogley et al., (1994)	Compiling land-use maps	4.6
Stillwell-Soller et al., (1995)	Combining Aslemann et al., (1989) and Klingers (pers. Comm.) political Alaska dataset	4.7
Kaplan, (2002)	Model parametrisation using FAO soil map, with BIOME4 derived soil wetness and a digital elevation model (DEM)	11
Lehner et al., (2004)	Combining existing map, data and information on GIS platform	9.1
Pringent et al., (2007)	Multisatellite method from SMI and ISCCp observations	5.8

Methane emissions from the global wetlands have been estimated by a number of modeling studies e.g. Walter & Heimann (2000), Granberg (2001), Segers and Leffelaar (2001), Gedney et al., (2004) etc using various parameterization. Among these studies, climatological fields from climate models are forced on global methane-hydrology model by Walter et al., (2000)

whereas a simple emission algorithm based on soil net primary productivity (NPP) and soil carbon content with soil temperature is adapted by Cao et al., (1995) and Gedney et al., (2004) respectively. Emission algorithm suitable for tundra wetland sites is adopted for global emission by Kaplan (2002), although after suitable modifications.

Apart from the modeling studies, there had been a number of observational studies on methane emission measurement at different ecological environments as well. Most of these observational studies are carried out using box chamber measurements at observational sites and a few by eddy-covariance technique. Among them, Devol et al., (1990) and Wassmann et al., (1996) studied the seasonal dynamics of methane emission from Amazon floodplain. Studies by Nakano et al. (1999), Bartlett et al., (1992), Whalen et al., (1990, 1992) and Mastepanov et al., (2008) describe methane emission from tundra wetlands. Phelps et al. (1998) carried out methane flux measurements from high-latitude lakes during spring ice melt. Wilson et al., (1989) did methane emission measurements from temperate swamp.

3.4 Model parameterisation of wetland methane emission

Original plan had been to use the Kaplan (2002) approach for wetland parameterisation which is based on parameters at atmospheric model resolution. The result using this method did not yield satisfactory results. Since we needed a parameterisation suitable for paleo simulations we had to develop our own parameterization. We actually tried to emphasize building a simple method, involving less number of control parameters which could be available over past climatic conditions.

The parameterisation is a two step process and combines the methods as described in Kaplan (2002), Gedney et al., (2004), and Shindell et al., (2004). In the first step, potential global wetlands are parameterized using basic surface and hydrological parameters and validated in comparison to GLWD (Lehner et al., 2004), the most reliable wetland database at present. In the second step, the strength of methane emission from the modeled potential wetlands has been estimated using various soil parameters like soil temperature and soil carbon.

3.4.1 Parameterisation of wetland area

We have used only a handful of surface and soil parameters in contrast to other modeling methods (Walter et al., 2001, Cox et al., 1999) which require a number of hydrological variables for wetland estimation to parameterize potential wetlands. This parameterization goes beyond them by choosing surface slope and soil water content to be the control parameters to determine potential wetlands. The choice relies on the assumption that only the moist and flat areas would support the formation and sustenance of potential wetlands. Flatness is determined

by terrain slope and the moistness by soil water content. We imposed conditional thresholds on both of these parameters to identify the possible potential wetlands in the first step.

The climatological soil moisture content is derived from the CARAIB vegetation model (Warrant et al., 1999, Otto et al., 2002, Laurent et al., 2008). It is also to be noted at this point that parameterisations at coarser resolution are prone either to over or underestimate the wetland area as well to miss a few of the well-known wetlands. In actual, wetlands are often small scale phenomena for which a sub scale parameterisation is needed. In view of that, in the present study, the parameterisation was carried out at a 10 minute spatial resolution and then interpolated to model grid of 2.8° in an area conservational approach.

CARAIB was chosen because we could get high resolution soil moisture map for paleo conditions as well for transient output between 1990 and 2006 from it. It also performed well in intercomparison of dynamic vegetation models.

Data and method

A detail of CARAIB and other inputs to the model

The CARAIB model is a large scale vegetation model designed to study role of vegetation in the global carbon cycle. The hydrological module calculates soil water content and several associated hydrological fluxes corresponding to the root zone, the active part within the soil layer for methanogenesis. It considers all the intermediate steps of precipitation, evapotranspiration, surface runoff and soil hydraulic activities (parameterized in terms of soil texture) to estimate the soil water output.

Soil water in CARAIB is normalised on the basis of field capacity (the maximum amount of water held by per unit soil) and wilting point (the lowest water content held by soil before the plant wilts), two extreme measures of water holding potential of soil. It is a dimensionless quantity in the CARAIB. For most of the work presented in the thesis, output from a climatological mean year was used. It provides an opportunity to study the seasonal trend of wetland as well. The surface slope map is obtained from FAO-UNESCO (<http://www.fao.org/nr/land>) which is derived from ETOPO5 surface elevation. Apart from these two major parameters, the other parameter we also used is the soil temperature.

Methodology

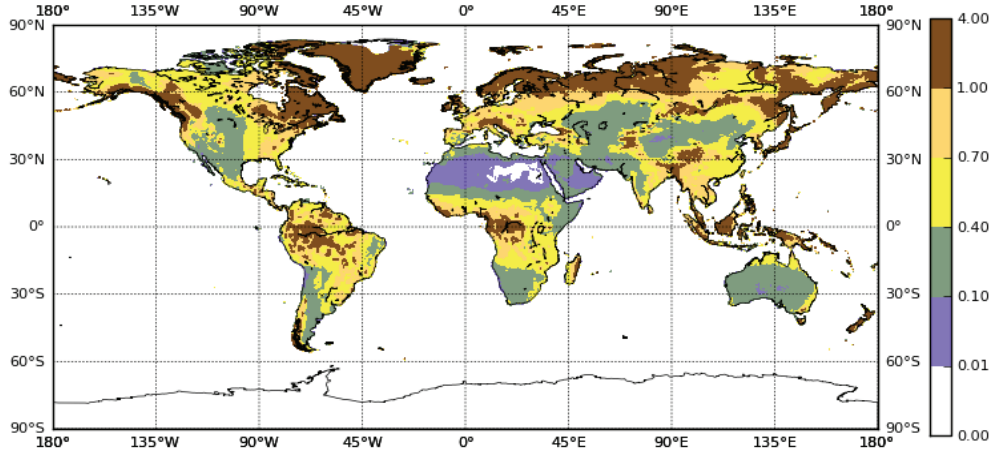


Figure 3.4: Annual mean CARAIB soil water content map for present day conditions

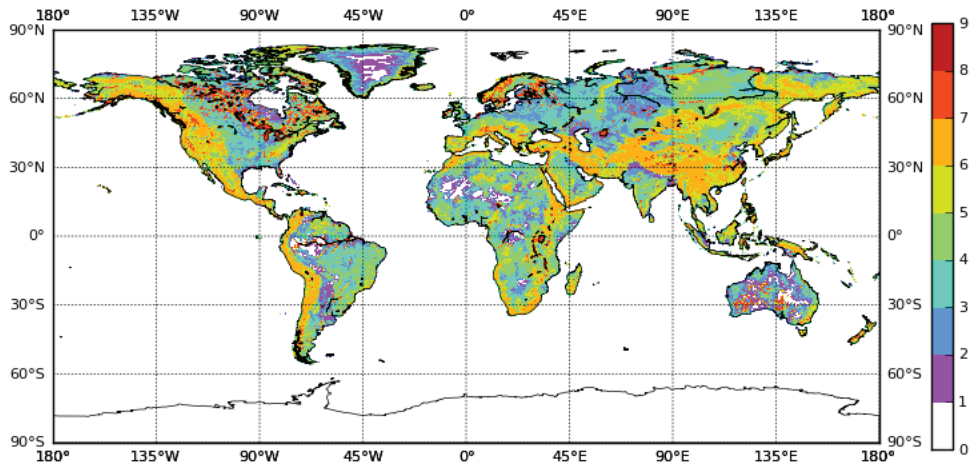


Figure 3.5: Surface slope map (percentage gradient) from ETOPO5 elevation data with distributions of nine slope gradient classes are given by 0–0.5°, 0.5–2°, 2–5°, 5–8°, 8–16°, 16–30°, 30–45°, and > 45°

In the parameterisation process, threshold values for soil water content and terrain slope were selected such that the resulting wetland distribution matched the Lehner et al., (2004) database as closely as possible. As soil water content is provided in the form of monthly maps, the threshold value is estimated from their yearly average distribution and later applied on monthly maps.

Two sets of threshold values for soil water are chosen separately, .3 for northern latitudes (30°N–90°N) and 1.1 for the rest of globe (30°N–90°S). The threshold value for surface slope is

2° everywhere. The CARAIB parameter of soil water yields larger values in the tropics and southern hemisphere compared to the high northern latitudes. CARAIB does not distinguish snowfall from liquid water precipitation. As a consequence, soil water content is over estimated during the winter season. In reality, wetlands could only be formed at the absence of snow and only when once the snow melts. Therefore we have introduced an additional threshold for soil temperature of 0° C.

Results and analysis

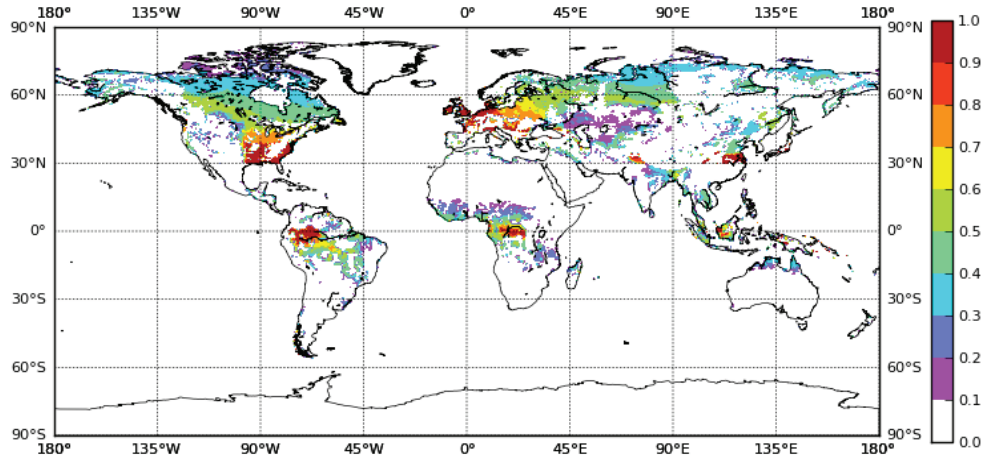


Figure 3.6: *Modeled wetland distribution with fractional inundation coverage*

Figure 3.6 shows the model derived wetlands with values between 0 and 1 corresponding to the inundated fraction of cells. It includes areas which are inundated even for a single month of a year. Its comparison with GLWD wetland map (Figure 3.2) shows that most of the major GLWD wetland areas are captured well in our modeled map. It holds most of its 50-100% wetlands over Northern American continent where it matches reasonably well with the GLWD. At the other places, GLWD classified swamp, flooded forest, fresh water floodplains are seen in the modeled map as well. The Siberian wetlands, classified as freshwater floodplain by GLWD, are reproduced well by the model. Over South America, GLWD locates scattered wetlands over the floodplains of major river basins in the form of swamp and flooded forest which are found more localized in the model map. In this region, model map shows wetlands only at the south of equator but misses a few in the north. In Africa, GLWD describes wetlands in form of freshwater floodplains and swamp forest which the model map is able to captures pretty well at similar locations. However, in Europe, model produces wetlands in south of the Scandinavian countries and in Western Russia which are not found in the GLWD.

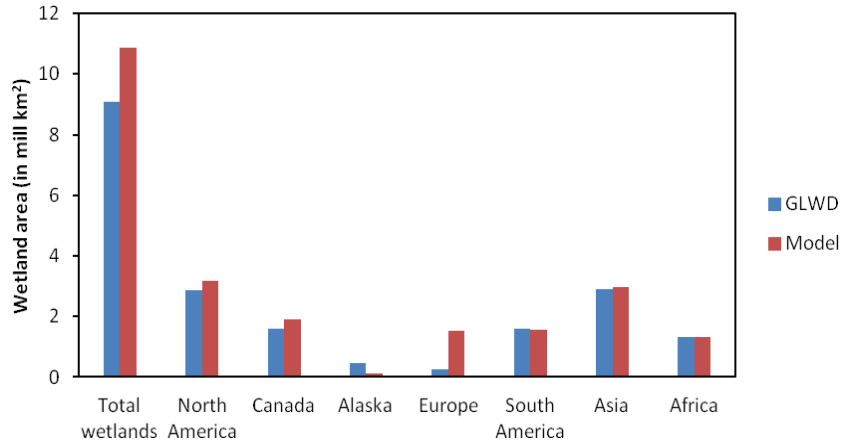


Figure 3.7: Regionally aggregated wetland areas from this study compared to GLWD

Figure 3.7 shows that our parameterisation estimates potential wetlands to be 10.8 million km² which lies in the higher range of presently available wetland databases (Lehner et al., 2004, Kaplan 2002, Aslemann et al., 1989). In comparison to GLWD, it overestimates the global wetlands by 17%. However the success of the present parameterization lies in its ability to capture wetlands at a regional scale. However the largest discrepancies are found in Europe (1.8 vs 0.2 mill km²) and in Alaska (0.4 vs 0.1 mill km²).

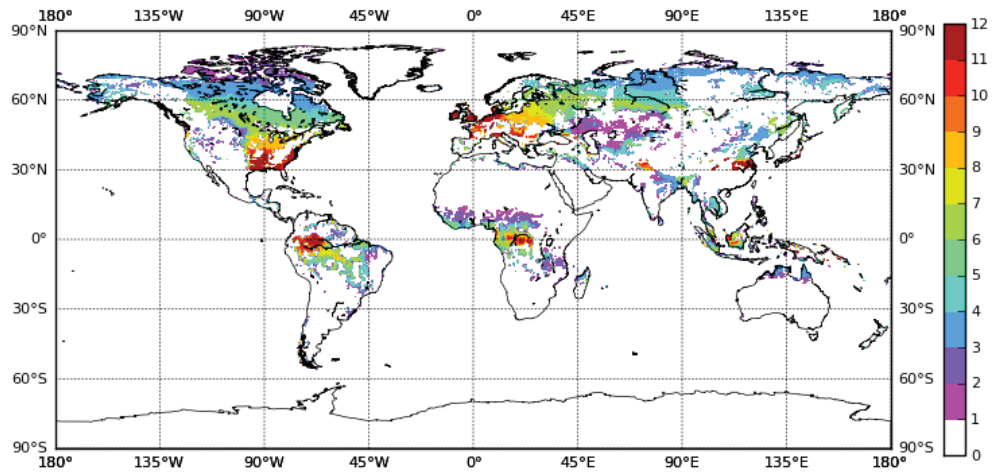


Figure 3.8: Duration of wetland inundation in months

It can be derived from the Figure 3.8 that vast regions over North America and Canada remain inundated for four to seven months of the year and behave as wetlands. However for some regions over Western Europe and Central America, shown in yellow patches, the inundation

occurs during eight to nine months of a year. Overall, over large areas over central Asia, wetlands are temporary and occur only for one to two months. Most of the wetlands over South American floodplain, located south of equator, and in central Africa are found to be inundated during half of the year. Central African plain also holds similar types of wetlands. However the parameterisation yields that there are some permanent wetlands, though very small in area, which are located at Central Africa and South America close to the equator. Some permanent wetlands are also found around 30°N at the East American coast, Western Europe and Northern India.

Seasonal pattern of wetlands

The seasonal cycle is an important aspect of inundation and wetland area for estimating CH₄ emissions correctly. According to Kaplan (2002), seasonal wetlands account for 61% of the total area. However, the range of wetland seasonality and its contribution to methane flux vary considerably among different studies.

Till date, hardly any observations of wetland dynamics are available over a full year or longer on a larger scale. Only Prigent et al., (2001) gives monthly wetland data for one full year (from July 1992 to June 1993) with a suite of passive and active microwave observations. Even though the microwave satellite data of Prigent et al., (2001) severely underestimates the global wetland area, they may give some hints about the seasonality.

At regional scale, however, there exist a number of wetland studies using remote sensing. Among these, Papa et al., (2006) studied northern wetland dynamics using Topex-Poseidon dual-frequency radar altimeter. Mialon et al., (2005) also carried out a detailed analysis of the wetland seasonal dynamics on a weekly basis over Canada-Alaska and northern Eurasia from 1988 to 2001 using DMSP SSM/I. Similarly over the tropics, a comparison of inundation patterns among major South American flood plains is carried out with SMMR by Sippel et al., (1994) and with SAR imagery over Central Amazon basin by Hess et al., (2003).

Although factors behind the periodic surface inundation differ between high latitudes and the tropics, the seasonal cycle of inundation is quite comparable. Maximum inundation is observed during May to September. In comparison to the boreal wetlands, the variation is weaker and less prominent in the tropics.

According to Hamilton et al., (2002) inundation extent is strongly correlated with the precipitation rate although in some areas of South American floodplains, a time lag exists between precipitation and inundation cycles. It is also found that this time lag increases with increasing distance from the main stream. A detail study into the South American floodplains proves the importance of ITCZ as tropical wetlands are often tuned to seasonal pulses of water caused by its seasonal movement (Mitsch et al., 2010). The river basins situated at the north of equator show a semi-annual phase shift in the seasonal cycle (Figure 3.11).

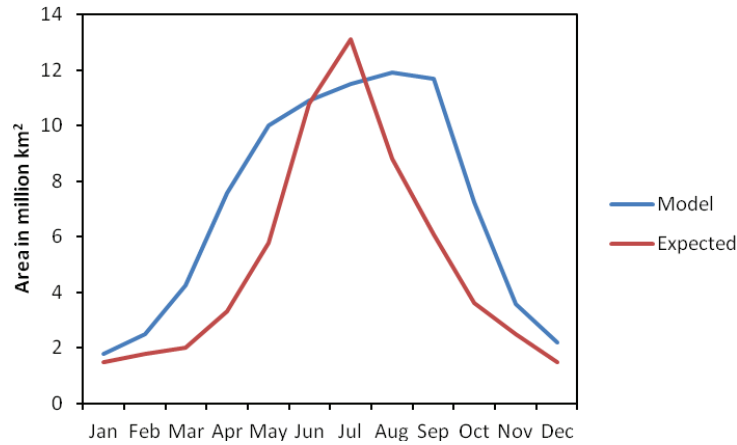


Figure 3.9: *Modeled and expected seasonality of wetland expansion for northern latitudes (40°N to 90°N)*

The ‘expected’ wetlands area in Figure 3.9 is an ensemble average of observational and modeling studies available from the literature. Wetlands in boreal latitudes show large seasonal variation compared to the tropical wetlands. While the areal extent for northern wetlands varies from 2 to 12 million km² annually, it is constrained between 3 to 5 million km² in the tropics. In boreal regions, both the parameterisation and the literature values show a pronounced summertime maximum which peaks in August and July respectively. However the peak in the parameterisation is broader than other studies suggest. The boreal wetlands, caused by temperature rise and snow melt starts spreading from March onwards and reaches maximum during July. After that they gradually decrease in area and shrink with the onset of winter. They show a low areal spread from October to March.

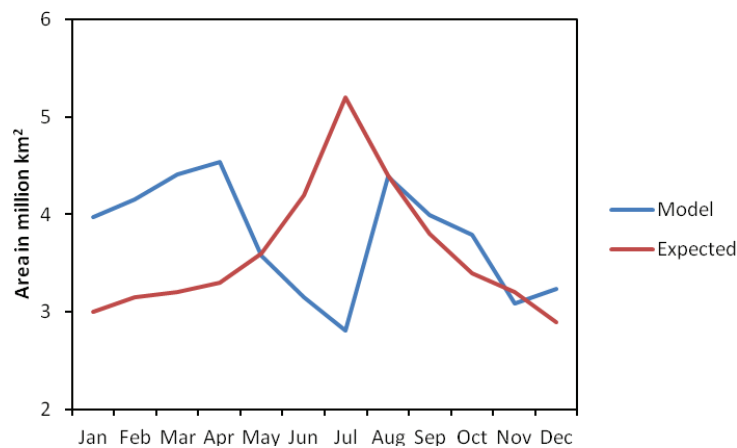


Figure 3.10: *Modeled and expected seasonality of wetland expansion for tropics (20°N-40°S)*

Over tropical wetlands, which are primarily formed due to excess rainfall, exhibits less variation. In fact, for the tropics, the model result shows two highs in seasonal cycle, once during April and the second in August with an intermediate low between May to July. The result does not really match with the overall tropical wetland trend from the observational studies and a clear phase difference is visible between May to September between them. In the following, we discuss the different seasonality of tropical wetlands depending up on their location with respect to the tropics.

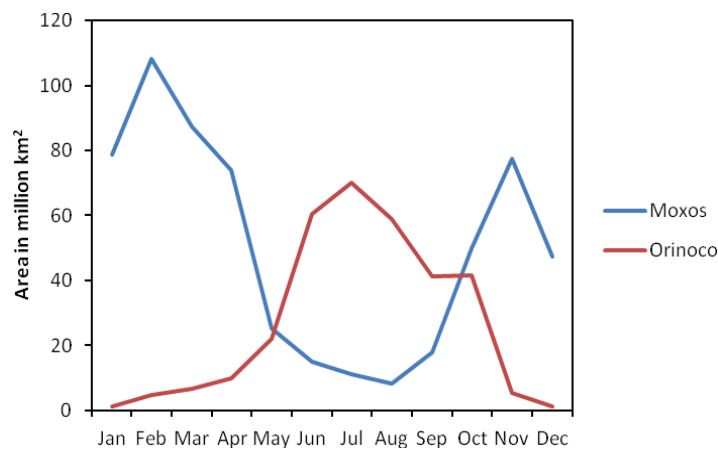


Figure 3.11: *Comparison of the seasonality between two major river floodplain areas in southern American wetlands of Moxos (60°W-68°W and 10°S-18°S) and Orinoco (64°W-74°W and 4°N-10°N)*

Moxos which is situated south of equator exhibits the inundation pattern quite similar to our model derived tropical wetlands. On the other hand, Orinoco, which is situated on the north of equator, has a completely different inundation pattern with high areal extent from May to September and low extent from November to April. This result could be validated by the study of Hamilton et al., (2002) who also observed that over the northern part of Latin American floodplains (Amazon, Roraima and Orinoco floodplain situated over the latitudinal range between (10°N-4°S) the inundation pattern is high from June to September in comparison to those river floodplains down south (Bananal, Moxos and Pantanal over the latitudinal range between (8°S-16°S) where the high is observed between September to April.

The phase difference over the tropics which is shown in Figure 3.10 could be attributed to the location of modeled wetlands which are found to form mostly south of 10°. The difference in wetland seasonality between wetlands, situated at northern belt of south American floodplain (above 10°S latitude) and below 10°S latitude, arises due to the north-south shift of the Inter

Tropical Convergence Zone (ITCZ) and corresponding shift in rainfall pattern (Hamilton et al., 2002). At the northern region all the major floodplains show high inundation from March to August but at south, the inundation is high during the winter from January to April. Our model result predicts dominance of wetlands in the southern part of South American floodplains and thus contradicts the expected seasonal pattern from observational studies which boast of wetlands primarily from northern equatorial part of South America.

3.4.2 Parameterisation of methane emission

Modeling methane emission from wetland soil is largely controlled by its dependence on soil temperature. This dependence takes a well documented exponential form so that the methane production $P(T)$ satisfies $P(T) = p \times Q_{10}^{(T-T_M)/10}$ for constant p , temperature T and the average temperature T_M at which the rate of production is known or can be calculated.

Over most of the studies, wetland methane emission is estimated empirically as a function of soil carbon and soil temperature (Cao et al., 1995, Gedney et al., 2004) where the emission rate (CH_4 emission) is linearly dependent on soil carbon and exponentially on soil temperature and expressed as

$$CH_4 \text{ emission} = KCH_4 \times C_{soil} \times Q_{10T_{soil}}^{(T_{soil}-T_{ref})/10} \quad (3.1)$$

In this relationship KCH_4 is a global constant which is optimised in view of global methane flux. C_{soil} is the amount of decomposable carbon which works as a substrate for methanogenesis. Q_{10} is defined as a factor that determines the rate of reaction with 10°C rise in temperature and lies in a range of 2-16 based on various studies (Walter and Heimann., 2000).

From Arrhenius equation Q_{10} is derived as, $Q_{10} = K_{t+10} / K(t) = \exp - E / R (\frac{1}{T+10} - \frac{1}{T})$ (3.2)

where E is the activation energy and R is the Universal gas constant.

In their study of modeling wetland methane emission, Gedney et al., (2004) chose a standard $Q_{10T_{ref}}$ value of 3.7 based on a set of model simulation and diagnosing the root mean square (r.m.s) error in comparison to observation. $Q_{10T_{soil}}$ at soil temperatures is given by

$$Q_{10T_{soil}} = Q_{10T_{ref}}^{T_{ref}/T_{soil}} \quad (3.3)$$

In other studies, in a slightly different approach, methane emission is parameterized as a fraction of soil respiration mainly because it is one of the major gases emitted from respiratory soils (Christensen et al., 2003). The soil respiration also has an exponential dependency on soil temperature.

As soil respiration does involve changing populations of many different organisms, each undergoing a complex series of reactions (Rees et al., 1998), there lays an obvious relation between respiration rate and Arrhenius equation.

Lloyd and Taylor (1994) parameterizes respiration rate as $R = R_{10}e^{308.56(1/56.02-1)/(T-227.13)}$ (3.4)

It was later used by Christensen et al., (2003) in order to estimate methane emission over Tundra regions. Christensen assumes methane emission as a percentage of total soil respiration. The same approach is followed in many of the other studies on global scale as well after suitable modifications.

So while comparing these two approaches as shown in equation 3.1 and 3.4, it can be concluded that they are not completely different from each other as both are derived from the Arrhenius equation on chemical rate constants.

It is noted that parameterizations of the CH_4 source term require knowledge about the available decomposable substrate on which the methanogenic reactions are instigated. Most studies substitute this with the soil carbon content (Gedney et al., 2004) while others use Net primary productivity (NPP) (Weber et al., 2009, Cao et al., 1996)

Data and method

In the present study, we adapt the empirical relation between methane emission rate and soil temperature and soil carbon as shown in equation 3.1 following Gedney et al., (2004) to estimate CH_4 emission.

For this study, KCH_4 is varied from 2.4×10^{12} to 5.4×10^{12} to produce corresponding wetland methane emission budget from 153 to 345 Tg per year, two extreme ranges of possible wetland methane fluxes as described in the literature. The comparison of the atmospheric model simulations (described in Chapter 4) with the NOAA CMDL data suggests that with a KCH_4 value of 2.4×10^{12} produces the lowest error between the model results and observations. The Q_{10} value for our estimation is fixed at 3.7 as used by Gedney et al., (2004).

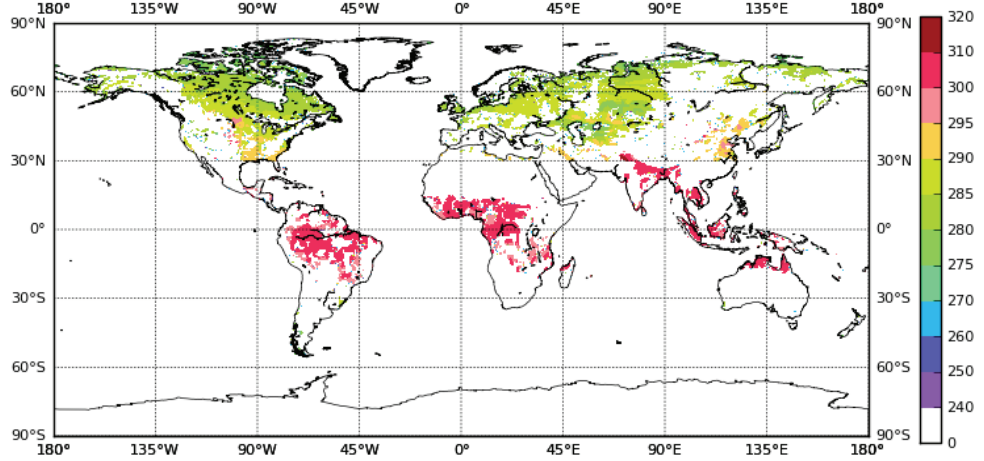


Figure 3.12: Average soil temperature distribution over potential wetlands

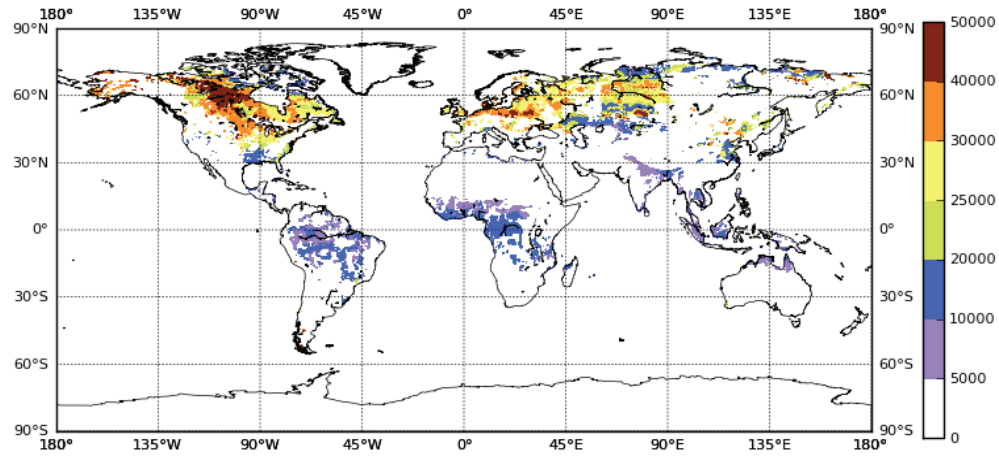


Figure 3.13: Average soil carbon distribution (g C/m^2) over potential wetlands

The average soil temperature (Figure 3.12) is always higher over tropics compared to northern latitudes. The value of average soil temperature over northern wetlands is 283 K and over tropics it is 300 K. On the other hand, the average soil carbon content for northern wetlands is $2.2 \times 10^4 \text{ g C/m}^2$ and it is $1 \times 10^3 \text{ g C/m}^2$ for tropics.

Hence, northern wetlands cover larger areas and are richer in soil carbon, while tropical wetlands emit more methane per unit area due to the higher soil temperatures.

3.4.3. Results

Wetland emission of present day

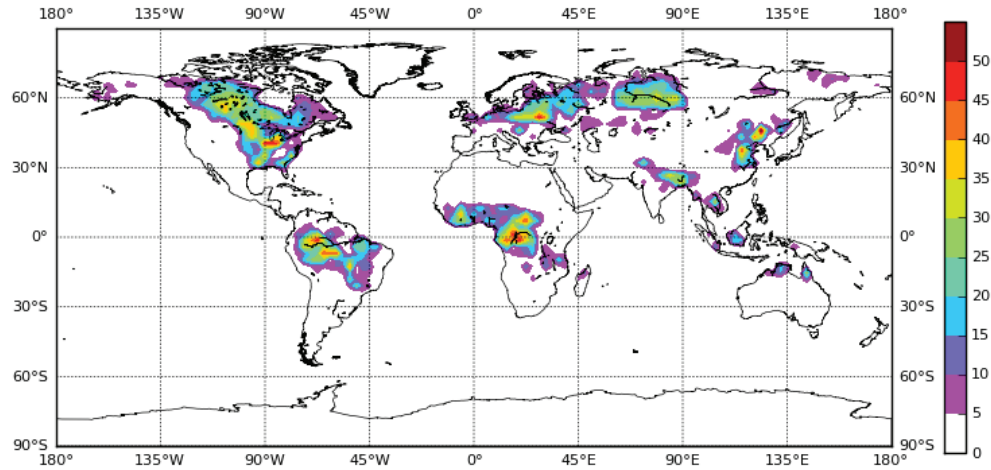


Figure 3.14: Annual mean Methane emission rate ($\text{mg/m}^2/\text{day}$). Shown here are the results with $KCH_4 = 2.4 \times 10^{-12}$ yielding a global total of 153 Tg/year

From the figure it is found that the average wetland methane emission is ranged between 10-30 $\text{mg/m}^2/\text{day}$ over a year in order to sustain the annual emission of 153 Tg. However a few of the hotspots are found where average emission rate reaches up to 55 $\text{mg/m}^2/\text{day}$. These locations include few wetland areas close to the equator as well as areas over high north latitudinal wetlands. Among the tropical wetlands, regions close to central Africa near the Congo basin and Amazonian floodplain are high emitting regions of methane. For the northern latitudes, boreal region over North America and Canada as well as few wetland areas over Western Europe are included in this category. However the factors behind high emission rates are different for equatorial and boreal regions. Over the tropics, the persisting higher temperature throughout the year causes strong methane emissivity whereas over the boreal regions it is high amount of soil carbon content.

The relative contributions from northern latitudes and tropics to global wetland methane emissions are very close to each other even though at the northern wetlands the area is twice that of tropical wetlands in our parameterisation. Northern wetlands emit around 81 Tg of methane per year whereas tropics emit annually 72 Tg of wetland methane for the global budget of 153 Tg.

Comparison between model results and field measurements

Due to issues with the representativeness of the localized field measurements the evaluation of the methane emission model remains semi quantitative. According to the field studies, for different fen and marsh types of wetlands across North America and Canada, average daily emissions vary between 10-200 mg/m² which are verified by Suyker et al., (1996) (measuring period between mid-May to early October over Saskatchewan), Bubier et al., (1993) (measuring period between May to mid September over Manitoba), Rinne et al., (2007) (measuring period between March 2005 to February 2006 over Ruovesi, Southern Finland), Crill et al., (1988), Moore et al., (1994) (measuring period between early June to mid August Over Hudson Bay). For the tropics, the box chamber measurements from different wetlands estimate average daily methane emission from 50 to 120 mg/m² and are referred in Wilson et al., (1989) (measuring period between April 1985 to May 1986 over Newport News Swamp), Bastviken et al., (2010) (measuring period between September to December 2006 over Pantanal floodplain). The modeled wetland emissions in the Saskatchewan, Manitoba regions range from 30 to 220 mg/m² overlaps well with the maximum fluxes in the observation range. However a few of the wetlands in this region reaches a high of 250 mg/m² in July and August. It reaches a low in May and October when it even dips down to 10 mg/m²/day. Since the model does not produce any wetlands in the Hudson Bay area, we cannot compare the Moore et al., (1994) observations.

Seasonality of wetland methane emission

The topic has not received much attention in the literature up to now, but a few case studies were carried in different wetland environments over a period of a whole year to study the seasonality. Whalen et al., (1992) and Nakano et al., (2000) analysed methane emissions from a tundra environment. Rinne et al., (2007) and Suyker et al., (1996) did that for boreal fen using eddy correlation whereas Wilson et al., (1989) does the same for temperate swamp. There are modeling studies by Walter et al., (2000) and Bohn et al., (2007) at different wetland sites including Siberian wetlands which look into the seasonal aspect. On a global scale there is not any model study in this regard so far.

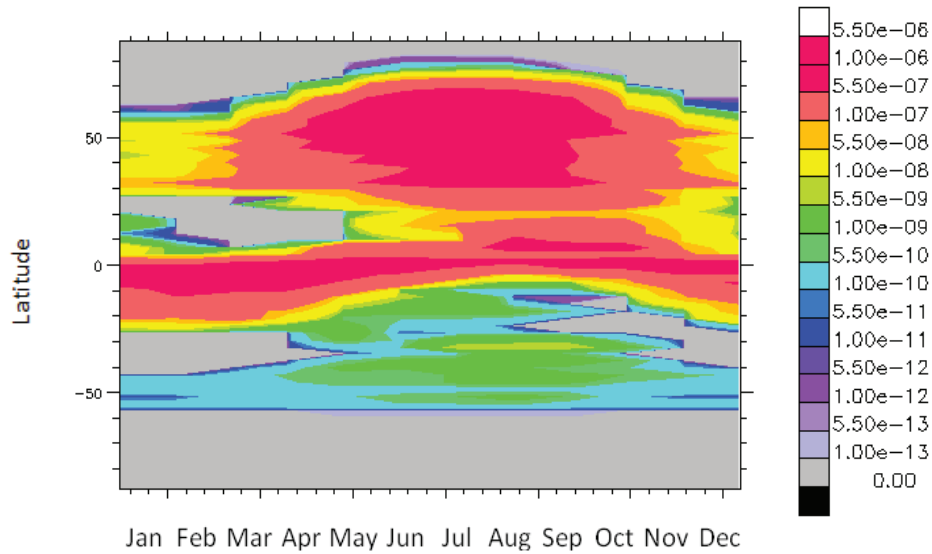


Figure 3.15: Zonal distribution of wetland methane emission rate ($\text{gm CH}_4 \text{m}^{-2} \text{sec}^{-1}$) over a climatological year

Figure 3.15 shows the zonal mean distribution of methane emission rate from global wetlands over a year from the model simulation. It shows that northern wetlands have a strong seasonal variability compared to the tropical wetlands confined between 10°N - 20°S . The northern wetlands emissivity is particularly low, in fact below $10^{-8} \text{ gm m}^{-2} \text{ sec}^{-1}$ during the winter months and intensifies up to $5 \times 10^{-6} \text{ gm m}^{-2} \text{ sec}^{-1}$ only in middle months from May to September. On the other hand, Tropical wetlands, though smaller in latitudinal spread shows a strong emissivity throughout the year.

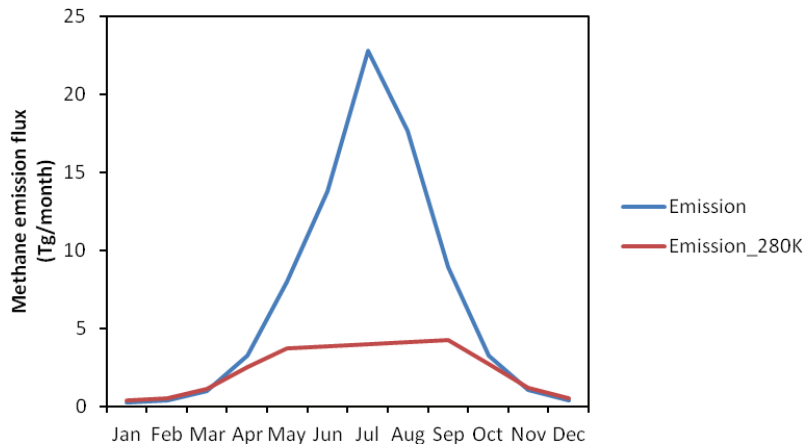


Figure 3.16: Seasonal variation of monthly emissions (Tg/month) from northern wetlands (shown in blue). The red plot shows the seasonal variation if the soil temperature is kept fixed at 280K throughout the year.

From the above figures, it can be derived that northern latitudinal wetlands exhibit a strong seasonal variability in methane emission. While the monthly emission in this region remains below 5 Tg from January to April and again from October to December, it shows a steep increase from April onwards. In the month of July, the highest of emissions is observed with a figure close to 25 Tg followed by a steep fall. The soil temperature across northern wetlands show strong seasonal trend and have a key impact behind the varied seasonality of emission. While the average soil temperature across the northern wetlands during the winter months remain as low as 279 K it reaches close to 293 K in summer. It can be observed from red curve in Figure 3.16 that if the soil temperature at the northern latitudes would have remained constant at 283 K, the wetlands should have very less seasonality. In that case, the difference between maximum and minimum emission would be less than 5 Tg. With varying soil temperature, this difference is close to 20 Tg.

The model result also shows that, among the yearly contribution of 81 Tg methane coming from northern wetlands, around 24 Tg is emitted from month of July itself. The rest of the contribution occurs during May to September in a range between 8 to 18 Tg. During the period from June to August, northern wetlands contribute approximately 65% of its annual budget. Over the winter months it remains extremely low. In fact over January, while winter at its peak, methane emission remains as low as .25 Tg. During the winter months, even if some of the wetlands continue to emit methane, they do that at a much weaker rate, almost one tenth compared to summer months. However, the effective wetland area drops down overwhelmingly during this period as well which results a reduction in net emission. With the onset of summer, soil temperature rises, so spreads the wetland extent all around to contribute at larger proportion to the annual budget.

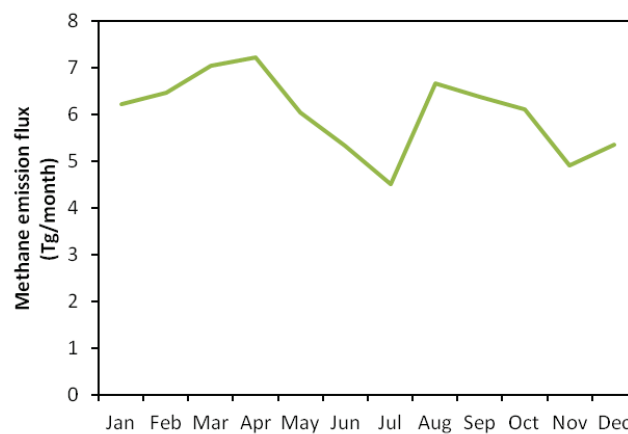


Figure 3.17: Seasonal variation of monthly emissions (Tg/month) from tropical wetlands

Tropical wetlands exhibit only little seasonality of methane emissions (Wilson et al., 1989). Throughout the year, the average emission rate over this region remains uniform and does not

undergo significant change. The primary factor behind this is the uniform soil temperature over this region. Throughout the year, average soil temperature over tropical wetlands remains close to 300 K. If we look at the average monthly emission strength over tropical wetlands, it lies between 4.5 to 7.2 Tg with small variation between June to August and then from October to December.

The seasonal trend of overall tropical emission is quite similar in pattern to the wetland areal seasonality. It suggests that while the tropical soil temperature remains largely unperturbed throughout the year, wetland dynamics is the sole factor which influences emission seasonality whatever observed.

3.5 Conclusion

The present study introduces a simple parameterization method to model wetland methane emissions under present day and paleo-climate conditions. The wetland parameterisation, described in this study follows the method developed by Kaplan, (2002). However, compared to Kaplan, the present method adopts an improved approach and succeeds in reproducing major features of the wetland distribution across globe. In fact in this study, significant attention has been given to validate the wetland parameterisation in comparison to GLWD database, the best available wetland inventory. We chose two threshold values for soil water content to parameterize wetlands, individually for boreal and tropical regions in view of their climatic differences, unlike the Kaplan approach, where a uniform global value had been selected. This approach is proved to be effective in capturing sparse wetland distributions. The overall global wetland area from this study estimates 10.87 million km² which proves to be reasonable in comparison to GLWD database. The model results capture the regional wetland distribution reasonably well particularly in the South America, Asia and African continents. However, some differences occur over Alaska and Europe. The major advantage of this method compared to other process based models lies in its dependence on limited number of control parameters which can be derived from a dynamic vegetation model also for past climatic scenarios, An important finding from the present study is that, being a local phenomena with scattered distributions, wetlands need to be modeled at a finer spatial resolution than the typical AOGCM grid scale.

Wetland methane emissions are parameterized as a function of soil temperature and carbon content. The emission strength is scaled in view of our current knowledge of global wetland methane budget which was evaluated by comparing CH₄ chemistry transport simulations with ground bases atmospheric CH₄ measurement (see Chapter 4, section 4.3.2) and estimated to be 142 Tg per year. Soil temperature largely dominates the wetland methane emission rate over the globe, and plays a vital role in its seasonality. Its persisting high value over the tropics causes high methane emission contrary to the boreal wetlands where the soil carbon that plays

more of the dominant role. The seasonality of methane emission from boreal wetlands is influenced by wetland area dynamics as well as soil temperature changes. In the tropical wetlands, seasonality is less significant and methane emissivity remains more or less uniform over the year.

4. Present day methane simulation

The atmospheric methane distribution shows considerable spatial and temporal variability. This variability is monitored by several station networks (CMDL, WDCGG, CSIRO) across the globe. In this study, we try to capture the atmospheric variability of methane using ECHAM5 MOZ chemistry transport model forced with the surface emissions compiled from different sources. The comparison between model and observation data helps to enhance our understanding of methane source distributions, their individual budget and their role in controlling atmospheric methane variability. It also validates the model performance to predict the methane at individual stations. Through this modeling study we also attempt to evaluate the wetland methane parameterization described in Chapter 3.

4.1 Methane sources and sinks

4.1.1 Sources for ECHAM simulation

In our model simulation, apart from wetlands and biomass burning, methane emissions from all the other sources are adapted from EDGAR 3.2 database provided by Peter Bergamaschi (pers. Communication 2009) of European Joint Research Commission, Italy. For wetland methane source, we have used emission map developed from our own parameterisation described in Chapter 3. Methane emissions from biomass burning are adopted from the “Reanalysis of the tropospheric composition over the past 40 years” (RETRO) project (Schultz et al., 2008). This inventory was constructed using a combination of reported and simulated data on burned area in different world regions. The seasonality and geographic distribution of the fires was taken from a satellite burned area product (GBA-2000, Tansey et al., 2004).

In our simulation, both the wetland and biomass burning emission have a seasonal distribution. However, rice emission from EDGAR 3.2 database was devoid of any such seasonality which ideally it should have. We have imposed the seasonality on rice emission by multiplying it with the monthly rice emission fraction from Matthews et al., (1991). In their study, Matthews et al., (1991) derived the seasonal distribution of cultivated rice areas by collating the rice cultivation activities and rice cropping practices for individual rice producing countries. All other sources are considered to emit constantly throughout the year.

Table 4.1: Comparison of global methane emissions used in the ECHAM model simulation with estimates reported in IPCC AR4

	IPCC 2007 (min-max) (Tg/year)	Emission in ECHAM simulation (Tg /year)
Natural		
Wetlands	100-231	142
Termites	20-29	19
Ocean	4-15	17
Hydrates	4-5	-----
Geological seepage	4-14	-----
Wild animals	15	8.5
Anthropogenic		
Wild fires	2-5	-----
Energy	74-77	83
Landfills and Waste	35-66	76
Ruminants	76-92	101
Rice (seasonal)	39-112	40
Biomass burning	14-88	35
Total	503-610	510

The annual total emission of 510 Tg in our model is close to the lower limit of IPCC AR4 (2007) which lies between 500 and 600 Tg. Compared to individual sources as prescribed in IPCC AR4 report (see Table 4.1), hydrates and geological emission are missing in our model which together contributes 8 to 18 Tg of methane to the yearly budget. In fact, methane emission budget from Geological seepage is still largely uncertain (Etiope et al., 2008). The source of wildfires is not treated individually in our model but included in the source of biomass burning. It should be noted that although fires caused by lightning account for some biomass burning events, the methane emission from it is significantly low and so merged with the anthropogenic biomass burning in the model. The strength of anthropogenic emissions used in the model is estimated to be 335 Tg per year which lies within the IPCC range. However as discussed in Chapter 2, the higher estimate of IPCC anthropogenic emission is attributed to unreasonably high rice sources of 112 Tg estimated by Chenn and Prinn (2005). If we consider realistic rice emission budget which is approximately 40 Tg (Wang et al., 2004, Olivier et al., 2005), and similar to our model assumption, the total anthropogenic emission strength in the model comes closer to the high range of IPCC. Our biomass burning emission matches several inverse modeling studies reported in IPCC (Houweling et al., 2000, Wuebbles et al., 2002, Wang et al., 2004) although isotope modeling (Fletcher et al., 2004) would yield larger values. Methane emissions from ruminants are divided into enteric fermentation and manure management and amount to 101 Tg which is higher than the IPCC maximum. Same is true for

Landfills and waste emission for which the model figure is 78 Tg and the IPCC high is 66 Tg. For the energy sector which consists of gas, oil and coal mining, the model emission lies in the middle of IPCC estimate. As for methane budget from natural sources is concerned, an estimate of 161 Tg is used in the model simulation, which lies close to the low IPCC range of 150 Tg, almost half of the high estimate of 314 Tg. The largest difference between model and IPCC high estimate arises due to the difference in wetland budget. The model wetland budget is estimated 115 Tg whereas the IPCC budget lies within 100 to 231 Tg range. In view of the recent global wetland studies (Kaplan et al., 2006, Webber et al., 2010) as well as the top-down estimates in IPCC (Wang et al., 2004, Chenn and Prinn 2006, Houweling et al., 2000), our model estimation is remarkably low. The absence of natural emission sectors of hydrates and geological emission in the model is compensated by ocean emission which lies above the IPCC maxima. However both the termites and wild animal emission in the model lies near the low end of IPCC budget.

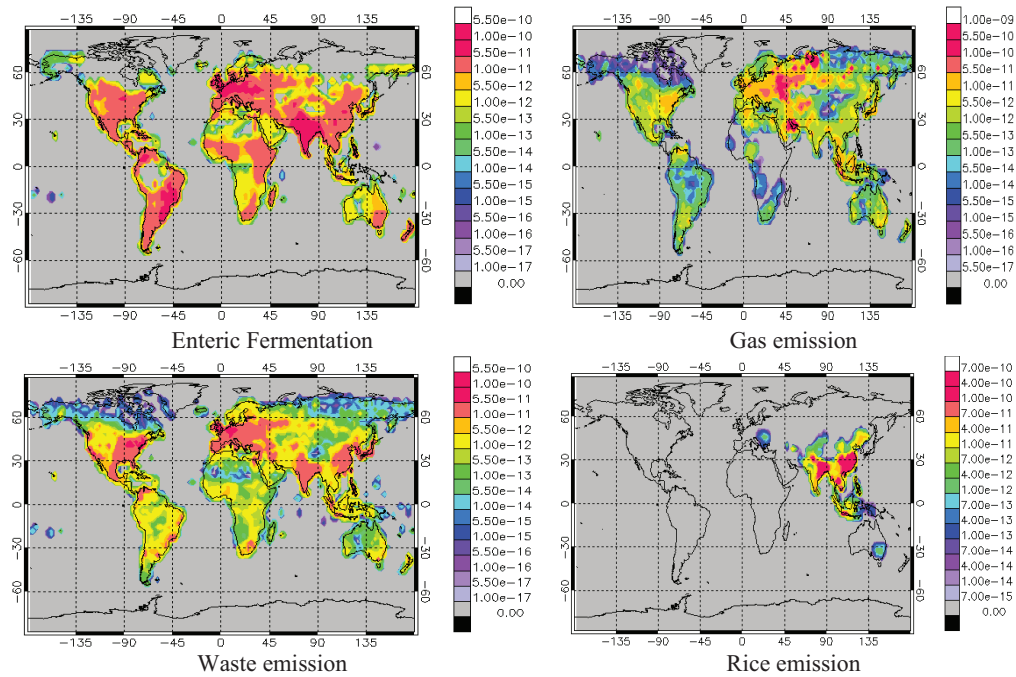


Figure 4.1: Global mean methane emission (in $\text{mg m}^{-2} \text{sec}^{-1}$) from various sources

It can be evident from the Figure 4.1 that methane emission from enteric fermentation is dominant over high over Indian sub continent, South of Europe and America. In fact the emission rate is high in all over India and countries like France, Germany and Austria in Europe and Brasil in South America. Methane emitted from Gas is significantly high in all over Europe and Middle East countries like Saudi Arab. Europe also stands high along with Eastern

America for high methane emission from waste disposal. India and Eastern China also shows significant methane emission from this sector. The rice methane emission map shows that rice paddies are the most localized of the methane sources. Methane from rice paddies are emitted only from Asia with countries like India, China, Thailand and Indonesia contributing the most.

4.1.2 Sinks for present day simulation

The atmospheric methane sink due to oxidation by OH was parameterized using a gridded monthly mean OH distribution from the multi-model mean of the ACCENT inter comparison activity (Stevenson et al., 2006). The global mean OH concentration is estimated to be 10.9×10^5 molecule cm^{-3} . The data were provided by M. Krol (pers. Communication, 2006). In the ACCENT project, 19 global models simulated the atmospheric composition around the year 2000 using different meteorological boundary conditions and different emission inventories. The mean methane lifetime from these models is 8.67 years (Stevenson et al., 2006), compared to the value of 8.4 years from IPCC (2001).

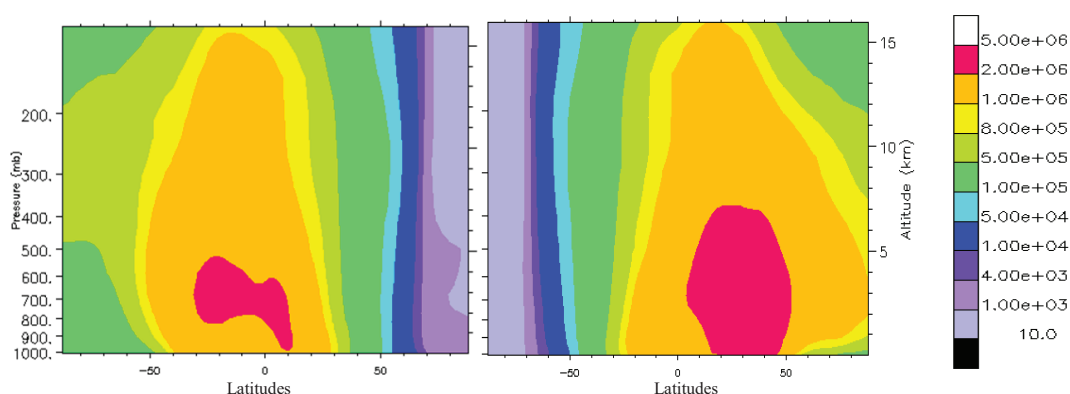


Figure 4.2: Zonal mean distribution of OH concentration (in molecule cm^{-3}). The left panel stands for January and the right panel for July

Figure 4.2 shows that the OH high in the tropical zone is more pronounced in the month of July than January. In January, the high OH concentration is found mainly in the tropical zone of Southern Hemisphere where it is extended up to 30°S. However in July, it is weaker in Southern Hemisphere and widely spread in Northern Hemisphere up to 50°N. In fact in July, the mean OH concentration stands high in Northern Hemisphere while it is exactly opposite in January.

4.2 Model description for methane simulation

The global chemistry climate model used in the present simulation is ECHAM5-MOZ. It was developed at the Max Planck Institute for Meteorology, Hamburg and consists of the general circulation model (GCM) ECHAM5 (Roeckner et al., 2003) and the chemistry transport model MOZART2 (Horowitz et al., 2003).

The dynamical core of ECHAM5 solves the prognostic equations for vorticity, divergence, temperature, and the logarithm of surface pressure in spectral space with a pre-defined triangular cutoff at wave number 31, 42, 63, 106, etc. (spectral resolution). Physical processes as advection of tracers and water vapor, convective and stratiform clouds, vertical diffusion, radiation and chemistry are calculated on an associated gaussian grid. The vertical axis uses a hybrid terrain-following sigma-pressure coordinate system (Simmons and Burridge., 1981). The model uses a semi-implicit leapfrog time integration scheme (cf. Robert, 1982) with a special time filter (Asselin., 1972). Details of the physical parameterisations including radiation, surface processes, gravity wave drag, convection, stratiform cloud formation, orbit variations, and subgrid scale orography can be found in Roeckner et al., (2003). In this study, the model was run in T42L31 resolution. This corresponds to a Gaussian grid with 128 longitudes and 64 latitudes ($\sim 2.8^\circ \times 2.8^\circ$ resolution). Sea surface temperatures (SST) and sea ice (SIC) fields were constrained by gridded fields from the Atmospheric Model Intercomparison Project 2 (AMIP2, Gates et al., 1999).

The chemical mechanism with 63 transported species and 168 reactions, and the backward Eulerian solver are adopted from the MOZART 2.4 model as described by Horowitz et al. (2003). The photolysis rates are computed by interpolation from a multivariate table originating from detailed radiative calculations with the Tropospheric Ultraviolet and Visible radiation model (TUV, version 3.0) by Madronich et al. (1998). Parameterisations of dry and wet deposition, surface ultraviolet (UV) albedo, and lightning NO_x production were modified according to ECHAM5-HAM (Stier et al., 2006), Seinfeld and Pandis (1998), Laepple et al., (2005), and Grewe et al. (2001), respectively.

4.3 Model results

4.3.1 Present day methane distribution

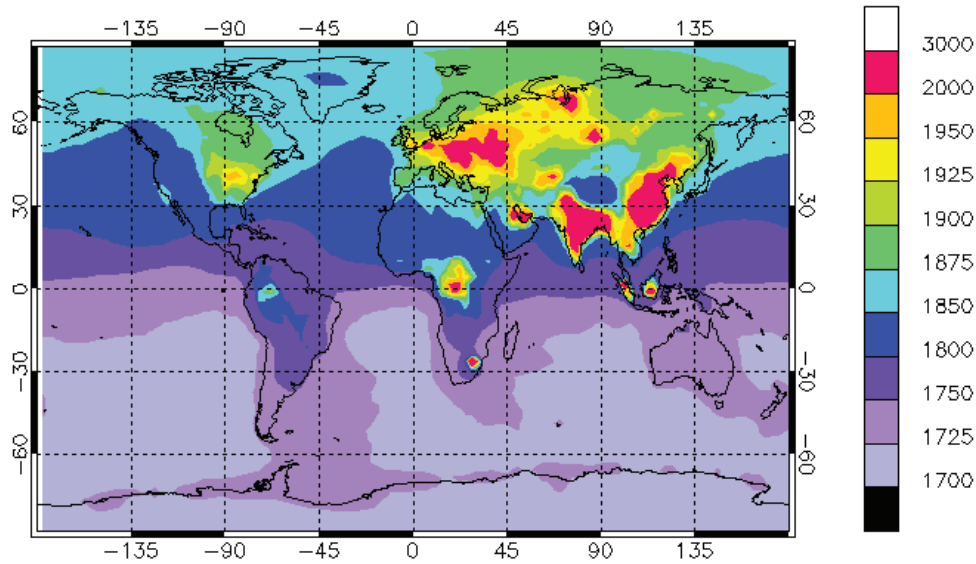


Figure 4.3: Annual mean present day surface methane distribution (in ppb) from ECHAM5 model simulation

The global mean methane mixing ratio at the lowest model level (0-50m) is 1790 ppb in the present day ECHAM simulation. This stands at par with the “present day” observations described by Dlugokencky et al., (1994), carried out by recording weekly data over a decade across globally distributed network sites. Methane concentration remained rather stable between 1998 and 2002, and has shown an increasing trend since then (see chapter 5). We chose this period to reach at the model equilibrium with the emissions prescribed in the model. Due to larger land mass, most of the methane sources, particularly the anthropogenic ones are distributed over Northern Hemisphere in the continents of Europe, America and part of Asia. The natural sources also have similar distribution, although significant areas of wetlands and termites are found in tropical region of Southern Hemisphere. As a consequence the methane level over the Northern Hemisphere shows a stronger variation compared to Southern Hemisphere where it is well mixed (Figure 4.3). It is found from the model result that methane level in the Northern hemisphere varies between 1800 to 2800 ppb while it ranges from 1700 to 1800 ppb except for a few equatorial hotspots over Central Africa and South East Asia. The difference between the hemispheric mean methane mixing ratios, known as inter hemispherical methane gradient, is estimated to be 145 ppb which is consistent with the hemispheric gradient found by Dlugokencky et al., (2008).

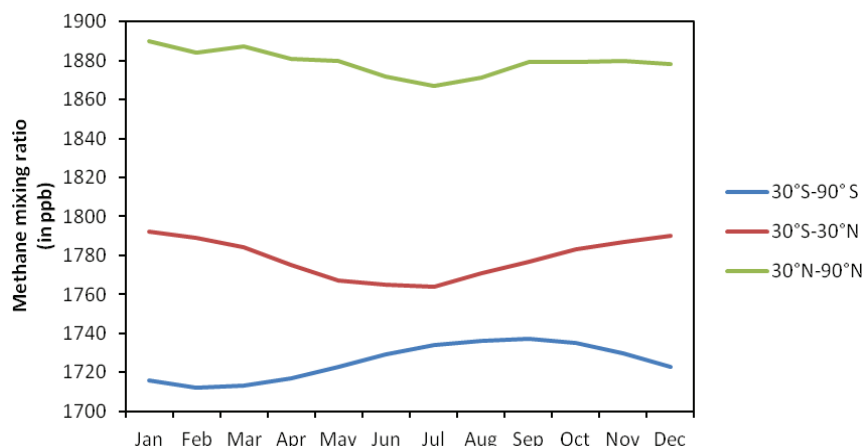


Figure 4.4: *The seasonal variation of mean surface methane mixing ratio at various latitude zones*

If we look at the atmospheric methane seasonality at various latitudinal belts, it is found that they have distinct characteristics. The average methane mixing ratio in the southern latitudes is high between July and October and low between January and April. On the contrary, both at tropics and at northern latitudes, methane concentration shows a high between January and March and low between June and August. The methane level in the Southern Hemisphere is mainly influenced by the OH loss. Here the seasonality of methane is in opposite phase with the OH seasonal pattern. On the other hand, methane in the northern latitudes is influenced by the spatial distribution of its sources, their seasonal emission pattern as well as their interplay with OH chemistry. In fact, OH shows a larger seasonal variability in Northern Hemisphere than the Southern Hemisphere.

Among the hotspots found in the Northern Hemisphere, a large part of Asia, particularly the whole of India and East china show high surface methane level. Perhaps this is attributed to the rice agricultural practice and animal farming which are dominant over both of these countries (Figure 4.1). A high methane region is also found to spread across the countries of Western Europe such as Germany, France, and Austria, caused from methane emission from gas and oil extraction (Figure 4.1). The mean methane surface mixing ratio over these countries is above 1950 ppb according to the model estimation. Small patches of methane hotspots are also found over the boreal region of Siberia and Central Russia which is attributed to wetland emission from peat and bogs (see Chapter 3, Figure 3.14). It is also found that compared to Europe, average methane mixing ratios over America are low. Except for a few hotspots close to the East American coast which do not exceed 1950 ppb, the average methane level lies between 1800 and 1875 ppb there.

Compared to Northern Hemisphere, the Southern Hemisphere has very few methane hotspots, which are also quite small in area. They mostly occur near to the equator. The most prominent methane maximum occurs at the Congo basin due to strong wetland emission (see Chapter 3, Figure 3.14) and biomass burning. It is well spread between 12°N and 5°S latitude and covers a significant area in central Africa. Here, the equatorial maximum reaches as high as 2600 ppb. A high methane mixing ratio of 2300 ppb is also found over Malaysia and Indonesia mainly due to strong wetlands and rice emissions. In South America, close to the Amazon floodplain exactly below the equator, a modest methane maximum is simulated with average value around 1850 ppb. It shows that although the South American wetland emission is dominant among the tropical emissions, it could not significantly influence the local methane level. OH concentration is also high in that region which acts as a local sink for methane. In this region, due to presence of sufficient water vapour and sunlight, OH production from ozone photolysis is expected to be high.

4.3.2 Comparison between model output and methane surface observations

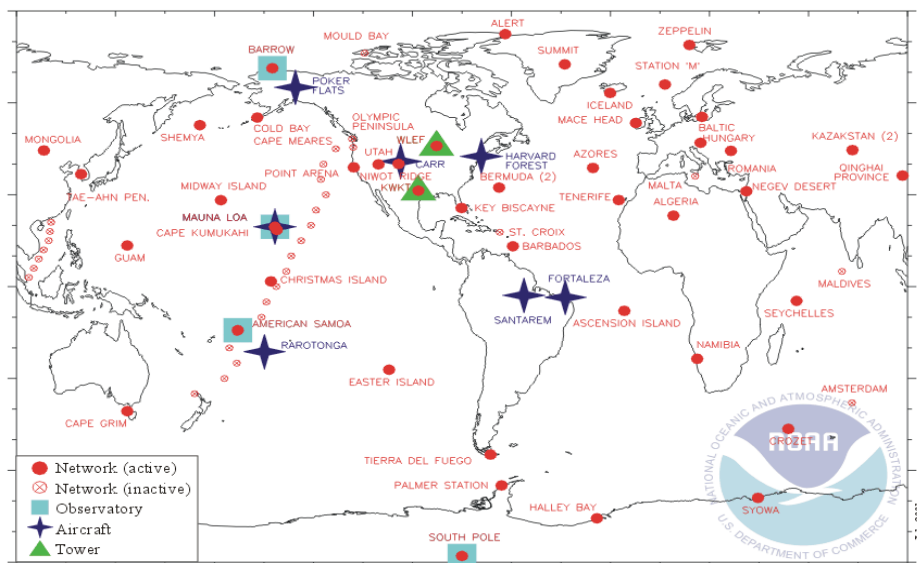


Figure 4.5: Global distribution of CMDL stations for green house gas observations
(source: http://www.esrl.noaa.gov/gmd/aggi/aggi_2008.png)

The NOAA Global monitoring division (GMD) provides high-precision measurements of the global abundance and distribution of long-lived greenhouse gases that are used to calculate changes in radiative climate forcing. Air samples are collected through the NOAA/ESRL global air sampling network, including a cooperative program where the Carbon Cycle

Greenhouse Gases (CCGG) group, which started in 1967 at Niwot Ridge, Colorado, makes ongoing discrete measurements from land and sea surface sites and aircrafts. It provides samples from about ~80 global clean air sites, including measurements at 5 degree latitude intervals from ship routes. Along with the GMD network, WDCGG (World Data Center from Greenhouse gas) network is also worthy to mention which is involved in data collection and data management. The WDCGG, which is one of the world data centers under the WMO GAW programme, has been operating since October 1990 at the Japan Meteorological Agency (JMA). Among various stations of NOAA GMD network which records the surface methane trend (starting from 1985 to 2006 depending on the station locations), 46 have been chosen to compare methane seasonality with model data. Figure 4.5 shows the CMDL station network in 2008. The majority of the stations are situated in the Northern hemisphere and at remote locations, particularly over islands or coastal areas.

Seasonality of methane

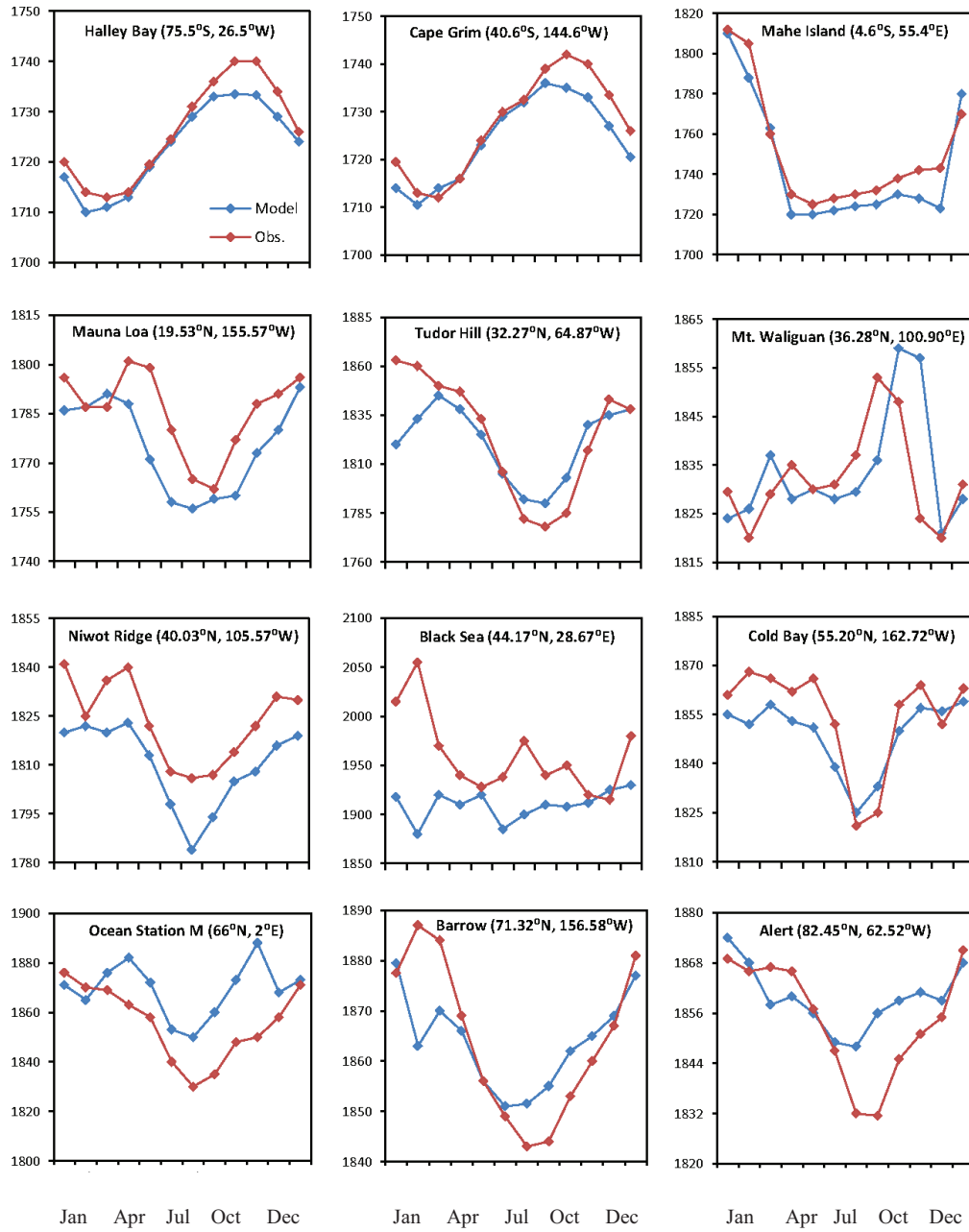


Figure 4.6: Model-observation comparison of surface methane mixing ratios (in ppb) at selected sites. Observations were averaged between 1986 and 2006.

In Figure 4.6, the methane mixing ratio at different CMDL stations are plotted as a monthly average of the observed data spanning over two decades, starting from late 1980s and till 2006 depending on the station locations. Similarly the model data is derived as the monthly average of model output of four years in its equilibrium state. In the Northern Hemisphere, both in Northern Hemisphere emission and OH oxidation influence the atmospheric in Northern Hemisphere mixing ratio. Apart from a few stations which are influenced by local emissions, majority of mid and high northern latitudinal stations show higher value during winter compared to the summer. This does not coincide with the seasonal cycle of average methane emission which suggests that OH has the most dominant effect in mid and high latitudes. Seasonality of surface methane over the Southern hemispheric stations shows a common trend which is of much smaller amplitude than Northern hemispheric stations. The lowest methane level is found in Austral summer. The seasonal pattern in the Southern Hemisphere is exactly at the opposite phase to OH seasonality which confirms that the methane mixing ratio is controlled by OH in Northern Hemisphere.

If we look into the stations situated near continental boundaries, the seasonal cycle in meteorology has a major impact on the methane seasonality. For these stations, such as Taean Peninsula (36.72°N, 126.12° E), Shemya Island (52.72°N, 174.08°E), situated at the ocean region of the Asian coast, monotonically decreasing methane mixing ratio is observed during the winter when the trade winds are directed from land to ocean. However during summer when the trade winds are from ocean to land, a strong methane gradient is found at the continental boundary.

The difference between the annual maximum and minimum varies between 10 ppb and 30 ppb for majority of the stations in the Southern Hemisphere while it ranges between 50 and 60 ppb for tropical and northern hemispheric stations. However for few stations such as Sary Taukum (44.45°N, 75.57°E) and Hegyhatsal (46.95°N, 16.63°E) the difference reaches as much as 100 ppb.

Over all the model-observation comparison shows that our model is able to capture the salient features in the observed seasonal cycle reasonably well across the stations. However, for those stations situated at high northern latitudes and a few in the extra tropics, the observed seasonality is not captured too well. Over the majority of the stations in the tropics and at all of the stations in the Southern Hemisphere, the model is able to reproduce the expected seasonality very well. The model bias is -5 to -10 ppb at the stations at Southern hemisphere and tropics. However for stations situated above 60° north, the model overestimates methane by 20 to 40 ppb. At the Northern mid-latitude stations situated near the high emission regions, the model does not fare well. In particular, it fails to produce highest methane mixing ratio observed at Black Sea (44.17°N, 28.67°E), Sary Taukum (44.45°N, 75.57°E) and Ulaan Uul (44.45°N, 111.08°E). Here the model underestimates by 100 ppb compared to the observed maxima at different months of the year. Over other months, the methane level is reasonable.

This underestimation is likely caused by a single missing source or a group of sources in the emission inventory used.

The background sites, e.g. Tudor Hill (32.27°N, 64.87°W), St. Davids Head (32.37°N, 64.65°W) and Terceira Island (38.77°N, 27.37°W), situated away from the continents, show a better seasonal match between model and observation. The same is observed at Point Arena (38.95°N, 123.73°W), Wendover (39.88°N, 113.72°W) and Niwot Ridge (40.03°N, 105.57°W) which have methane mixing ratio close to the background level. At Shemya Island (52.72°N, 174.08°W), Cold Bay (55.20°N, 162.72°W) and Barrow (71.32°N, 156.58°W) the model performance is excellent. The Asian sites of Mt. Waliguan (36.28°N, 100.90°E) and Tae-ahn Peninsula (36.72°N, 126.12°E) which are influenced by local emission have higher methane mixing ratio up to 40 to 100 ppb compared to the background sites. The model methane value at Mt. Waliguan which is located at a height of 3810 meter shows excellent match with the observation which proves the model suitability to produce realistic mixing ratio even at relatively high altitudes.

Table 4.2: Pearson correlation statistics and r.m.s error of the monthly mean model simulated atmospheric methane mixing ratio in comparison to the CMDL surface stations. The sites are listed from North to South

Location of Stations (in degree)	Pearson correlation co-eff	r.m.s.error (in ppb)
Alert (82.45N,62.52W)	0.88	10.6
Zeppen (78.9,11.88E)	0.78	16.6
Barrow (71.32,156.58W)	0.86	9.7
Ocean Station (66N,2E)	0.71	18..7
Heimaey (63.33N,20.28W)	0.75	11.9
Baltic Sea (55.35N,17.22E)	0.21	35.7
Cold Bay (55.2N,162.72W)	0.87	9.3
Mace Head (53.32N,9.9W)	0.28	17.7
Shemya Island (52.72N, 174.08E)	0.89	11.0
Hegyhsal (46.95N,16.63E)	0.25	41.1
Ulan Uul (44.45N, 111.08E)	-0.16	37.6
Sary Taukum (44.45N, 75.57E)	0.60	34..6
Black Sea (44.17N,28.67E)	-0.24	70.0
Plateau Assy (43.25N, 77.87E)	-0.24	9.5
Niwot Ridge (40.03N, 105.57W)	0.91	14.4
Wendover (39.88N, 113.72W)	0.79	16.1
Point Arena (38.95N,123.73W)	0.77	14.4
Tae-ahn Peninsula (36.72N,126.12E)	0.33	36.7
Mt. Waliguan (36.28N, 100.9E)	0.31	12.1
St. Davids Head (32.37N, 64.65W)	0.87	17.2
Tudor Hill (32.27N, 64.87W)	0.92	15.4
Sede Boker (31.12N,34.87E)	-0.39	17.3
Tenerife (28.3N, 16.47W)	0.41	17.6
Sand Island (28.2N, 177.37W)	0.89	10.0

Key Biscayne (25.67N, 80.2W)	0.85	14.5
Assekrem (23.17N, 5.42E)	-0.40	12.5
Mauna Loa (19.53N, 155.57W)	0.82	13.7
Cape Kumukahi (19.52N, 154.82W)	0.83	12.2
Ragged Point (13.17N, 59.42W)	0.79	12.5
Christmas Island (1.7N, 157.17W)	0.91	9.6
Mahe Island (4.67S, 55.17E)	0.98	10.2
Ascension (7.92S, 14.42W)	0.88	13.4
Tutuila (14.23S, 170.57W)	0.16	13.4
Easter Island (27.13S, 109.45W)	0.97	7.3
Cape Grim (40.68S, 144.68E)	0.98	4.1
Crozet (40.68S, 51.85E)	0.97	3.9
Palmer Station (64.92S, 64W)	0.99	3.6
Syowa Station (69S, 39.57E)	0.99	3.7
Halley Bay (75.57S, 26.5W)	0.99	3.2
South Pole (89.98S, 24.80W)	0.99	3.4

In Table 4.2, a quantified representation of model-observation seasonal match is given by showing the Pearson correlation coefficient and root mean square (r.m.s.) error between them.

As it can be derived from the table that over the eight stations located between 30°S to 89°S, the correlation is very high with a mean value of 0.98. For the tropical stations between 13°N to 8°S, it is not as good, still figures around .90. For the set of stations situated within the latitude range of 15 to 30°N, the correlation reduces further and estimated to be .77. However, for those extra-tropical stations which are around 18 in numbers and situated between the 30 and 60°N, the mean correlation is as low as .61. If for few of the stations (e.g. Tudor Hill 32.27°N, 64.87°W, Niwot Ridge 40.03°N, 105.57°W, Shemya Island 52.72°N, 174.08°E, Cold Bay 55.20°E, 162.72°W) the correlation is 0.9 and above, for few others (Hegyatsal 46.95°N 16.63°W, Mace Head 53.32°N, 9.90°W), it is close to 0.3. In fact, for the stations (e.g. Plateau Assy 43.25°N, 77.87°E, Black Sea 44.17°N 28.67°W, Ulaan Uul 44.45°N, 111.08°E), the model seasonality is found to be in the opposite phase to that of observation and the correlation between them is negative. It suggests that for the high emitting terrestrial region in the northern latitudes, the model sometimes fails to capture each of the local sources, which cause the apparent seasonal mismatch. There the sources present, have their individual seasonal variability and strong regional signature. Once we get further up in north, the correlation improves for the high latitudinal stations and shows a mean correlation value of 0.8. This is perhaps due to the fact that the boreal region is mainly dominated by wetland emission which is parameterized well in the model.

Another aspect to evaluate the model results is by looking at the r.m.s. error of the model methane output at the stations compared to observation. The average r.m.s error in the southern latitudinal belts is 4.2 ppb which shows that model perform at its best in this region. Over the tropical region it has a value between 11 to 13 ppb which increases up to 20 ppb at the high northern latitudes. Overall the global average is estimated to be 13 ppb which indicates the

suitability of the model to produce a realistic methane distribution both at the global and regional scale. Compared to the modeling study by Patra et al., (2009) which estimated a r.m.s statistics of 18.6 ± 4.2 ppb for the stations situated between the latitude 5 and 60°N, our model shows an improvement by 2 ppb and finds an average r.m.s error of 16 ppb.

It is to be noted here that to reach this optimum match between model and observation on the basis of average correlation and r.m.s. error, we modified the base source strength of wetland and biomass burning regionally. The best seasonal match for northern latitudinal stations occurs with the wetland emission being reduced by a factor of 1.2 above 45°N. For the same purpose, the biomass burning emissions have to be reduced by factor of 1.8 above 35°N. In order to improve correlation over the southern hemispherical stations, biomass burning emission is increased by a factor of 1.48 below 35°N. The emission scenario after the regional scaling has been regarded as the optimized emission scenario for model simulation. It is noted here that after the modification, both the wetland and biomass burning source remain within the IPCC range with the strengths of 142 and 31 Tg respectively. It proves that the wetland methane model in Chapter 3 overestimates methane emission in the high northern latitude which would ideally be low. Perhaps for a better representation of regional wetland methane emission, one has to have a low KCH_4 in Northern Hemisphere value for boreal regions than the rest of the globe.

Latitudinal distribution of methane

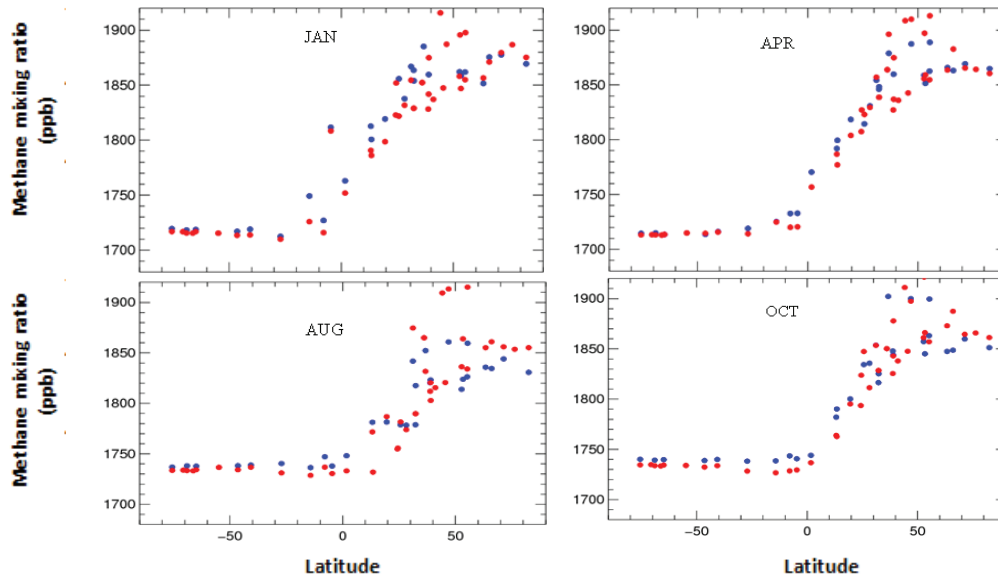


Figure 4.7: Comparison between model and observations for the latitudinal distribution of surface methane mixing ratio at different months of the year (January, April, August and October). The red and blue line stands for the observation and model respectively.

Figure 4.7 confirms the good agreement between observation and model and summarizes the latitudinal distribution of surface methane with a common pattern which does not vary much over the months in a year. It shows that over the Southern Hemisphere, average methane mixing ratio does not show any significant spatial variability and remains between 1700 to 1750 ppb depending on months. It shows an increasing trend close to the equator between 15°S to 5°N and continues to rise up to 1850 to 1900 ppb till 50 to 60°N. It stabilizes there but shows a decline at the pole where it holds an average mixing ratio of 1850 ppb. It can be seen from Figure 4.7 that the model captures well the overall methane latitudinal trend at both the hemispheres.

According to Dlugokencky et al., (1994), the Inter hemispherical gradient of surface methane varies between 130 to 150 ppb which the model produces reasonably well over the months. However, in the high northern latitudes, particularly in the latitude range of 40 to 60°N, the model shows a scattered distribution which is less prominent in the observation. It is evident that in this region the model has a tendency for overestimation. If we look into individual months, it is found that in the Southern Hemisphere, the model methane pattern matches very well with the observation particularly in January, April and August. However, in October the model underestimates in the range of 5 to 10 ppb. In the Northern Hemisphere, the trend is more complex while even the closely situated stations show varied methane level. Here the

model shows a tendency to underestimate in tropics while it overestimates in high north. This pattern is followed over the year. For stations, located between 40 and 50°N, the observations show a methane value close to 1900 ppb in the month of October which is highest in a year. At these same locations, the simulated methane level is 50 ppb low in August. The model seems to produce it well in October but not so well in August and overestimates between 20 and 40 ppb.

4.4. The sensitivity analysis of model with changes in source strengths

In order to improve the performance of the model at regional scale as well as to evaluate the impact of individual sources on the global methane abundance, a sensitivity analysis has been done. Eight classes were created from the twelve methane source sectors considering their similarity in emission processes and regional distribution. Two sets of model simulation have been carried out for each of the eight groups of sources one by enhancing and the other by reducing the respective source strength by 10 Tg. The source strengths always remain within the range of IPCC estimates. For each of these sixteen simulations, the correlation co-efficient and the r.m.s. error of the model output is estimated with respect to observation which is shown in Table 4.3.

Grouping of the sources

In view of their distinctive emission characteristics, wetlands, rice, biomass burning and ocean have been treated as individual methane source classes in the sensitivity analysis. Although the process of methane production from the soils of wetlands and rice paddy fields are quite similar, which is due to decomposition of soil organics in anaerobic condition, rice emission is mainly concentrated in the Asian continent. Wetlands, on the other hand are distributed all over the world at various climate zones. These two sources also have completely different seasonal emission pattern. Similarly ocean emission has a distinctive signature compared to territorial sources. Among the other sources, we have considered termites and wild animals in the same class as they are emitted without any human influence and together counted a mere 5 % of the total budget. Among the anthropogenic sources, industrial waste from solid and water are taken into one class. The other major anthropogenic sources from industry which include gas, oil and coal mine emissions are grouped into one because of their identical nature and similar regional distribution. The last group in our analysis consists of enteric fermentation and manure management from domestic animals, both of which depend on animal farming.

Most of the simulations listed in the Table 4.3 degrade the quality of the simulation. Only five out of the sixteen simulations yield r^2 close to that obtained from the base case simulation and show promises for further improvement on the model-observation seasonal match. These five sets are obtained from the model simulations with Wt-10, TeA+10, EnM+10, CoG+10 and Wa+10. Among them, for Wt-10, the average correlation value improves from .61 to .64 at temperate region (32-55°N), from .89 to .93 at tropics (15°S to 15°N) and from .76 to .81 at northern extra tropics (20-30°N). However it could not improve the correlation for stations situated at high north (above 60°N) where it degrades to .78 from .80. Among the set of stations, it is very difficult to come up with a good seasonal match for those situated at high north. It is seen in this sensitivity analysis that while trying to improve the seasonality at those locations, we end up reducing it elsewhere. For other set of simulations apart from Wt-10, the average correlation values at high north are lower with respect to the base case one. In fact for Rc-10, it dips down to .70 even if the tropical and extra tropical stations show higher correlations. For simulations with a 10 Tg enhanced emission in each of the anthropogenic sources as given by EnM+10, CoG+10, Wa+10 and TeA+10, the correlation in the temperate region improves to .66 and that in tropics improves to .91. For extra tropics it reduces to .74 and for high north it reduces to .75. So overall, it seems that it is with the wet-10 simulation that results in a better seasonal match than the standard one globally. However, if one looks at the r.m.s error between model and observation with the Wt-10 simulation, it shows a huge increase compared to the base case one. Globally it results in r.m.s error of 44 ppb which is approximately 25 ppb high than the base case. It is consistently high by 20 to 30 ppb both in Northern and Southern Hemisphere. For other set of simulation with the enhanced anthropogenic sources, the average r.m.s. error figures between 28 and 35 ppb, lower than Wt-10 but still 10 to 15 ppb higher than the base case simulation. It indicates that even if any modification of the sources could result in better seasonal match than the base case scenario between model and observation, it could not produce the observed surface methane mixing ratio at the stations. It is not possible to come up with a better correlation without hampering the global methane abundance. It can be concluded that the base case scenario used in the standard model simulation serves best to capture the observed seasonality remaining closely to the station recorded data.

4.5 Conclusion

The present study shows the success of the ECHAM MOZ model simulation to reproduce major features of methane distribution across the globe using anthropogenic emission from EDGAR and RETRO inventory and the wetland emission from the newly developed wetland parameterisation. It is able to capture the seasonal variability pretty well although shows a tendency to overestimate between 20 and 40 ppb over high northern latitudinal stations which could be attributed to overestimation of an individual or a group of sources. In Southern

Hemisphere the model observation correlation is quite high. In fact major effort has been gone in this chapter to look in to the seasonal variation of model methane and optimize the global methane budget. The optimized global methane budget is estimated at 510 Tg which falls in the lower end of IPCC AR4 report. The optimized emission scenario which produces the best model observation match has been emerged by some regional modification of wetland and biomass burning emissions. The modification has been done in the form of reducing both wetland and biomass burning emissions above 45° N and enhancing the later below 35° N. The optimized wetland and biomass burning methane budget is estimated to be 142 Tg and 31 Tg respectively which indicates to a weak wetland source that falls in the low end of IPCC. This is an important finding from this chapter since majority of the previous modeling studies prescribe a higher wetland methane budget. It is also to be mentioned that a set of sensitivity studies which has been carried out by changing the strength of group of methane sources within ± 10 Tg, do not result in an overall improvement in model observation correlation. This reinstates the suitability of the optimized methane budget as estimated in the study to produce best possible model observation match.

5. Methane trend at present

Atmospheric methane concentrations showed a steady increase of about 15 to 20 ppb per year until the early 1990s. Between 1990 and 2006, the growth rate was much lower, averaging to only 5 ppb per year, and some years even showing negative growth rates (Figure 5.4, Dlugokencky et al., 2011). Several theories were put forward in order to explain this apparent “stabilization” of methane concentrations (Dlugokencky et al., 2003, Rigby et al., 2008, Khalil et al., 2007) and a few model studies have been performed trying to reproduce and to explain the changes in the methane growth rate and its inter annual variability (Bousquet et al., 2006, Dentener et al., 2003, Fiore et al., 2006). More recent measurements show a renewed rise in global average methane concentrations <http://www.esrl.noaa.gov/gmd/aggi>). The previous studies attributed the variability of methane concentrations to a combination of emission changes, changes in meteorology, and variations in the atmospheric oxidation rate, i.e. the OH concentration. Here, we attempt to reproduce the observed methane changes between 1990 and 2006 with the ECHAM-MOZ chemistry climate model, and we try to separate influences of changing emissions from meteorological variability. We do not consider fluctuations in the OH concentration as other studies have done, because we trust the results from Montzka et al., (2011) who found that the OH variability between 1998 and 2007 was not more than $2.3 \pm 1.5\%$, and there is no reason to believe that it should have been any larger in the years before 1998.

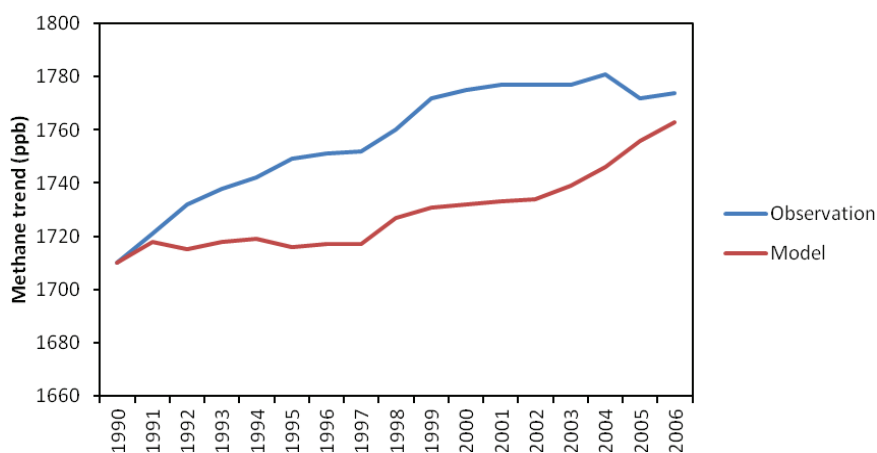


Figure 5.1: Time series of the global average CH_4 mole fraction derived from the surface sites operated by NOAA/GMD (blue line) from 1984 to 2006. Red lines depict annual average, global mean surface mole fractions from the ECHAM-MOZE base run

5.1 Simulation set-up

For the transient methane simulation between the year 1990 and 2006, the methane emissions from anthropogenic sectors except the biomass burning are adopted from the EDGAR V4.2 inventory (<http://edgar.jrc.ec.europa.eu/overview.php?v=42>). Biomass burning emissions were adopted from the RETRO emission inventory (Schultz et al., 2008; see also chapter 4, section 4.1.1.) Wetland emissions were calculated with the new parameterization described in Chapter 3. For this purpose, a new CARAIB simulation was performed to generate monthly estimates of soil moisture for the entire period from 1990 to 2006 (L. Francois, personal communication, 2012). As described in chapter 3, soil moisture and terrain slope together are used to determine the potential wetland areas. Note that this simulation was performed with an updated CARAIB model version compared to the results shown in previous chapters of this thesis. This implied that we had to adjust the threshold parameters for soil moisture from .3 to .6 for northern latitudes (30°N-90°N) and from 1.1 to 1.25 for the rest of the globe. Figure 5.2 shows the resulting wetland areas. While our parameterization suggests that the global wetland area remained stable around 9 ± 0.5 million. km² until 2004, it drops below 8.5 million km² in 2005 and 2006. In fact, the time series exhibits a continuous decline after 1998. As can be seen from Figure 5.2, this decline is largely due to a decreasing wetland area in the Northern latitudes (30°N-90°N). The tropical wetlands do not so much variability during this period.

For ocean and termites methane emission, we use the value of 1990s for the seventeen years of simulation since there is no proof that they underwent any significant change over these years.

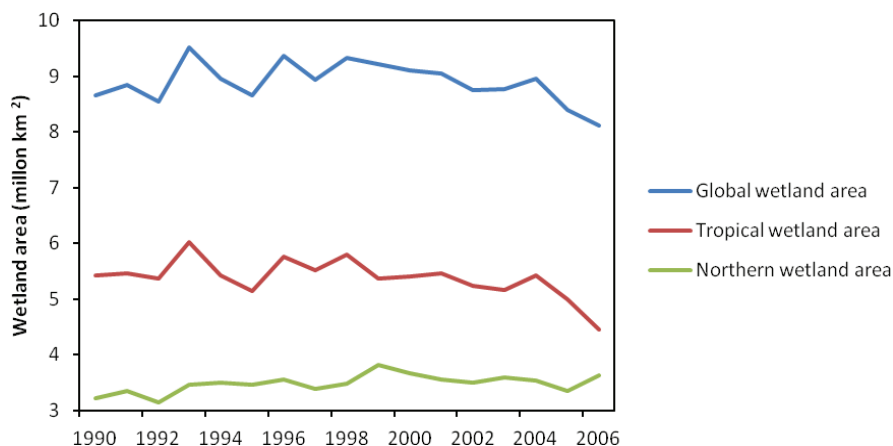


Figure 5.2: The variability of global, tropical (30° S to 30° N) and northern (30° N-90° N) wetland area between 1990 and 2006

As the EDGAR V4.2 inventory contains a rather detailed sector split, we chose to group some of them into broader categories for the discussion of the simulation results (see Table 5.1).

Table 5.1: *Origin and sector classification of methane emissions used in the transient ECHAM-MOZ simulation*

Emission category	Reference	Original sector classification
Oil and gas extraction	EDGAR 4.2	Gas production & distribution (GPD), Fossil fuel fires (FFF) Energy manufacturing and transformation (EMT)
Industrial and residential fossil fuel combustion	EDGAR 4.2	Industrial process and product use (IPU), Residential emission (RCO), Non road transportation (TNR)
Waste treatment	EDGAR 4.2	Fugitive from solid (FFS), Solid waste disposal (SWD), Waste water treatment (WWT)
Animal emission	EDGAR 4.2	Enteric fermentation (ENF), Manure Management (MNM)
Biomass burning	RETRO	
Rice emission	EDGAR 4.2	Agricultural soil
Wetland emission	Parameterized from CARAIB	
Other natural sources	GEIA	Termites, ocean, Wild animals

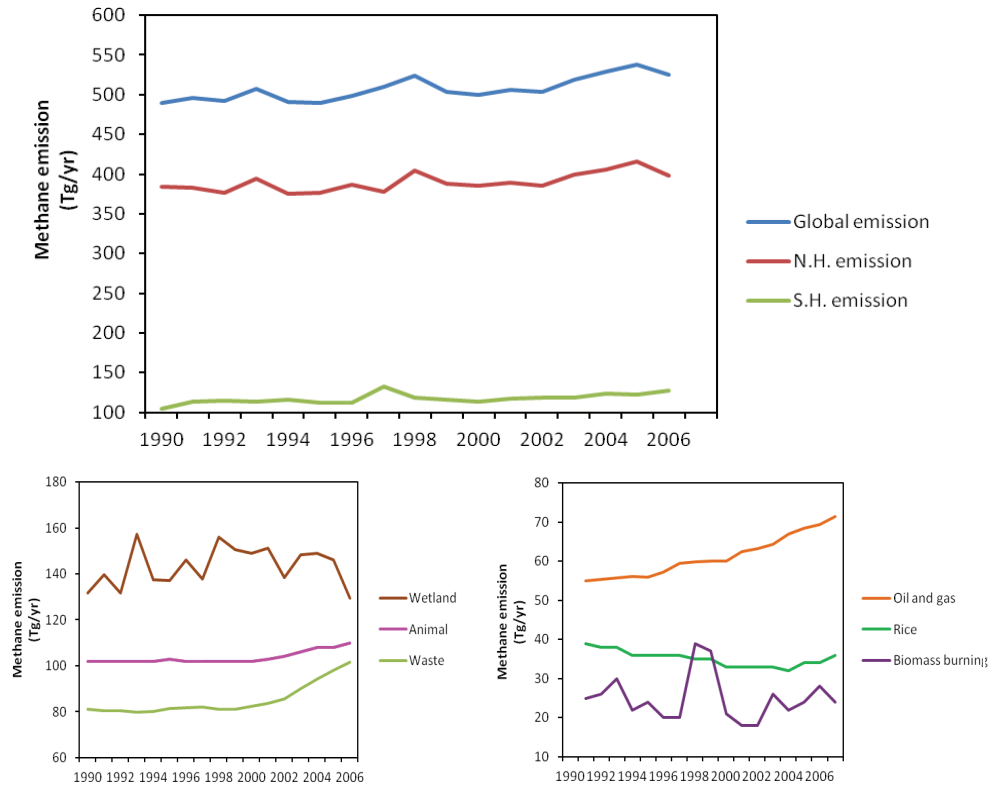


Figure 5.3: The top panel shows the trend of global methane emission and its contribution from Northern and Southern Hemisphere. The panels below split the emission trend depending up on the strength of the sources, the left one shows annual emissions above 80 Tg and right one below that

It is evident from Figure 5.3 that Northern Hemisphere has larger methane sources, almost 3.5 times than Southern Hemisphere. It also shows stronger variability with annual emission ranging between 375 and 425 Tg over the simulation period. The Southern Hemispheric sources show less variability with annual strength lying within 110 and 120 Tg. Only in the year 1997, it reaches up to 132 Tg. The global methane emission trend between 1990 and 2006 is more influenced by Northern Hemispheric emissions than by Southern Hemispheric sources.

If we look at the changes of various methane sources during this period, wetlands does not show any particular trend although having a significant inter annual variability with its emission ranged between 130 to 160 Tg annually. It shows large emission in the year of 1993, 1998, 2000 and 2004 with a value ranging between 150 and 160 Tg. The highest increase in its emission is observed between 1992-1993 and 1997-1998 in a scale of 20 Tg.

Both the animal and the waste emission remain constant between 1990 and 2000 with values close to 100 and 80 Tg per year respectively. They both show a steady rise only after 2001, with waste methane shows maximum and finishes close to 102 Tg of annual emission at the end of 2006. The right panel at the bottom of Figure 3 shows an increasing trend for methane emission sourced from oil and gas extraction which is particularly dominant since 1999. It remains uniform between 1990 and 1994 with 55 Tg, increase up to 60 Tg till 1999 and then starts to grow at a steady rate, reaching 72 Tg at the end of 2006. Rice emission on the other hand seems to weaken over the years as it declines from 40 Tg to 32 Tg between 1990 and 2003 followed by a late increase. Methane emission from biomass burning hardly shows any significant variability apart from a huge growth in 1997-98.

Following Montzka et al., (2011) we assume that the variability of the global mean OH concentration was rather small during the 1990 to 2006 time period. We therefore used the same monthly varying multi-model OH climatology as in our previous simulations (see section 4.1.2) and did not change these values between years.

This is in contrast to the previous modeling studies on atmospheric methane trend (Fiore et al., 2006, Bousquet et al., 2006) which considered significant variability in OH level in their simulations. However, our assumption is based on the study by Montzka et al., (2011) who finds very small inter annual variability of global OH between 1998 and 2007. Although there have been studies (Krol et al., 1998, Prinn et al., 2005, Bousquet et al., 2005) which found large OH inter annual variability derived from CH_3CCl_3 measurements in the order of order of 7 to 9% (in some cases up to 25%), Montzka et al., (2011) provide evidence that these results suffer from large uncertainties which were dominant before 1998 due to large CH_3CCl_3 emission. Post 1998, there is a significant reduction in global CH_3CCl_3 emission which should reduce the uncertainty in OH estimation as well. Montzka et al., (2011) found OH inter-annual variability in the order of $2.3 \pm 15\%$ between 1998 and 2007 which is significantly less than the previous modeling studies. This difference arises due to reduced uncertainties in the analysis of CH_3CCl_3 data rather from actual reduction of OH variability.

Contrary to the other simulations described in this thesis, we also include a sink term for the surface uptake of methane. This was parameterized as a first order loss with a constant and uniform deposition velocity V_d over land. The deposition velocity was adjusted to yield 25 Tg annual methane deposition for a global average mole fraction of 1780 ppb (Curry et al. 2007, Kightley et al. 1995, Whalen et al.1990). The resulting V_d is $8.5 \times 10^{-7} \text{ m s}^{-1}$.

5.2 Results

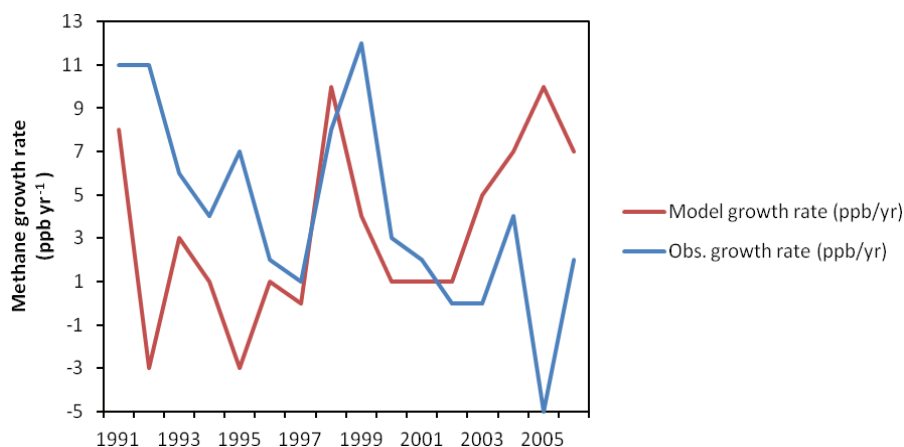


Figure 5.4: Time series of annual growth rate derived from NOAA/GMD sites (blue line) and ECHAM-MOZ base run (red line)

From Figure 5.4, it can be derived that the observed methane growth rate is showing a declining trend between 1990 and 2006, apart from a sudden rise at 1998 and 1999. Starting from 11 ppb/yr at 1991 and 1992, it shows a steady decline and reaches close to 0 in the year 1997. It increases again to 12 ppb/yr in the year 1998 followed by a steep fall. Between 2000 and 2003, the growth rate remains within 0-2 ppb/yr. It shows a negative growth in 2005 only to increase again in 2006. In comparison to the observation, the model derived methane shows a lower growth rate between 1991 and 1995 and a higher growth between 2003 and 2006 with a mean value 1.5 and 7 ppb/yr respectively. The trend of growth rate between model and observation are very close to each other between 1996 and 2002. It proves that the model is able to reproduce the methane inter annual variability pretty well in the mid of simulating period but not so well at the initial and terminal four years.

As shown in Figure 5.1, our model simulation reproduces the average surface methane mole fraction between 1990 and 2006 reasonably well. The mean observed methane mixing ratio during this period was 1755 ppb (CMDL), while the model mean mixing ratio is 1730 ppb. The model also shows a rather steady methane level during this period with a small, but steady growth over time. In fact, the overall increase in the simulation (50 ppb) is even smaller than the observed increase (65 ppb). This indicates that the long-term changes in methane emissions are relatively well captured, and that our assumption of small OH variability is robust.

One of the differences between the observation and model result is visible between 1990 and 1997. During this period, the model methane mixing ratio remains constant at a value close to 1720 ppb although the observed methane shows a steady increase and reached 1750 ppb at the

end of 1997. However, since 1997 both the model and observation shows a brief increase till 1999 followed by a temporary stabilization till 2002. Between 2002 and 2006, although the observed methane level remains close to 1775 ppb, the model methane shows a rising trend and reaches 1765 ppb at the end of 2006.

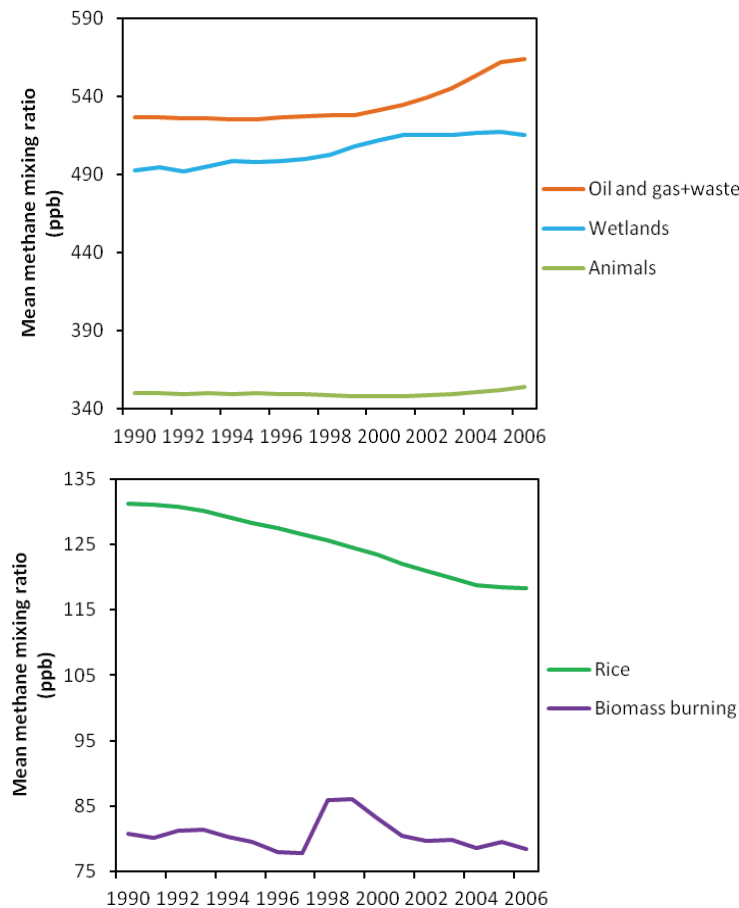


Figure 5.5: The trend of various methane tracers between 1990 and 2006 derived from ECHAM-MOZ simulation

If we look at the model derived methane tracer trend for major sectors we could see that apart from wetlands none of the others shows any growth for the first seven years of simulation, when the model shows a negative bias compared to the observation. Methane tracer from oil extraction and waste which together constitutes a large part of anthropogenic methane seems to be at equilibrium between 1990 and 1998 with a value of 527 ppb. It shows a rising trend only after 1999 and reaches to 560 ppb at 2006. Even the methane tracer from animal emission shows the same trend although in a smaller scale during this period. This pattern is

consistent with the trend of their emission as shown in Figure 5.3. In contrast to both of these anthropogenic tracers, wetland methane mixing ratio shows a steady increase since 1992 and ends up at 515 ppb at the end of 2006 which is 20 ppb higher compared to its 1990 value. Methane mixing ratio sourced from biomass burning follows the same trend as its emission pattern (see Figure 5.3), showing a 9% increase during 1998 and 1999 compared to its mean value over the simulated years, which is approximately 80 ppb. In this El Nino year, with a widespread dryness across the globe, the increase of fires in the tropical zone and boreal regions cause an overwhelming methane emission from biomass burning in the range of 40 Tg, which is 15 Tg high than its mean.

Methane from rice paddies shows a decreasing trend over the entire simulation period. It is concomitant with the trend of methane emission from rice fields (see again Figure 5.3) which shows a continuous decline from 1990 to 2003. During this period, the strength of annual rice emission slips from 40 Tg to 32 Tg mainly due to changes in agricultural practices in China (Li et al., 2002), one of the largest contributor to the global rice methane emission. Two most important changes occur in form of reduced use of organic amendments and increased practice of intermittent flooding. From the early 1980s, Chinese farmers began draining the paddies midway through the rice growing season which resulted in a drastic mitigation of methane emission from the fields. Li et al., (2002) has stated that this practice replaced continuous flooding over most of the paddy areas over China. The other large contributor, India does not show any significant change over the last two decades in rice methane emission. According to Garg et al., (2011), there is a reduction of only .39% from 1995 to 2008 methane production from Indian rice paddies which perhaps has no role behind the reduction of global rice methane budget.

Figure 5.5 gives an indication that perhaps the model observation mismatch between 1990 and 1997 occurs due to flattened anthropogenic emissions which constitute approximately 60% of the total source. There is no existing proof which could indicate to a different anthropogenic emission pattern and eventually a possibility that it would have contributed to the methane rise in the early nineties. In fact there are number of evidences which suggest that the reduction of fossil fuel sources in the nineties which inhibited the methane growth rate of 1980s. Statistical Review of World Energy (2002) suggested that there have been significant drop in fossil fuel production in the mid and late nineties. They have come up with the fact that extraction of oil and coal which peaked in the late 1980s, dropped to less than two thirds of their peak values by mid to late 1990s. It is also speculated that the natural gas extraction which peaked in the late eighties fell by 17% between 1991 and 1997. According to Reshetnikov et al., (2000) and Dedikov et al., (1999), the methane emission decreased by more than 20 Tg in Russia alone during this same period. Worthy et al., (2009) also found significant reduction in anthropogenic methane emission in the order of 30 Tg from Europe and Siberia after 1987. However, Dlugokencky et al., (2003) stated that there is no evidence

in Gazprom (Russia's state owned gas company) which could support such a large reduction in methane emission.

Some recent studies also suggest a different view on that. In the recently concluded 2012 ACCENT-IGAC-GEIA Conference at Toulouse, evidence was presented (presentation by G. Pétron) that methane emissions from fuel extraction in the state of Colorado, USA have been grossly underestimated in the past. This is associated with the hydraulic fracturing or fracking technique which is also applied in other parts of USA as well. According to Pétron et al. (2012), who carried out their study in the Weld County and surrounding, the methane source from natural gas system in Colorado is most likely underestimated by a factor of at least 2. If we follow the estimation of Pétron et al., (2012), the CH₄ emissions from fossil fuel extraction in the US might have to be increased up to 15 %. Assuming that fracking accounts a considerable fraction of the total fuel extraction, global emissions from this sector could be larger than estimated by EDGAR 4.2. This could potentially explain the differences between model and observational methane trend between 1990 and 1997. However, the fracking technique had not been used in a wide-spread fashion until the mid 2000's and it showed a rather steady increase since then. It is therefore unlikely that this can account for the observed discrepancies between the model and the observations. At the same time it is to be noted that apart from USA, in many a West European countries like Germany and Netherlands, and in Russia, fracking has been practiced since 1970s, although regionally (http://en.wikipedia.org/wiki/Hydraulic_fracturing). In view of that, an underestimation of methane emission from natural gas extraction on a global scale cannot be ruled out even before 2000s.

Another possibility is the underestimation of wetlands emission at the early 1990s which holds a mean value of 140 Tg during that period. However this possibility does not seem plausible as per findings stated in Chapter 4 which suggests that the wetland methane budget has to be at the lower end of IPCC table, between 130 to 140 Tg, to match with the station data across the globe. It negates any possibility to increase wetland methane emission to produce a better model methane variability.

Apart from long term CH₄ changes, the model is able to represent inter annual variability rather well. For example, the model is able to produce the rising trend in methane mixing ratio between 1998 and 2001 which is visible in the observational trend (see Figure 5.1). This model methane rise is attributed to increase in both wetland and biomass burning methane tracers. As it has been discussed earlier that the 1998 El Nino year increased methane emission from biomass burning, our wetland emission also shows a steep increase during this period (see Figure 5.3) similar to by Fiore et al. (2006), although the later estimated a larger increase. The 1997-98 rise in wetland emission can be associated with globally high temperature trend and high precipitation at southern tropics and north of 30°N (Dlugokencky et al., 2001, Fletcher et al., 2004). Our model wetlands also show a decreasing trend in methane emission (see again Figure 5.3) after 2000 as suggested by Bousquet et al., (2006)

who concluded a concomitant increase in methane from oil and gas extraction which possibly cause in the overall stabilization of global methane level. Overall, it can be concluded that changes in certain emissions, particularly the oil and gas extraction as reported to EDGAR inventory may be wrong and results in the model bias between 1991 and 1997.

5.2.1 Simulations with different model set ups

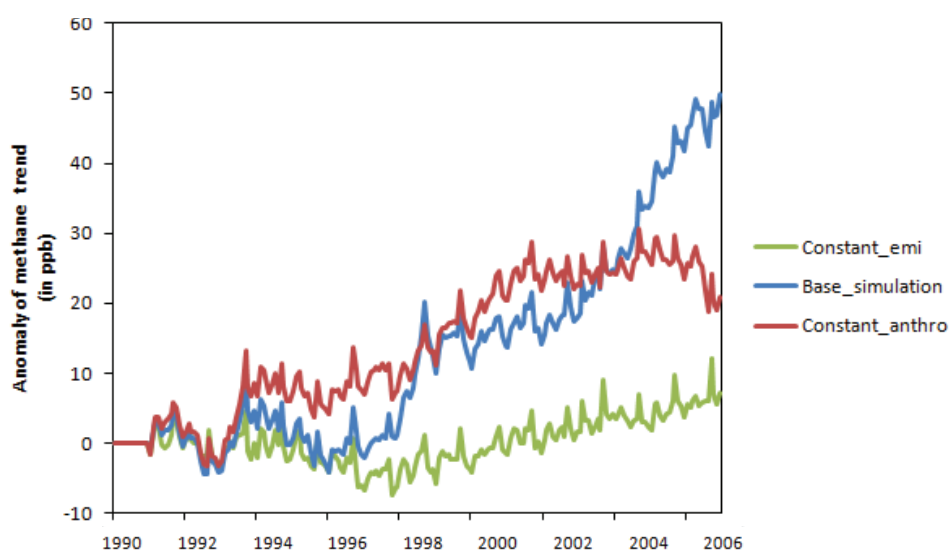


Figure 5.6: The figure represents the anomaly of methane trend for different model simulations with respect to model methane mixing ratio of 1990. The blue line shows the methane variability for BASE simulation with changing emissions. The red (Constant_anthro) and green line (Constant_emi) shows the methane variability for model simulation keeping anthropogenic emission and total emissions at their 1990 values respectively

The Constant_anthro and Constant_emi model simulations helps to isolate the impact of varying wetland emission and meteorology on the overall model methane trend. It can be derived from Figure 5.6 that with constant anthropogenic emission, the mean methane level in the atmosphere would have been 30 ppb less than the scenario of BASE simulation. In general, the Constant_anthro shows a higher than BASE methane variability between 1990 and 2002 in the range of 5 to 10 ppb. However with the BASE methane concentration showing a continuous rise since 1999, it crosses the Constant_anthro methane and extends the difference up to 30 ppb. The Constant_anthro methane remains in the equilibrium state between 2000 and 2006. If we compare the long term variability of Constant_anthro methane with the observed methane from Figure 5.1, we found some close similarity between their features. Both of them shows a steady increase between 1990 and 1997 with a diminishing

growth rate which is suddenly raised between the year of 1997 and 2000 (see Figure 5.4). Even between 2000 and 2006 both these trends are similar when methane concentration reaches to stabilization. It proves that the model simulation only with wetland methane variability does produce the key features of observational trend which is missing from the results with a varying anthropogenic methane emission prescribed in the model. Between the year 1990 and 1997, the increasing methane trend as shown in Constant_anthro due to wetland emission gets reduced by the depleting anthropogenic trend in the BASE simulation. If we look at the methane variability due to meteorology in the Constant_emi plot, we could see its close similarity with BASE simulation between 1990 and 1997. Constant_emi methane however shows a negative anomaly between 1997 and 2000 which goes down as much as -8 ppb in 1998. The anomaly shows a positive trend after 2000 and reaches 10 ppb in the year 2006. Over all the changing meteorology in the model due to sea surface temperature and sea ice concentration seems to have a negligible impact on overall methane trend.

5.3 Conclusion

Our model simulation reproduces the average surface methane mole fraction between 1990 and 2006 reasonably well with some differences between 1990 and 1998 in the magnitude of 20 to 40 ppb. This difference could be associated with changes in certain emissions, particularly the oil and gas extraction as reported to EDGAR inventory which may be underestimated and results in the negative model bias in this period. The role of oil and gas emission is emphasized mainly because implausibility of changes in natural emissions, particularly the wetlands. Moreover, the recent findings by Pétron et al., (2012) which indicates underestimation of gas extracted methane from fracking technique by a factor of 2 at Boulder, USA. The history of gas extraction from hydraulic fracking dates back to early 1990s at USA along with several European countries. This would also put focus on the uncertainty in the budget of oil and gas extracted methane, which would have a substantial role to explain the apparent model observation difference. However the practice of shale gas extraction grew only after mid 2000 at USA. It should be noted that the model simulation is also able to produce short term inter annual methane variability rather well particularly between 1997 and 98 and in early 2000s. The wetland methane tracer shows the expected variability over the simulated years, which proves the success of wetland methane parameterization using CARAIB vegetation model for transient simulations.

It is to be mentioned that, in this study, we used a constant OH concentration throughout the simulation in contrary to previous modeling studies, based on recent findings of Montzka et al., (2011) who found that that OH variability is significantly less than the established figures. This is a more realistic approximation which deviates from earlier methane model assumptions on OH variability. Our assumption rules out role of sink in our simulation to explain model methane variability which is presumed to be entirely source driven. However,

according to Montzka et al., (2011), the maximum range of OH variability could be 3.8%, which if applied in our simulation could actually impose some additional variability over the simulated results. Adapting some probabilistic distribution of the OH variability within the maximum range in future simulations would be further development on this work and along with sources could explain the recent methane trend better.

6. Methane at past climate: LGM, Pre-industrial

Atmospheric methane underwent significant transition from past to present climate. These changes in methane concentration are recorded in isotopes trapped in ice cores. Due to prevailing uncertainties in methane source and sink estimation, it is difficult to reproduce the ice core methane data using models. In this chapter, we address the range of this uncertainty over two key past climatic periods, the Last Glacial Maximum (LGM) and pre-industrial (PI) time and attempt to produce methane concentration using ECHAM MOZ chemistry climate model simulation. We chose Last Glacial Maximum (LGM) and pre-industrial (PI) for the model study mainly because these two periods mark important phases in climate change and precede drastic increase in global methane level. The other motivation to carry out past climatic methane study is to evaluate the wetland methane parameterization which is developed keeping in mind the paleo climatic conditions. Since wetlands were the main methane source in past, the success of methane simulation will largely depend on the performance of the wetland methane parameterization.

6.1 Methane budget during LGM: Role of sources and sinks

The Last Glacial Maximum (LGM) is an interesting time period for biogeochemical studies as there are major changes of vegetation patterns, ice cover and sea level during the episode about 19,000-20,000 years ago. During this time, vast ice sheets covered much of North America, northern Europe and Asia which had a profound impact on Earth's climate.

The atmospheric composition was also very different from present day or pre-industrial (PI) time. Atmospheric methane concentrations were very low compared to present day. According to the ice core records (Chappellaz et al., 1990, Stauffer et al., 1988), the LGM methane concentration was as low as 350 ppb half of pre-industrial level.

Several hypotheses have been proposed by various studies in order to explain such a low concentration of atmospheric methane over LGM and its subsequent rise. The most prominent ones are the wetland hypothesis (Chappellaz et al., 1993), the clathrate gun hypothesis (Kenett et al., 2003) and a combination of these two (Maslin and Thomas 2003). Inverse modeling studies constrained by observations from ice cores (Crutzen et al., 1993, Martinerie 1995, Chapellaz 1997, Brook et al., 2000, Dällenbach et al., 2000) tend to support the wetland hypothesis and suggest that the low LGM atmospheric CH₄ can be explained solely by decline in tropical and high latitude wetland sources of methane during the glaciation. Wetlands, the largest natural source for atmospheric methane are highly climate sensitive and were likely to undergo drastic reduction during LGM, at a scale of 70 to 94% reduction (Chappellaz et al. 1997, Cao et al., 1995) with a low surface temperature and a completely different vegetation

regime dominated by tundra, semi desert type temperate grasslands. However this theory encounters major challenges from process based ecosystem simulations which indicate that the sensitivity of wetland CH₄ emissions at LGM has been over estimated by top-down modeling and other factors must be responsible for the low LGM methane levels (Adams et al., 2001, Kaplan 2002, Valdes et al., 2005). However one of the modeling studies (Kaplan 2002) found an insignificant change in LGM wetland extent over this period and emphasizes on the low emission rate due to a colder temperature. Some of the studies (Charman 2002, Kenett et al., 2003) suggest that wetland expansion is a slow process and cannot explain the rapid post glacial climatic warming. According to them, the wetland temperature sensitivity should be capable of producing a fast response to rapid climatic warming post LGM, without the wetland expansion to increase methane fluxes. There is no doubt that the LGM climate and low CO₂ curtailed the primary production of vegetation and which according to Valdes et al. (2005) lowers wetland methane emissions by 27% relative to pre industrial value, in agreement to other work (Kaplan 2002). The post LGM increase of NPP and soil temperature raises the methane emissivity which would contribute to high methane flux.

It is also certain that cooler and drier LGM climate decreased the global wetlands extent compared to present, mainly over high northern latitude due to physical presence of ice sheets. However, the exposure of coastal shelves due to ocean retreat could produce additional wetlands both over tropics and boreal uplands, which may offset the assumption of wetland loss across northern latitudes.

On the other hand the clathrate gun hypothesis which implicates post LGM methane release from ocean bottom due to decomposition of clathrates accounts for a small fraction of the abrupt post glacial increase and could not be hold majorly responsible for this transition of methane budget (Kennet et al., 2003). The drier LGM climate also reduces the frequency of biomass burning and hence CH₄ emissions from this source, whilst cooler sea surface temperature would have lowered ocean emission

Some studies (Valdes et al., 2005, Kaplan et al., 2006) also consider sink processes of methane to explain the low LGM ice core records. Valdes et al., (2005) suggest that the probable cause is a strong reduction of biogenic volatile organic compound (BVOC) emissions during LGM which has a major impact on OH, the main sink of methane in the atmosphere. BVOCs which include isoprene, terpenes, acetone, methanol as well as other short lived compounds are produced from various types of vegetation and react with OH to get oxidized. Low BVOC implicates rise in OH concentration in the atmosphere which is concomitant to methane drop. During LGM, due to large ice covers in high northern latitudes and absence of vegetation, BVOC emissions are low which increases only after deglaciation with the establishment of temperate and boreal vegetation and subsequent development of cold-need leaved forests. The enhancement of tropical sources stimulated by increased humidity and CO₂ fertilization are also responsible for post glacial BVOC rise (Kaplan et al., 2006). Valdes et al., (2005) simulate a 25% increase in OH during LGM compared to pre-

industrial while Kaplan et al. (2006) find a 22% rise. Thus, the modeling studies (Adams et al., 2001, Valdes et al., 2005 and Kaplan et al., 2006) are able to explain the glacial ice core methane records with the weakened methane source combined with the enhanced sink, responsible for a reduced methane lifetime.

6.1.1 Modeling of LGM wetlands

Methodology

The wetland and methane emission parameterisation described in Chapter 3 was adapted to LGM conditions as follows. First, except for the sea level retreat and the resulting exposed shelf areas there is no change on the terrain pattern during LGM which could influence wetland formation. We use soil temperature and territorial elevation as control parameters to consider the influence of ice sheets and coastal shelves in our parameterisation.

CARAIB simulated normalised soil water content for LGM is used in the parameterisation as the key input. The threshold values for soil water are applied as .3 for northern latitudes and 1.1 as tropics for wetland formation similar to present day. We also consider the present day value of surface slope for LGM surface in the parameterisation. However, it is not possible to implement the parameterisation at the coastal land mass due to unavailability of surface slope values. In general, the coastal shelves should have a low elevation and thus contain a low surface slope value. So at those places the surface slope should not pose any condition to wetland formation and therefore can be ignored. We only put the soil wetness condition on the coastal shelves to estimate the potential wetlands. Then we add it to the continental wetlands to come up with the total wetland extent during LGM.

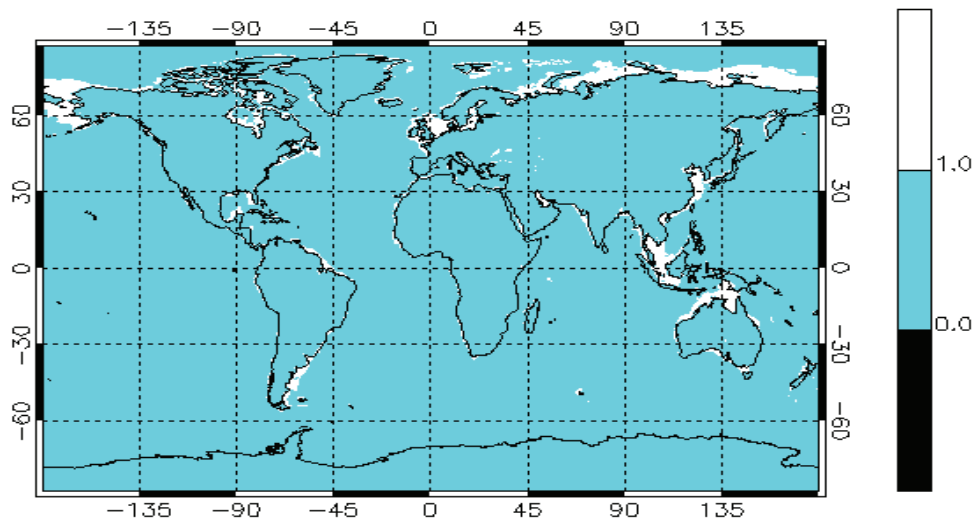


Figure 6.1: The exposed continental shelves during LGM with a value of 1

It is found that even if the exposed coastal shelves (Figure 6.1) are estimated to be as large as 22 million km² of area during LGM, a mere 10% of it actually contributes to wetland formation on a global scale (see Figure 6.2). Among it around 1.3 mill km² of wetlands occur in the tropical regions where 1.1 mill km² at the boreal regions. The presence of ice sheets inhibits wetland formation at the northern continental boundary whereas dry soil across South American continental shelves is unlikely to favour wetland formation. However, pacific coastal land mass at the East Asia and Atlantic land mass of East American continent are found to be suitable for wetland formation.

It is to be noted that CARAIB provides monthly values for LGM soil water content a seasonal LGM wetland map is produced from the parameterisation. However, since there is no available knowledge about LGM wetland seasonality, we consider all the inundated areas as wetlands.

Results

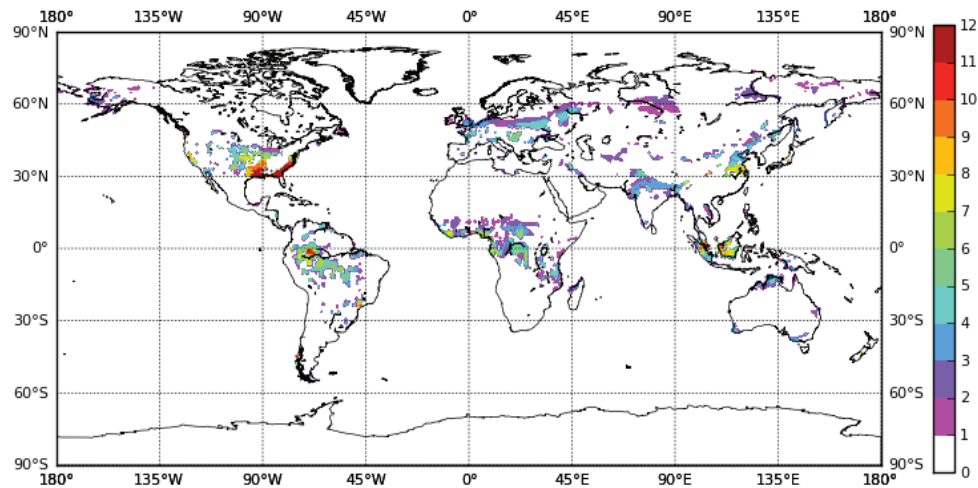


Figure 6.2: *Distribution of potential LGM wetlands with the colour bar indicating monthly frequency of inundation over a climatological year*

The annual mean of wetland area at LGM is estimated to be 7.75 million km² which is significantly lower than at present. It is found that northern latitudes (30-90°N) contribute only 3.4 million km² of wetland areas compared to 4.36 million km² from tropics (30°N-30°S). It is quite opposite to the present day wetland distribution, where north latitudinal wetlands dominate over the tropical wetlands. Compared to present day, northern latitudes show significant decrease in wetland formation during LGM, with a reduction of more than 50%. On the other hand, the tropical wetlands show an increase of almost 15% than present day. This increase of tropical wetland area is attributed to the eastern coastal shelves.

Compared to Figure 3.8 in Chapter 3, it is evident that wetlands are missing from large part of northern latitudes, particularly northern America, Scandinavia, and Siberia. The main reason for it is the presence of large ice sheets over these regions which largely limit the wetland formation. However, the parameterisation suggests additional wetlands at coastal shelves at the continental boundary of western Alaska. These are ephemeral with inundation occurring only during one month. The same is true for areas at the central Siberia and regions across eastern Asia. However there are some regions close to the 30°N, where permanent wetlands are found particularly at the east coast of North America. Coastal shelves in eastern China are also mapped as permanent wetlands.

On the other hand, the LGM tropical wetlands are similar to the present day distribution, particularly in the South American floodplain and central African basin. A significant additional contribution comes from the exposed shelf close to the Gulf of Thailand and Malaysia known as Sunda shelves, which contribute significantly to the global estimate. However, it could not compensate for the missing wetlands at the boreal uplands and the total LGM wetland extent is reduced by 28% compared to present day.

As described above, other studies (Kaplan et al., 2006, Weber et al., 2010, Valdes et al., 2005), also show a reduction of LGM wetland areas within a range of 10-25% compared to pre-industrial or present day. Our model result shows a 25% reduced LGM wetlands than present day, which lies in the higher range as compared to the previous studies. However Kaplan (2002), simulated LGM wetland extent to be larger than Pre-industrial area up to 13% and found the LGM wetland area to be within the uncertainty of the present day estimate. It is unacceptable in view of the huge loss of boreal wetlands.

Table 6.1: *Comparison between LGM wetland areas derived from different model studies*

Wetland model studies	Estimated area (x 10⁶ km²)
Kaplan et al., 2006	6.8
Valdes et al., 2005	6
Webber et al., 2010	7.6
Present study	7.75

It shows that, although the trend of wetland evolution since LGM differs between the models studies, in terms of total LGM wetland area estimation, these models are not very different. However, it is highly possible that the regional distribution of wetlands do not match between these studies. In view of that, to check how far our model is able to capture the regional wetlands compared to others, we carry out a comparison of our wetland spatial distribution with that of Kaplan 2002 (see figure 6.3).

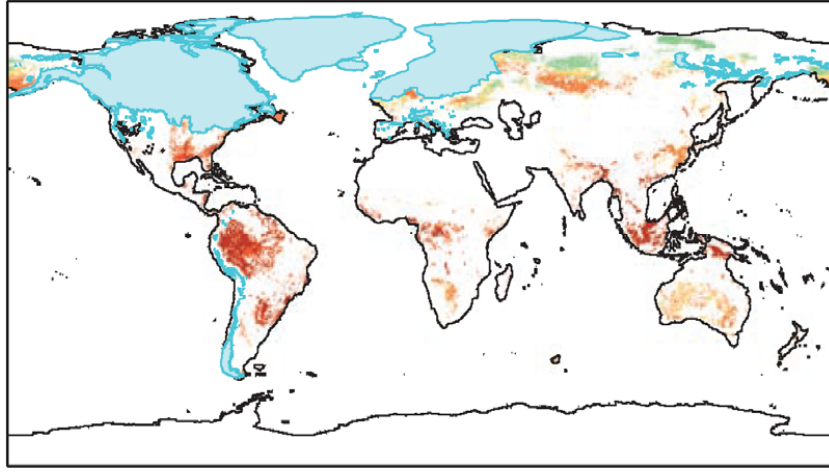


Figure 6.3: *LGM wetland distribution is shown in grey colours on the global map, based on Kaplan, (2002)*

Although Kaplan (2002) LGM wetland map estimates wetland area more than the acceptable range, we chose it for model evaluation since it is the only LGM wetland map available in the literature that provides some idea on spatial distribution of LGM wetlands. From the comparison, it can be found that our model is able to produce major wetlands on the continents as well as on the shelves compared to Kaplan (2002). On the continents, our model could produce wetlands over South American river plain, central African basin as well as Eastern America and Central Asia. Among the coastal wetlands, it could produce major wetlands over Sunda and New Guinea shelves, East Asian and Atlantic coast of South America. Our model overestimates some temporary wetland areas over Western European continents and adjacent Atlantic coast. Kaplan (2002) mapped large wetland area over Australia which is missing in our map.

6.1.2 Modeling methane emissions from LGM wetlands

In order to parameterize the methane emission from LGM wetlands, we used the same approach as described in Chapter 3, section 3.4.2. In fact we retained the same value of KCH_4 and Q_{10} as used in present day modeling described in section 3.4.3., mainly because of lack of evidence in literature regarding rescaling these parameters for LGM. In fact, Weber et al., (2010) in their LGM wetland methane modeling used the Q_{10} value based on present day reference temperature of 273K following Gedney et al., (2004). They also tuned the LGM KCH_4 value based on present day wetland methane budget of 150 Tg, similar to our assumption.

Results

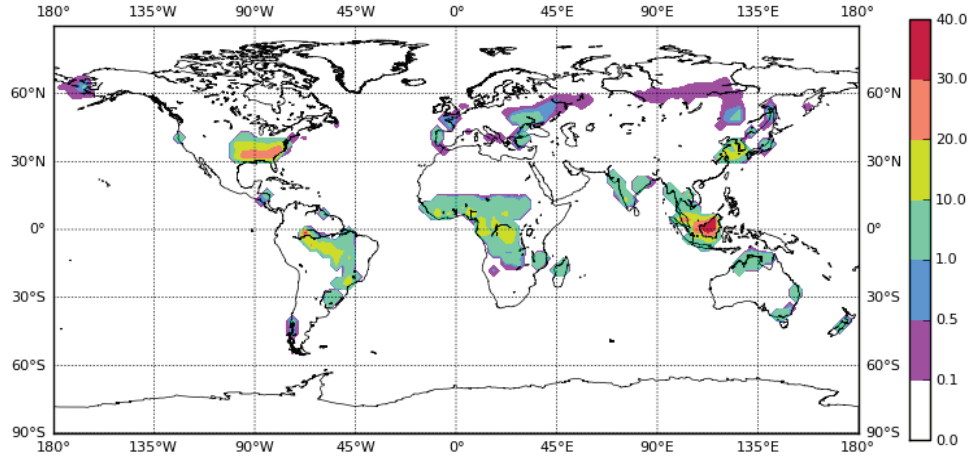


Figure 6.4: The average methane emission rate ($\text{mg}/\text{m}^2/\text{day}$) from LGM potential wetlands

The annual methane emissions from LGM wetlands are estimated to be 72 Tg and therefore about 50% of the present day value (see Chapter 3). It can be derived from Figure 6.4 that the methane emission strength ranges between .05 and $35 \text{ mg}/\text{m}^2$ per day. The boreal wetlands, north of 40°N , are found to emit less than 1 mg m^{-2} methane per day due to the persisting low soil temperature. This is significantly low compared to present day boreal emission (see Figure 3.14). On the other hand wetlands in the tropics and extra tropics show stronger emissions. Over few hotspots located at the Sunda shelves, close to the equator, the emission rate reaches as high as to the present day maximum. Other hotspots are located at eastern American coast, South American floodplain and African plain land. On an average, the daily tropical wetland methane emissivity at LGM lies in the range of 5 to 15 mg m^{-2} , whereas the same at present day lies between 10 to 25 mg m^{-2} . If we look at the regional contribution of LGM wetlands to the annual methane budget, the wetlands at high northern latitude contribute only 24%. The rest is coming from the tropical wetlands which figures around 55 Tg per year. In comparison to present day, the LGM wetland methane emission scenario was quite different. During LGM, the boreal wetland methane budget is significantly low, only one fourth of its present day value. Tropical wetland contribution, on the other hand was not that low, still 25% less than present. If the annual LGM wetland methane budget between this study and the other modeling studies are compared, we would find that our parameterization is prone to underestimation compared to others even though wetlands cover larger area (Table 6.2).

Table 6.2: Annual wetland methane emission (in Tg/year) during LGM and PI from various studies. The numbers in parentheses gives the ratio of PI to LGM wetland methane emission

Model studies	LGM wetland emission	PI wetland emission
Valdes et al., 2005	108	148 (1.3)
Kaplan et al., 2006	150	180 (1.2)
Webber et al., 2010	89	105-128 (1.2-1.4)
Present study	72	115 (1.5)

It is evident from Table 6.2 that the LGM wetland methane emission varies between 89 and 150 Tg over different modeling studies. Compared to those, our LGM wetland methane budget is significantly low. However in our model study, we found a ratio of Pre industrial to LGM wetland methane budget to be 1.5 which is pretty close to the other studies. It shows that with consistent methodology, our wetland methane parameterization is able to produce a realistic PI to LGM ratio which is comparable to others.

It should be noted here that Valdes et al., (2005) who used Sheffield dynamic vegetation model (SDGVM) to simulate LGM tracer emissions, estimated the wetland methane emission to be 108 Tg per year in which tropics (30°N-30°S) contributes 98 Tg and Northern Hemisphere (90° N-30°N) a mere 10 Tg. The difference of methane flux between Valdes et al., (2005) and our study arises due to disparity in ratio of tropical to SH wetlands emission. Our study lowers the tropical wetland methane flux of Valdes et al., up to 50%. However, the wetland emission from northern latitudes does not differ much between the studies.

6.1.3 Methane sources for LGM

There has been some discussion in the literature concerning the potential role of other natural sources during the LGM. For example, Valdes et al., (2005) quantify the strength of these sources such as biomass burning, ocean and termites which are shown in Table 6.3.

Table 6.3: Strength of LGM methane sources (in Tg per year) according to Valdes et al., (2005)

Source sectors	Emission strength (Tg/year)
Wetland	72 Tg
Biomass burning	7 Tg
Ocean	10 Tg
Termites	27 Tg

The estimation of methane surface flux from biomass burning is estimated from a fire module included in the University of Sheffield Dynamic vegetation model (SDGVM) by Valdes et al. (2005). The fire module is based on soil dryness and assumes 80% of the above-ground carbon and nitrogen are lost by fire which is triggered when the litter content reaches a critical

dryness (Beerling and Woodward 2001). The drier and cooler climate during LGM had less litter amount in the soil which would probably decrease the burning of biomass and thus had a reduced methane emission compared to present day. The colder sea surface temperature (SST) in LGM could also reduce the oceanic methane since its emission rate depends upon the SST pattern. For termites, at the absence of reliable evidences, present day emission field have been used. Here we adopt the estimates from Valdes et al., (2005) in the model simulation. Hence, together with the wetland source described above, the global annual LGM methane emission flux is 116 Tg/yr. This value is lower than Valdes et al., (2005) and Kaplan et al., (2006).

6.1.4 Methane sinks for LGM

As discussed earlier, the major sink of atmospheric methane, the hydroxyl radical (OH) was high during LGM and acts as a major factor behind the lower methane concentration (Adams et al., 2001). Reductions in global forest cover and cooler climate during LGM resulted in low BVOC emissions which are presumed to cause a rise in atmospheric OH. However, a number of recent studies (Hofzumahaus et al., 2009, Taraborelli et al., 2012) found a much lesser influence of BVOCs on OH than previously assumed. They found a high OH concentration in field campaigns where BVOC emissions are also quite high. These studies conclude that there might be some unknown pathway of OH recycling from peroxides even in the presence of BVOCs. These findings eventually suggest that low BVOCs must not always lead to a high OH as expected in the LGM chemistry modeling studies.

However, reduction of biogenic emissions is not the only factor behind the perturbation of oxidizing capacity in the LGM climate. In fact, changes in albedo at the presence of sea ice and land ice covers, reduced water vapour, lightning and soil sourced NO_x emissions as well as dust effect on photolysis had their individual impacts on the OH concentration and are often ignored while modeling OH concentration.

Changes in Earth's albedo from presence of sea ice and ice sheets have an effect on the global radiation budget. Ultraviolet (UV) radiation flux in the 290-310 nm range controls tropospheric ozone photolysis and therefore has a strong influence on OH abundance. However, tropospheric ozone is not believed to change much (less than 2%) between LGM and pre-industrial (Pinto and Khalil 1991, Martinerie et al., 1995) which indicates that perhaps the impact of changing albedo on OH level is not significant.

Water vapour in the LGM atmosphere was lower than the present day level. Martinerie et al., (1995) suggested that lower water vapour would decrease OH concentration by 7%, resulting in a 6% increase of CH₄ life time. This would result larger CH₄ concentration. Another uncertainty which is also not addressed in most of the model studies are changes of NO_x production due to lightning. Kaplan et al., (2006) could not find any changes in the convective

precipitation rate and inferred that changes in lightning produced NO_x were very small. The soil NO_x production is not estimated in those studies either.

However a study on LGM atmospheric chemistry using the MOZART chemistry transport model by Thomas Laepple (Unpublished results, pers. comm. 2009) shows that the effect of these individual factors, which are often ignored, does not alter the LGM oxidation capacity much. In the following figure (Figure 6.5), briefing of these factors and their apparent effect on OH concentration are given.

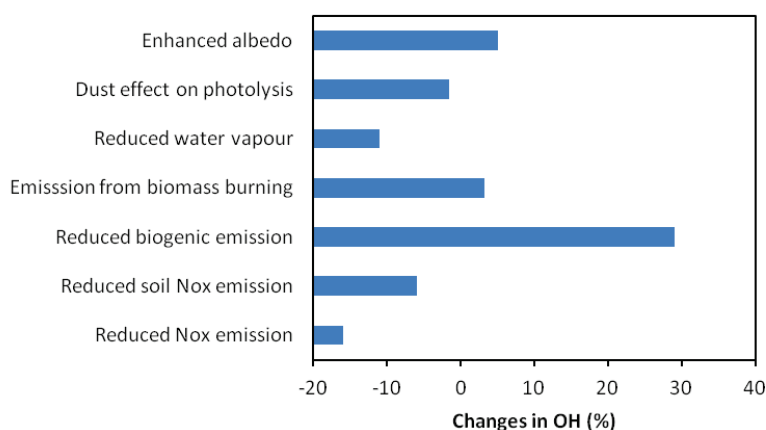


Figure 6.5: *The potential changes in OH concentration due to changes of various factors in LGM*

Overall, Laepple found that the net increase in annual mean concentration of LGM OH is 26% compared to present day. This agrees well with other modeling studies on chemistry climate interaction, (Martinerie et al., 1995, Valdes et al., 2005, Kaplan et al., 2006, Adams et al., 2010). The tropospheric mean value was between 10 and 13×10^5 molecules/cm³. In our LGM methane simulation with ECHAM5, in the absence of interactive OH chemistry, we have used a tropospheric mean OH concentration of 12.3×10^5 molecules/cm³, derived by scaling the present day distribution with a factor of 1.25.

6.1.5 Model Simulation for LGM methane

The boundary conditions for climate model simulation between LGM and present day are very different and could have serious impact on model simulation. The present simulation had to be done with input from different sources which are described in the following sub-section.

Boundary conditions for ECHAM5 simulation

In our model simulation the land sea mask, glacial mask and topography are derived from Paleoclimate Modelling Intercomparison Project 3 (PMIP3). The sea surface temperature are obtained from GLAMAP (Sarnthein et al., 2003) whereas the sea ice concentration is given by Uwe Mikolajewicz (Pers. Comm. 2011). The rest of the data containing surface variables (surface geopotential, snow depth, surface roughness, orography) are sourced from Community Earth System model (COSMOS) output, from Xu Zhang (Pers. Comm.2010). The meteorological prognostic variables (temperature, divergence, specific humidity and vorticity) are provided from COSMOS output and used as initial condition to the ECHAM5 model simulation.

Orbital forcing and tracer gas concentrations are prescribed from Coupled Model Inter-comparison Project (CMIP5) simulations for LGM. Obliquity, eccentricity and perihelion are set at values of 22.95° , 0.018994 and 294.42° respectively. LGM CO_2 concentration is fixed at 185 ppm in accordance to CMIP5.

Results from LGM ECHAM simulation

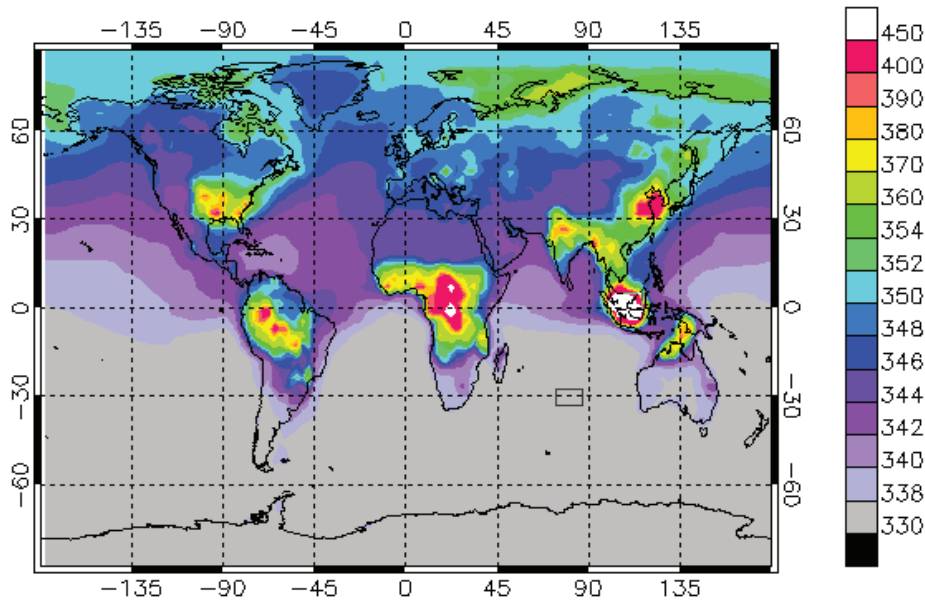


Figure 6.6: *The spatial distribution of the annual mean surface methane mixing ratio (in ppb) for LGM from ECHAM5 simulation*

The global mean for LGM methane is found at 345 ppb from the model simulation which is in close agreement with ice core records (Dällenbach et al., 2000), who find 350ppb. The tropical mean methane level is always high compared to rest of the globe (Figure 6.6). The

Northern Hemisphere exhibits part holds a higher mean methane value of 20 ppb than its southern counterpart. The hotspots of methane are found over South American, African and East Asian continents with average values lying between 370-430 ppb. The Sunda shelf region near present Malaysia shows a methane level more than 450 ppb which is influenced by the local wetland source. Generally, the exposed shelf areas with additional wetland sources during the LGM (see section 6.1.2) appear to exert a strong influence on the atmospheric CH₄ concentration. This suggests that the spatial pattern of LGM surface methane distribution was more influenced by local wetland emission than any other factor.

The inter-hemispheric difference of methane is a good indicator of its source distribution, transport and mixing between the hemispheres. In this study, the inter polar gradient is estimated by calculating the difference of mean methane mixing ratio of latitudinal bands surrounding Greenland and Antarctica. From our model simulation, we get an average methane mixing ratio of 352 ppb in the zone of Greenland and 338 ppb in Antarctica which indicates to a polar gradient of 16 ppb strength. In the “Greenland Ice-core Project (GRIP)” (Dällenbach et al., 2000), where CH₄ records measured from the ice cores drilled in Central Greenland (72°34'N, 37°37'W), Byrd station, West Antarctica (79°59'S, 120°01'W) and in Vostok, East Antarctica (78°28'S, 106°48'E), the inter polar difference is found to be 14 ± 4 ppb during the cold phase of Last Glacial period. This matches pretty well with our model results. Compared to the present day and the Pre-industrial time which is discussed in section 6.2.5., the LGM Inter polar gradient was only between 10% and 30% of their respective values. In LGM, the tropics (10°S to 30°N) are the main source from where methane gets transported to both Greenland and Antarctica. The boreal methane sources are either absent or much smaller compared to present day. As a result, the inter hemispheric gradient was much smaller during LGM.

6.2 Methane budget during pre-industrial (PI) era

6.2.1 Transition of methane from LGM to PI

From ice core records, it has been found that the average methane level during pre-industrial (PI) Holocene (200 years before present) was around 700 ppb (Loulergue et al., 2008). The post glacial methane rise is often perceived either to be an effect of changing sources, sinks or combination of both. Most of the bottom-up studies suggest that the increase must have resulted from a change in methane sources (Valdes et al., 2005, Kaplan et al., 2006, Weber et al., 2010.), such as wetlands, the largest natural source of methane. Chappelaz et al., 1993b estimated that wetlands emissions increased by 80% between the LGM and PI which explains half of the 94% increase in methane concentration. Valdes et al., (2005) found a much smaller increase in wetland emissions, only 36%. There are also studies by Kaplan et al., (2002),

which estimates increase in wetlands since the last glacial period. Recent estimation by Weber et al., (2010) from the second phase of Paleo climatic modeling inter comparison project (PMIP2) suggests an increase of wetland emission between 54 and 72%. They discuss the large uncertainty involved in source driven hypothesis of LGM-PI methane change. Apart from wetlands, there are indications of anthropogenic methane sources during pre-industrial Holocene, particularly from agricultural activities, biomass burning and enteric fermentation, which could also contribute to the methane rise (Ruddiman et al., 2001). A high resolution Holocene record of methane changes from Greenland ice (Blunier et al., 1995) shows around 100 ppb rise in methane values that occurred between 5000 years ago and 17000 A.D. Ruddiman et al., (2001) estimated an additional methane source of 32 Tg per year to support this observed rise which they claimed to come from anthropogenic activities. In their study the wetland expansion hypothesis are largely rejected.

However, there could be a potential role of OH as well to explain the increase in methane level. The boreal vegetation changed drastically since the termination of glacial period with establishment of temperate and boreal vegetation and development of cold-need leaved forests. The increase of Non methyl volatile organic compounds (NMVOCs) emission from these plants has the potential to reduce the OH concentration (Adams et al., 2001) which causes the rise in methane lifetime. It is obvious that, in the absence of large spread vegetation, the LGM OH concentration would have been significantly high than the post glacial period. NMVOC emission is also likely to increase due to rise in mean tropical temperature (5-6°C). The size of the post LGM NMVOCs increase however remains uncertain.

Changes in the amount of Nitrogen Oxides (NO_x) emitted from climate sensitive source such as soils, lightning and biomass burning could also affect the OH level in the atmosphere since it is closely involved in the NO_x-O₃-CH₄ cycle. All these sources of NO_x are also climate sensitive and likely to undergo changes during the glacial transition. The estimates of lightning and soil strengths are subject to large uncertainties as well and so the NO_x budget.

6.2.2 Atmospheric methane in PI: In perspective to present day

From the ice core measurements, it can be inferred that anthropogenically induced upward trend of methane started about 1800 A.D and ended up at the present value of 1780 ppb. In perspective of present day, the low methane level before the 1850s is attributed to the absence of the human influenced emissions which accounts for almost 330 Tg per year, approximately 70% of the annual methane budget. Although, there are indications that some of the anthropogenic sources were contributing to PI methane budget, namely rice emission, biomass burning and ruminants (Ruddiman et al., 2001), their individual strengths suffer from

large uncertainty. They are believed to have contributed not more than 15% of the PI methane budget.

There are speculations about the changes in OH level as well post 1800s due to the onset of industrialization. The estimates from different model studies vary between 20% decrease to 5% increase of PI OH to reach the present value. Most of the studies point to a reduction of OH post 1800s due to industrialization, related to relatively strong increase in CH₄ and CO. This is somewhere compensated to some extent by increased NO_x emissions and depletion of stratospheric ozone which have resulted in the stabilization of OH in the last two decades (Prinn et al., 1995, Krol et al., 1998, Montzka et al., 2011). However there are also some studies which suggest that OH does not change between PI and present and the sharp methane rise is entirely source driven.

There are evidences of other factors which could also play a potential role in the methane rise. One of such factors came into light in a study by Singarayer et al., (2011), where they have found the role of earths orbital configuration change in the anomalous increase of atmospheric methane since the mid Holocene period, 5000 years ago before present.

6.2.3 Methane sources in pre-industrial epoch

It has been discussed in section 6.2.1 that there remains considerable uncertainty in the quantification of individual PI methane sources as well as the global budget. The source strengths of termites, ocean and biomass burning in this study were adopted from Valdes et al., 2005 (see Table 6.4). Valdes et al., (2005) estimated methane flux from biomass burning to be 10 Tg per year which lies in the range of previous estimates (Kammen et al., 1993). There are estimates as large as 30 Tg by Subak et al., (1994) which can be ruled out by the carbon isotope evidence of Quay et al., (1988). Quay et al. found a $\delta^{13}\text{C}$ value of -60‰ which would have not been possible with such a huge biomass burning source. The ocean emission was parameterized from Sea surface temperature (SST) by Valdes et al., (2005). In the absence of other evidence, termite methane emission is retained at its present day value. According to Harder et al., (2007), the wetland source may have been 10% larger than present owing to drainage and cultivation of wetland area since 1800 A.D. In the present study, we considered two scenarios, one with the present day wetland methane budget and the other with a higher emission of 10% (accounts for 12-15 Tg). However one of the major limitations of Valdes et al., (2005) is that they did not include any of the anthropogenic methane sources such as rice emission or ruminants in the pre-industrial methane budget which is likely contributed during 18th century. In another modeling study by Houweling et al., (2000) on constraining PI wetland budget, methane emission from rice agriculture, domestic ruminants and even waste treatment are considered. Houweling et al., (2000) also considered emission from additional natural sources such as wild fires, volcanoes and wild animals. Although

these emissions are based on crude assumptions and suffer from huge uncertainties, their existence during Pre Industrial period cannot be completely ruled out.

In the present simulation we included the rice emissions and emissions from livestock and animal waste from Ruddiman et al., (2001). They linearly scaled the anthropogenic methane emission based on population and estimated methane emission from rice farming to be 25% of present day. They also estimated around 11 Tg per year methane emission from live stock and animal waste which together constitutes 10% of the present day budget. For wild animals, as described in Houweling et al., (2000), a global strength of 15 Tg has been derived by Chappellaz et al., (1993) based on estimated number of bisons and buffaloes which is supported by Subak (1994). In the PI simulation, along with wild animal, wild fires emission has also been considered following Chappellaz et al., (1997) and Kammen et al., (1993).

The PI methane source strengths are shown in Table 6.4.

6.2.4 Methane sinks

A number of studies in the literature have attempted to assess changes in the global tropospheric OH distribution from the pre-industrial to present. These studies include the one by Kieslev et al., (2000) on northern hemispheric OH trend post 1850 to 1995, which shows that the lower tropospheric OH photochemical production was enhanced more rapidly than its sink mainly due to increase in NO_x surface emission. However, in the higher troposphere, increasing CO causes photochemical destruction of OH. It has found that even if there is an increase of OH concentration in the lower troposphere from PI to present day both at tropics and southern hemisphere, it gets balanced with the reduced OH in the high northern latitude and the net change is insignificant.

Law et al. (1990) found small changes in OH due to the conflict between NO_x and the CH₄ – CO-Non methyl Hydrocarbon (NMHC) cycle. According to them, the oxidation of CH₄, CO and NMHCs by OH leads to an increase in OH as these source gases are reduced. It competes with the effect from reduced NO_x which will lead to less OH production.

The lack of correct NO_x pre-industrial source estimations proves to be a substantial flaw in determining OH level since NO_x together with CO, CH₄ and O₃ is responsible for tropospheric OH chemistry. According to Lelieveld et al. (1998), if the NO_x level is relatively high, CH₄ and CO oxidation in the atmosphere provides for a net source of O₃ and OH radicals, whereas net destruction of O₃ and OH prevails in the NO_x poor troposphere. As evident from modeling studies of Kieslev et al., (2000) and Lelieveld et al., (1998), different assumptions for post industrial NO_x increase results in completely opposite OH trend. Therefore, the OH behaviour in the troposphere depends critically between its sink and source intensity changes, i.e., CO, CH₄ and NO_x emission rates.

Houweling et al., (2000) and Wang et al., (1998) suggest 7 to 9% higher PI OH level compared to present day. In their study, Houweling et al., (2000) rescaled the global OH concentration to match the observed trend of methyl chloroform (CH_3CCl_3), during 1980-1992. The simulation for 1860 indicates a 7.5% higher average OH level, as compared to the other simulation for present day. Wang et al., (1998) found similar result, a 9% higher global mean OH than present day using the same approach.

In the present study, we have considered four different scenarios of PI OH level for the simulation (present day OH, 8% higher OH, 20% higher OH, 5% less OH) and tried to balance the emissions within the uncertainty of all the sectors except termites and ocean which remain the same over all runs.

Table 6.4: *Strength of PI sources and sink of methane for ECHAM5 simulation*

PI sources and sinks	Sources and sinks strength
Mean OH concentration	$10.9 \times 10^5 \text{ molecule cm}^{-3}$ (= present day OH)
Wetland	115 Tg/year
Biomass burning	10 Tg/year
Ocean	15 Tg/year
Termites	20 Tg/year
Rice	10 Tg/year
Live stock and animal waste	11 Tg/year

6.2.5 Results from PI ECHAM model simulation

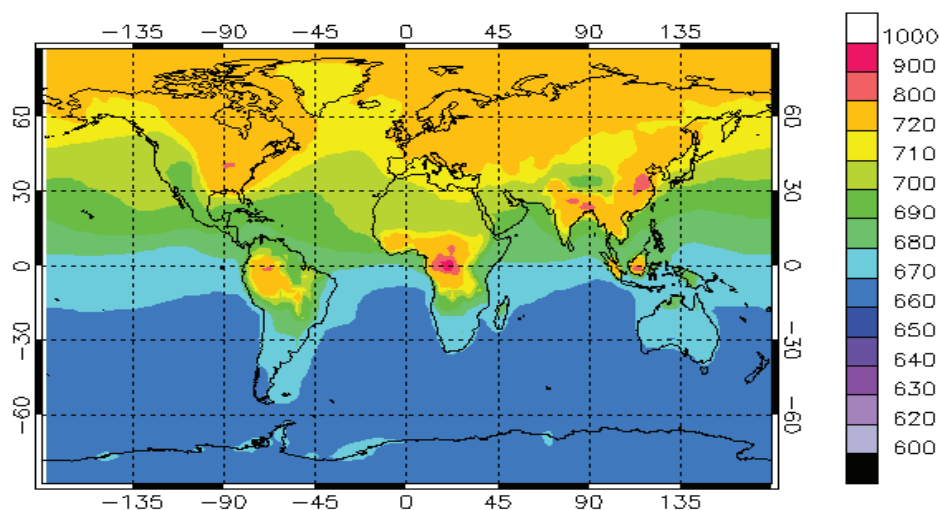


Figure 6.7: *Spatial distribution of annual mean surface methane mixing ratio (in ppb) from PI ECHAM simulation*

The average surface methane level from the base case simulation is estimated to be around 695 ppb which matches well with the ice core records. Figure 6.7 depicts that in the southern hemisphere methane is homogenously mixed and hold a mean value between 650 to 670 ppb. On the other hand, methane mixing ratio in the northern hemisphere varies from 680 to 900 ppb. This is quite obvious due to the presence of large land mass in the northern hemisphere, which holds most of the Methane hotspots with a mixing ratio of more than 800 ppb were found in the tropical region, between the equator and 30°N, mainly due to the effect from local sources such as tropical wetlands. From the perspective of LGM, the higher surface methane levels particularly at the tropics agree with Chappellaz et al., (1993) which attribute the Pre-industrial methane rise to massive expansion in tropical wetland emissions.

The PI inter hemispherical gradient is estimated to be around 52 ppb. This is not unrealistic compared to the methane isotope measurements from ice cores by Chappellaz et al., (1997) although the model polar gradient lies in its higher range of the ice records. Chappellaz et al., (1997) found inter polar difference of 44 ± 7 ppb from 5 to 2.5 kyr before present. And thus the model reproduces the observations fairly well.

6.2.6 Conclusion

ECHAM model simulations for LGM and PI produce reasonably well the methane distribution which is highly comparable with the isotope records found in the ice cores. It proves the successful adaptation of wetland methane parameterisation in these climatic scenarios although compared to previous modeling studies both the LGM wetland extent and methane budget is estimated low. In reality, a weaker LGM source is possible if the OH concentration was low too. This proposition is highly feasible since the recent studies by Hofzumahaus et al., (2009), and Taraborelli et al., (2012) indicate to a less pronounced OH – BVOC chemistry than previously thought which could alter the understanding of LGM OH chemistry modeling. However, in this study, a 26% increase in LGM OH than present has been considered following the interactive chemistry study of Thomas Laepple (Pers. Commn.) which considered the cumulative effects of various factor changes on LGM OH concentration. Contrary to LGM, the PI methane modeling has been simpler since there were no evidences of significant changes in OH and wetland methane budget compared to present day. For the other natural emissions and much weaker anthropogenic emissions from rice, animals and biomass burning, estimates of Valdes et al., (2005) and Ruddiman et al., (2001) is used. With these assumptions, the model produces PI methane concentration of 700 ppb and inter hemispherical gradient of 55 ppb which are pretty close to the ice core records.

7. Summary and conclusion

In this thesis, a simplified global tropospheric methane model has been developed for application under present-day and paleo-climate conditions. Much emphasis has been placed on the parameterization of methane wetland emissions, which constitute the largest natural source of methane and which have been speculated to contribute significantly to the observed variability of atmospheric methane concentrations. The model has been validated with present-day and pre-industrial observations, and the methane budget under these conditions has been discussed. The model was also applied to simulations of the last glacial maximum, and in a transient simulation spanning the past two decades. The main results found from this work are discussed here on the basis of individual chapter.

Chapter 2 is based on literature review, shows that at present, the global methane budget is approximately balanced with sources and sinks contributing between 430 and 507 Tg per year (IPCC AR4). It is highlighted in this chapter that even though the global methane budget is well constrained, large uncertainties exist about the relative contribution of various sources to the global budget and their spatial distribution. Among the studies, reported in IPCC AR4, the source strength of natural emission lies in a range between 145 and 260 Tg and anthropogenic emissions are between 310 and 428 Tg. For wetlands, the largest natural source, the reported budgets vary from 100 to 220 Tg.

Chapter 3 shows that the parameterization of methane wetland emissions requires a high-resolution model for soil moisture and vegetation dynamics. In this study, the new wetland parameterization is derived from soil water field and soil carbon of the CARAIB dynamic vegetation model and uses ECHAM temperature fields together with the Gedney et al., (2004) formulation to compute methane fluxes. It is found that the soil wetness distribution from CARAIB yields a good representation of the potential wetland areas globally as well as on the regional scale. The global wetland area that is derived after applying two different threshold parameters for boreal and tropical wetlands, respectively, lies in the higher range of other inventories. The global potential wetland area from the parameterisation is estimated to be 10.8 million km². Except for Europe and Alaska, the wetland areas in each continent are well captured with reference to the Lehner and Döll Global Lakes and Wetlands Database (Lehner et al., 2004). A major strength of the new wetland parameterisation is that it can be applied consistently for different climatic conditions, provided that CARAIB output is available. In this thesis, wetland areas have been reconstructed for present-day, preindustrial, and last glacial maximum conditions. In this study we emphasize the wetland seasonal behaviour which has been largely neglected in previous modeling studies. Annual wetland methane emission shows strong seasonal variability which depends on the seasonality of wetland area as well as control parameters such as soil carbon content, soil temperature etc. In reality, the northern latitudinal wetlands show larger seasonal variability than the tropical ones, which along with the soil temperature pattern influences on methane emission pattern. The

difference between the tropical and northern wetlands seasonality is captured well with our parameterisation. Tropical methane emissions are found to less vary over the year, not much affected by wetland variability which is also less pronounced here. It should be noted that our parameterisation could not produce the expected wetland seasonality in the tropics due to the excessive amount of wetlands placed north of the equator where the precipitation cycle is opposite to that south of the equator. Although northern wetlands cover larger areas and are richer in soil carbon, tropical wetlands emit more methane per unit area due to higher soil temperatures. This results in almost equal contributions from boreal and tropical wetlands to the global methane budget.

Chapter 4 shows that ECHAM model simulation with the inputs from EDGAR 3.2 inventory along with the parameterized wetland methane source proves suitable to produce atmospheric methane as observed by the station data from NOAA CMDL. The surface methane level in the Northern Hemisphere is found to vary between 1800 and 2200 ppb whereas in the Southern Hemisphere, it is well mixed and ranges between 1700 and 1800 ppb. The inter-hemispheric methane gradient which is estimated to be 145 ppb from the model output is also consistent with observations (Dlugokencky et al., 1994). The model is able to produce the salient features of observed methane seasonality and the surface methane mixing ratio reasonably well across most stations. The model matches observations pretty well for Southern Hemispheric and tropical stations with an average bias of -5 to -10 ppb. However, for high northern latitudinal stations, the model overestimates by 20 to 40 ppb. For a few stations situated at high emission regions at northern mid latitudes such as Sary Taukum (44.45°N, 75.57°E) and Black Sea (44.17°N, 28.67°E), the model underestimates as much as 100 ppb likely to be caused by a missing source or a group of sources in the emission inventory used. The background sites on the other hand show a better seasonal match between model and observation. Pearson correlation statistics between model and observation shows an average co-efficient value of .95 in the Southern Hemispheric stations. For the tropical stations the correlation is calculated to be .84 and for the high northern latitude it is .68. The average r.m.s error of model for the stations situated between 5 to 60° N is found to be 16 ppb which is among the best values found in the literature to date. To improve the correlation between model and observation, a few modifications have been done to the prescribed source strengths of wetland and biomass burning. To represent a better seasonality for northern latitudinal stations, wetland emissions above 45°N have been reduced by a factor of 1.2 whereas the biomass burning emission have been reduced by factor of 1.8 above 35°N. To improve the same for the southern hemispherical stations, biomass burning emission is increased by a factor of 1.48 south of 35°N. The emission scenario after the regional scaling has been regarded as the optimized emission scenario for model simulation. The resulting wetland methane source from our model parameterisation of 148 Tg, comes close to the lower end of wetland emission inventories reported to IPCC AR4. Based on the optimized emissions data, a set of model sensitivity simulations was carried out with the modification of individual

groups of sources (enhancement or reduction by 10 Tg) in order to evaluate how well the observations constrain specific source categories or regional distributions of emissions. It was found that alterations of the wetlands, animal and gas extraction sectors (s) lead to slight improvements of correlation values at tropics and extra tropics, although imposing larger rms error. It is however very difficult to improve the correlation at stations situated above 60°N. However, it is to be noted that there is insufficient evidence to fully attribute the remaining deviations of the simulated methane concentrations to specific errors in the underlying emissions.

Chapter 5 shows the results from model simulations using annually varying emissions from EDGAR 4.2 and the wetland parameterization with dynamically varying soil moisture fields from CARAIB. Importantly in the present simulation a sink term for the surface uptake of methane has been considered which was mostly ignored in previous studies. The model approximately reproduces the methane concentrations from 1990 to 2006 although the rise in model methane concentrations appears to be a bit different from the observation. The model does not reproduce a considerable increase in methane concentration between 1990 and 1997 when we expect a fast rise. On the other hand, after 2002 the model methane rise is faster compared to the observed value. This study indicates that the probable cause of this model observation difference is the methane budget from oil and gas extraction as reported to EDGAR inventory. Recent study by Pétron et al. (2012) indicates considerable underestimation of gas extracted methane using fracking technique over Boulder, USA. This possibility could hold true over several European countries which started practicing fracking technique to extract gas during 1980s. However, shale gas extraction at USA which is potentially a source of methane emission showed a significant rise only after 2005 when it increased from 4% to 24% in 2012 (The Economist, June 2012). So any major methane contribution from hydraulic fracking does not seem much plausible before 2000 in USA and over Europe. At the same time, any potential role of wetlands to explain the 20 to 40 ppb model observation difference is not given much importance since the wetland methane budget and its variability lies well within the expected range. The other important aspect of this study is that, in contrary to previous studies, a uniform OH field has been used in the simulation following the recent revelations by Montzka et al., (2011) which shows small variability of OH than previously thought. Even the recent study by Hofzumahaus et al., (2009) also shows less influence of VOC emissions on OH variability which challenges the previous studies. By adapting these findings in our simulation, this study goes a step further to seek the role of sources in order to explain the present day methane rather to held OH responsible.

Chapter 6 is dedicated to analysis of methane trend at LGM and Pre-industrial era with the help of new wetland methane model and existing knowledge of other methane sources and sinks. The LGM wetlands parameterized from CARAIB derived soil wetness estimates 7.75 million km² in area which is high compared to the modeling studies such as Valdes et al., (2005), Kaplan et al., (2006) and Webber et al., (2010). However, the Global methane

emission from LGM wetlands is estimated significantly lower than these studies. Our LGM methane source strength also lies in the low range of other model studies. However, as discussed earlier, the recent findings by Hofzumahaus et al., (2009) indicate to a lesser dependence of OH on BVOCs which potentially supports a low LGM OH concentration than presumed in other modeling studies. It indicates the possibility of a weaker methane source as well and in that sense our LGM source strength could well be close to reality. In the ECHAM model simulation with the LGM wetland source and other natural sources adapted from Valdes et al., (2005) and an assumption of 25% higher OH level than present produces LGM surface methane mixing ratio close to 350 ppb which is in reasonable agreement with the ice core records. It suggests that the model assumptions for the LGM sources and sinks are well balanced to produce the realistic signature of LGM methane. It also proves the success of wetland parameterisation in the LGM climate. For the Pre-industrial methane simulation present day wetland methane sources and OH level with reduced sources of biomass burning, rice and animal emissions as reported in Ruddiman et al., (2001) has been used. The model simulation produces an average surface methane concentration of 695 ppb which also agrees with the ice core records.

It should be mentioned that the new wetland parameterisation developed in this work can now be applied to other climate simulations to study methane budget during those periods, if one looks for the future possibilities as a follow up to this present study. It includes various time phases in past climate where methane could potentially be an important factor for climate change. The simulations could also include projection of future methane trend. In this context, the logical next step would be to implement wetland emissions directly in CARAIB and couple CARAIB with ECHAM. Also, in the light of new findings concerning the OH chemistry and its dependence on BVOC emissions, paleo methane studies need to undergo further review in order to reexamine the relative role of methane sources and sinks while explaining the observed methane trend.

Bibliography

- Adams, J. M., J. V. H. Constable, A. B. Guenther, and P. Zimmerman (2001), An estimate of natural volatile organic compound emissions from vegetation since the Last Glacial Maximum, *Chemosphere*, Vol. 3, 73-91.
- Aselmann, I., and P. J. Crutzen (1989), Global Distribution of Natural Freshwater Wetlands and Rice Paddies, their Net Primary Productivity, Seasonality and Possible Methane Emissions, *J. Atmos. Chem.*, Vol. 8, 307 – 358.
- Bastviken, D., A. L. Santoro, H. Marotta, L. Q. Pinho, D. F. Calheiros, P. Crill, and A. Enrich – Prast (2010), Methane Emission from Pantanal, South America, during the Low Water Season: Toward More Comprehensive Sampling, *Envir. Sci. Tech.*, Vol. 44, 5450 – 5455.
- Beck, L. L., (1993), A Global Methane Emissions program for Landfills, Coal mines, And Natural Gas Systems, *Chemosphere*, Vol. 26, Nos. 1-4, pp 447-452.
- Beerling, D. J., and F. I. Woodward (2001), Vegetation and the Terrestrial Carbon Cycle. *Modelling the first 400 million Years*, Cambridge Univ. Press. New York
- Bergamaschi, P., C. Frankenberg, J. F. Meirink, M. Krol, F. Dentener, T. Wagner, U. Platt, J. O. Kaplan, S. Körner, M. Heimann, E. J. Dlugokencky, and A. Goede (2007), Satellite cartography of atmospheric methane from SCIAMACHY on board ENVISAT: 2. Evaluation based on inverse model simulations, *J. Geophys. Res.*, Vol. 112, D02304.
- Bergamaschi, P., C. Frankenberg, J. Meirink, M. Krol, M. G. Villani, S. Houweling, F. Dentener, E. J. Dlugokencky, J. B. Miller, L. V. Gatti, A. Engel, and I. Levin (2009), Inverse modeling of global and regional CH₄ emissions using SCIAMACHY satellite retrievals, *J. Geophys. Res.*, Vol. 114, D22301.
- Bergamaschi, P., M. Krol, F. Dentener, A. Vermuelen, F. Meinhardt, R. Graul, M. Ramonet, W. Peters, and E. J. Dlugokencky (2005), Inverse modelling of national and European CH₄ emissions using the atmospheric zoom model TM5, *Atmos. Chem. Phys.*, Vol. 5, 2431-2460.
- Blunier, T., J. Chappellaz, J. Schwander, B. Stauffer, and D. Raynaud (1995), Variations in atmospheric methane concentration during the Holocene epoch, *Nature*, Vol. 374, 46-49, doi:10.1038/3740461a0.
- Bogner, J., K. Spokas, E. Burton, R. Sweeney, and V. Corona (1995), Landfills as atmospheric methane sources and sinks, *Chemosphere*, Vol. 31, No. 9, 4119-4130.
- Bohn, T. J., D. P. Lettenmaier, K. Sathulur, L. C. Bowling, E. Podest, K. C. McDonald and T. Friborg (2007), Methane emissions from western Siberian wetlands: heterogeneity and sensitivity to climate change, *Environ. Res. Lett.*, Vol. 2, 045015.

- Bousquet, P., D. A. Hauglustaine, P. Peylin, C. Carouge, and P. Ciais (2005), Two decades of OH variability as inferred by an inversion of atmospheric transport and chemistry of methyl chloroform, *Atmos. Chem. Phys.*, Vol. 5, 2635 – 2656.
- Bousquet, P., P. Ciais, J. B. Miller, E. J. Dlugokencky, D. A. Hauglustaine, C. Prigent, G. R. Van der Werf, P. Peylin, E. G. Brunke, C. Carouge, R. L. Langenfelds, J. Lathière, F. Papa, M. Ramonet, M. Schmidt, L. P. Steele, S. C. Tyler, and J. White (2006), *Nature Letters*, Vol. 443
- Brook, E. J., Susan Harder, J. Severinghaus, E. J. Steig, and C. M. Sucher (2000), On the origin and timing of rapid changes in atmospheric methane during the last glacial period, *Global Biogeochem. Cy.*, Vol. 14, NO. 2, 559-572.
- Bryant P. (1979), Microbial Methane Production-Theoretical Aspects, *J. Anim. Sci.*, Vol. 48, 193-201
- Bubier, J. L., T. R. Moore, and N. T. Roulet (1993), Methane emissions from mid-boreal wetlands of northern Ontario, Canada, *Ecology*, Vol. 74, 2240-2254
- Cao, M., S. Marshall, and K. Gregson (1996), Global carbon exchange and methane emissions from natural wetlands: Application of a process – based model, *J. Geophys. Res.*, Vol. 101, No. D9, 14,399 – 14,414.
- Cao, M., J. B. dent., and O. W. Heal (1995a), Modelling of methane emission from rice paddies, *Global Biogeochem. Cy.* Vol. 9, 183-195.
- Chappellaz, J. A., and I. Y. Fung (1993), The atmospheric CH₄ increase since the Last Glacial Maximum (1). Source estimates, *Tellus*, Vol. 45B, 228-241.
- Chappellaz, J., J. M. Barnola, D. Raynaud, Y. S. Korotkevich, and C. Lorius (1990), Ice – core record of atmospheric methane over the past 160,000 years, *Nature*, Vol. 345.
- Chappellaz, J., T. Blüner, S. Kints, A. Dällenbach, J. –M. Barnola, J. Schwander, D. Raynaud, and B. Stauffer (1997), Changes in the atmospheric CH₄ gradient between Greenland and Antarctica during the Holocene, *J. Geophys. Res.*, Vol. 102, 15987-15997
- Charman D. J., H. M. Roe, and W. R. Gehrels (2002), Modern distribution of saltmarsh testate amoebae: regional variability of zonation and response to environmental variables, *J. Quat. Sci.*, Vol. 17, 387–409.
- Chen, Y., and Ronald G. Prinn (2005), Atmospheric modeling of high–and low–frequency methane observations: Importance of interannually varying transport, *J. Geophys. Res.*, Vol. 110, D10303.
- Christensen, T. R., A. Ekberg, L. Ström, M. Mastepanov, N. Panikov, M. Öquist, B. H. Svenson, H. Nykänen, P. J. Martikainen and H. Oskarsson (2003), Factors controlling

- large scale variations in methane emissions from wetlands, *Geophys. Res. Lett.*, Vol. 30, NO. 7, 1414.
- Christensen, T. R., I. C. Prentice, J. Kaplan, A. Haxeltine, and S. Sitch (1996), Methane flux from northern wetlands and tundra, *Tellus*, Vol. 48B, 652 – 661.
- Cogle, J. G., GGHDR0-Global Hydrographic Data, Release 2.1, 23pp., (1994), *trent climate Note 91-1*, Department of Geogrpahy, Trent University, Petersbourgh.
- Cox, P. M., R. A. Betts, C. B. Bunton, R. L. H. Essery, P. R. Rowntree, and J. Smith (1999), The impact of new land surface physics on the GCM simulation of climate and climate sensitivity, *Clim. Dynam.*, Vol. 15, 183-203
- Crill, P. M., K. B. Bartlett., R. C. Harris, E. Gorham, E. S. Verry, P. I. Sebacher, L. Madzer, and W. Sanner (1988), Methane flux from Minnesota Peatlands, *Global Biogeochem. Cy.*, Vol. 2, 371-384
- Crutzen, P. J., and C. Brühl (1993), A model study of atmospheric temperatures and the concentration of ozone, hydroxyl and some other photochemical active gases during The glacial, The preindustrial Holocene and the present, *Geophys. Res. Lett.*, Vol. (20), 1047-1050
- Crutzen. P. J., Methane sources and sinks (1991), *Nature*, Vol. 350, 380-381.
- Cunnold, D. M., L. P. Steele, P. J. Fraser, P. G. Simmonds, R. G. Prinn, R. F. Weiss, L. W. Porter, S. O'Doherty, R. L. Langenfelds, P. B. Krummel, H. J. Wang, L. Emmons, X. X. Tie, and E. J. Dlugokencky, 2002, In situ measurements of atmospheric methane at GAGE/AGAGE sites during 1985-2000 and resulting source inferences, *J. Geophys. Res.*, Vol. 107
- Curry, C. L., (2007), Modeling the soil consumption of atmospheric methane at the global scale, *Global Biogeochem, Cy.*, Vol. 21, GB4012.
- Dällenbach A., T. Blunier, J. Flückiger, B. Stauffer, J. Chappellaz, D. Raynaud (2000), Changes in the atmospheric CH₄ gradient between Greenland and Antarctica during the last Glacial and the transition to the Holocene, *Geophys. Res. Lett.*, Vol. 27, No. 7, 1005 – 1008.
- Dedikov, J. V., G. S. Akopova, N. G. Gladkaja, A. S. Piotrovskij, V. A. Markellov, S. S. Salichov, H. Kaesler, A. Ramm, A. M. von Blumencron, and J. Leileveld (1999), Estimating methane releases from natural gas production and transmission in Russia, *Atmos. Environ.*, Vol. 3(20), 3291-3299.
- Dentener, F., M. van Weele, M. Krol, S. Houweling, and P. van Velthoven (2003), Trends and inter – annual variability of methane emissions derived from 1979 – 1993 global CTM simulations, *Atmos. Chem. Phys.*, Vol. 3, 73 – 88.

- Devol, A. H., J. E. Richey, B. R. Forsberg, and L. A. Martinelli (1990), Seasonal Dynamics in Methane Emissions from the Amazon River Floodplain to the Troposphere, *J. Geophys. Res.*, Vol. 95, No. D10, 16,417 – 16,426.
- Dlugokencky, E. J., Euan G. Nisbet, Rebecca Fisher, and David Lowry (2011), Global atmospheric methane: budget, changes and dangers, *Phil. Trans. R. Soc., Vol. A 369*, 2058-2072.
- Dlugokencky, E. J., L. P. Steele, P. M. Lang, and K. A. Masarie (1994), The growth rate and distribution of atmospheric methane, *J. Geophys. Res.*, Vol. 99, No. D8, Pages 17,021 – 17,043.
- Dlugokencky, E. J., S. Houweling, L. Bruhwiler, K. A. Masarie, P. M. Lang, J. B. Miller, and P. P. Tans (2003), Atmospheric methane levels off: Temporary pause or a new steady state?, *Geophys. Res. Lett.*, Vol. 30, NO. 19, 1992.
- Dlugokencky, E. J., K. A. Masarie, P. M. Lang, J. B. Miller, and P. P. Tans, (2003), Atmospheric methane levels off: Temporary pause or a new steady state? *Geophys. Res. Lett.*, Vol. 30, 1992
- Donner, L., and V. Ramanathan, (1980), Methane and Nitrous oxide; Their effects on terrestrial climate, *J. Atmos. Sc.*, Vol. 37, 119-124
- Dueck, T. A., R. D. Visser, H. Poorter, S. Persijn, A. Gorissen, W. Vissers, A. Schapendonk, J. Verhagen, J. Snel, F. Harren, A. Nagai, F. Verstappen, H. Bouwmeester, L. Voesenek, and A. Werf (2007), NO evidence for substantial aerobic methane emission by terrestrial plants: a ¹³C-labelling approach, *New Phytologist*, Vol. 175, 29-35.
- Etheridge, D., L. Steele, R. Francey, and R. Langenfelds (1998), Atmospheric methane between 1000 A.D. and present: Evidence of anthropogenic emissions and climate variability, *J. Geophys. Res.*, Vol. 103, 15979-15993
- Etiope, G. (2009), Natural emissions of methane from geological seepage in Europe, *Atmos. Environ.*, Vol. 43, 1430 – 1443.
- Ferretti, D. F., J. B. Miller, J. W. C. White, K. R. Lassey, D. C. Lowe, and D. M. Etheridge (2007), Stable isotopes provide revised global limits of aerobic methane emission from plants, *Atmos. Chem. Phys.*, Vol. 7, 237-241.
- Finlayson, C. M., and A. G. van der Valk (1995), Wetland classification and inventory: A summary, *Vegetatio*, Vol. 118, 185 – 192.
- Finlayson, C. M., N. C. Davidson, A. G. Spiers, and N. J. Stevenson (1999), Global wetland inventory – current status and future priorities, *Mar. Freshwater Res.*, Vol. 50, 717 – 727.

- Fiore A. M., L. W. Horowitz, E. J. Dlugokencky, and J. J. West (2006), Impact of meteorology and emissions on methane trends, 1990 – 2004, *Geophys. Res. Lett.*, Vol. 33, L12809.
- Fletcher, S. E., Pieter P. Tans, L. M. Bruhwiler, and J. B. Miller, M. Heimann (2004), CH₄ sources estimated from atmospheric observations of CH₄ and its ¹³C/ ¹²C isotopic ratios: 1. Inverse modeling of source processes, *Global Biogeochem. Cy.*, Vol. 18, GB4004.
- Frankenberg C., I. Aben, P. Bergamaschi, E. J. Dlugokencky, R. van Hees, S. Houweling, P. van der Meer, and P. Tol (2011), Global column-averaged methane mixing ratios from 2003 to 2009 as derived from SCIAMACHY: Trends and variability, *J. Geophys. Res.*, Vol. 116, D04302.
- Fung, I., J. John, J. Lerner, E. Matthews, M. Prather, L. P. Steele, and P. J. Fraser (1991), Three-Dimensional Model synthesis of the Global Methane Cycle, *J. Geophys. Res.*, Vol. 96, NO. D7, 13033-13065.
- Garg, A., B. Kankal, P. R. Shukla (2011), Methane emissions in India: Sub-regional and sectoral trends, *Atmos. Env.*, Vol. 45, 28, 4922-4929.
- Gates, W. L., Boyle, J. S., Covey, C., Dease, C. G., Doutriaux, C. M., et al.: An Overview of the Results of the Atmospheric Model Intercomparison Project (AMIP I) (1999), *Bull. Am. Meteorol. Soc.*, Vol. 80(1), pp. 2955.
- Gedney, N., P. M. Cox, C. Huntingford (2004), Climate feedback from wetland methane emissions, *Geophys. Res. Lett.*, Vol. 31, L20503.
- Granberg, G., M. Ottosson-Löfvenius, and H. Grip (2001), Effect of climatic variability from 1980 to 1997 on simulated methane emission from a boreal mixed mire in northern Sweden, *Global Biogeochem. Cy.*, Vol. 15, 977-991.
- Grewe, V., D. Brunner, M. Dameris, J. L. Grenfell, R. Hein, D. Shindell, and J. Staehelin (2001), Origin and variability of upper tropospheric nitrogen oxides and ozone at northern mid-latitudes, *Atmos. Environ.*, Vol. 35, 3421--3433.
- Hamilton, S. K., S. J. Sippel, and J. M. Melack (2002), Comparison of inundation patterns among major South American floodplains, *J. Geophys. Res.*, Vol. 107, 10.1029/2000JD000306.
- Harder, S. L., D. T. Shindell, G. A. Schmidt, and E. J. Brook (2007), A global climate model study of CH₄ emissions during the Holocene and glacial-interglacial transitions constrained by ice core data, *Global Biogeochem. Cy.*, Vol. 21, GB1011.
- Hein, R., P. J. Crutzen, and M. Heimann (1997), An inverse modeling approach to investigate the global atmospheric methane cycle, *Global Biogeochem. Cy.*, Vol. 11, 43-76.

- Hess, L. L., J. M. Melack, E. M. L. M. Novo, C. C. F. Barbosa, M. Gastil (2003), Dual – season mapping of wetland inundation and vegetation for the central Amazon basin, *Remote Sens. Environ.*, Vol. 87, 404 – 428.
- Hofzumahaus, A., F. Rohrer, K. Lu, B. Bohn, T. Brauers, C. Chang, H. Fuchs, F. Holland, K. Mita, Y. Kondo, X. Li, S. Lou, M. Shao, L. Zhang, A. Wahner, Y. Zhang (2009), Amplified Trace Gas Removal in the Troposphere, *Science*, Vol. 324, 1702, DOI:10.1126.
- Horowitz, L. W., Walters, S., Mauzerall, D. L., Emmons, L. K., Rasch, P. J., Granier, C., Tie, X., Lamarque, J.-F., Schultz, M. G., Tyndall, G. S., Orlando, J. J., and Brasseur, G. P.: A global simulation of tropospheric ozone and related tracers: Description and evaluation of MOZART, version 2, *J. Geophys. Res.*, Vol. 108(D24), 4784
- Houweling, S., F. Dentener, and J. Lelieveld (2000), Simulation of preindustrial atmospheric methane to constrain the global source strength of natural wetlands, *J. Geophys. Res.*, Vol. 105, No. D13, 17,243 – 17,255.
- Houweling, S., F. Dentener, and J. Lelieveld, B. Walter, E. Dlugokencky (2000), The modeling of tropospheric methane: How well can point measurements be reproduced by a global model ?, *J. Geophys. Res.*, Vol. 105, No. D7, Pages 8981 – 9002.
- Houweling, S., G. R. van der Werf, K. Klein Goldewijk, T. Röckmann, and I. Aben (2008), Early anthropogenic CH₄ emission and the variation of CH₄ and ¹³CH₄ over the last millennium, *Global Biogeochem. Cy.*, Vol. 22, GB1002.
- Houweling, S., T. Kaminski, F. Dentener, J. Lelieveld, and M. Heimann (1999), Inverse modeling of methane sources and sinks using the adjoint of a global transport model, *J. Geophys. Res.*, Vol. 104, No. D21, 26137-26160.
- Johnson, D. E., K. A. Johnson, G. M. Yard, and M. E. Branine (2000), Ruminants and other animals, Chapter 8, Pages 112-133 in *Atmospheric Methane: Its role in the Global Environment*, M. A. K. Khalil, ed. Springer-Verlag, Berlin Heidelberg, Germany.
- Kammen, C. M., and B. D. Marino (1993), On the origin and magnitude of pre-industrial anthropogenic CO₂ and CH₄ emissions, *Chemosphere*, Vol. 26, 69-86.
- Kaplan, J. O. (2002), Wetlands at the Last Glacial Maximum: Distribution and methane emissions, *Geophys. Res. Lett.*, Vol. 29, No. 6, 1079.
- Kaplan, J. O., G. Folberth, and D. A. Hauglustaine (2006), Role of methane and biogenic volatile organic compound sources in last glacial and Holocene fluctuations of atmospheric methane concentrations, *Global Biogeochem. Cy.*, Vol. 20, GB2016.

- Kennett, J. P., Cannariato, K.G., Hendy, I.L., Behl, R.J., 2003. Role of Methane Hydrates in late Quaternary Climatic Change: The Clathrate Gun Hypothesis, *American Geophysical Union 2003*, 216.
- Keppler, F., J. T. G. Hamilton, M. Barß, and T. Röckmann (2006), Methane emission from terrestrial plants under aerobic conditions, *Nature*, Vol. 439, 04420.
- Khalil, A. K., C. L. Butenhoff, and R. A. Rasmussen (2007), Atmospheric Methane: Trends and Cycles of Sources and Sinks, *Envir. Sci. Tech.*, Vol. 41, 2131 – 2137.
- Khalil, M. A .K., and R. A. Ramussen (1995), The changing composition of Earth's atmosphere, in Composition, Chemistry, and climate of the Atmosphere, edited by H. B. Singh, pp. 50-87, *Van Nostrand Reinhold, Hoboken, N. J.*
- Kightley, D., D. B. Nedwell, and M.Cooper (1995), Capacity for methane oxidation in landfill cover soil measured in laboratory-scale soil microcosmos, *Appl. Environ. Microbio.*, Vol. 61, 592-601.
- Kirschbaum, M.U. F., and A. Walcroft (2008), No detectable aerobic methane efflux from plant material, nor from adsorption/desorption processes, *Biogeosciences*, Vol. 5, 1551-1558.
- Krol, M., and J. Leliveld (2003), Can the variability in tropospheric OH be deduced from measurements of 1,1,1-trichloroethane (methylchloroform)? (2003), *J. Geophys. Res.*, Vol. 108 D3, 10697-10711, 4125.
- Krol, M., P. Leeuwen, and J. Leileveld (1998), Global OH trend inferred from methylchloroform measurements, *J. Geophys. Res.*, Vol. 103, D9, 10697-10711.
- Laepple, T., M. G. Schultz, J. F. Lamarque, S. Madronich, R. E. Shetter, B. L. Lefer, and E. Atlas (2005), Improved Albedo Formulation for Chemistry-Transport Models based on satellite observations and assimilated snow data and its impact on tropospheric photochemistry, *J. Geophys. Res.*, 110(D11), D11308, doi:10.1029/2004JD005463.
- Laurent, J., M.,L. François, A. Bar-Hen, L. Bel, and R. Cheddadi (2008), European Bioclimatic Affinity groups: data model comparisons, *Global Planet Change*, Vol. 61, 28-40.
- Law, K., and Pyle , J. (1993), Modelling trace gas budgets in the troposphere, 2. CH₄ and CO, *J. Geophys. Res.*, Vol. 98, 18401-18412
- Lehner B., and P. Döll (2004), Development and validation of a global database of lakes, reservoirs and wetlands, *J. Hydro.*, Vol. 296, 1 – 22.
- Lelieveld, J., P. J. Crutzen, and F. J. Dentener (1998), Changing concentration, lifetime and climate forcing of atmospheric methane, *Tellus*, Vol. 50B, 128 – 150.

- Levin., L. A., and R. H. Michener (2002) Isotopic evidence for chemosynthesis-based nutrition of macrobenthos. The lightness of being at Pacific methane seeps, *Limnology and Oceanography*, Vol. 47, NO.5.
- Levine, J. G., E. W. Wolff, A. E. Jones, L. C. Sime, P. J. Valdes, A. T. Archibald, G. D. Carver, N. J. Warwick, and J. A. Pyle (2011), Reconciling the changes in atmospheric methane sources and sinks between the Last Glacial Maximum and the pre-industrial era, *Geophys. Res. Lett.*, Vol. 38, L23804.
- Li, C., J. Qui, S. Frohling, X. Xiao, W. Salas, B. Moore III, S. Boles, Y. Huang, and R. Sass (2002), reduced methane emissions from large scale changes in water management in China's rice paddies during 1980-2000, *Geophys. Res. Lett.*, Vol. 30, No. 7, 1414.
- Lloyd, J., and J. A. Taylor (1994), On the temperature dependence of soil respiration, *Funct. Ecol.*, Vol. 8, 315 – 323.
- Madronich, S., and S. Flocke, The role of solar radiation in atmospheric chemistry. In: P. Boule, editor, *Handbook of Environmental Chemistry*, Springer-Verlag, 1998.
- Martinerie, P., G. P. Brasseur, and C. Granier (1995), The chemical composition of ancient atmospheres: A model study constrained by ice core data, *J. Geophys. Res.*, Vol. 100, No. D7, 14,291 – 14,304.
- Matthews, E., Inez Fung (1987), Methane emission from natural wetlands: Global distribution, area, and environmental characteristics of sources, *Global Biogeochem. Cy.*, Vol. 1, No. 1, 61 – 86.
- Matthews, E., Inez Fung, Jean Lerner (1991), Methane emission from rice cultivation: Geographic and seasonal distribution of cultivated areas and emissions, *Global Biogeochem. Cy.*, Vol. 5, No. 1, 3 – 24.
- Melack, J. M., and L. L. Hess (2004), Remote Sensing of Wetlands on a Global Scale, *Sil news*, Vol. 42.
- Melack, J. M., L. L. Hessi, and S. Sippel (1994), Remote Sensing of Lakes and Floodplains in the Amazon basin, *Remote Sens. Review.*, 994, Vol. 10, 127-142.
- Mialon A., A. Royer, M. Foly (2005), Wetland seasonal dynamics and interannual variability over northern high latitudes, derived from microwave satellite data, *J. Geophys. Res.*, Vol. 110, D17102.
- Mialon, A., A. Royer, and M. Fily (2005), Wetland seasonal dynamics and interannual variability over northern high latitudes, derived from microwave satellite data, *J. Geophys. Res.*, Vol. 110, 17182

- Mitsch, W. J., A. Nahlik, P. Wolski, B. Bernal, L. Zhang, L. Ramberg (2010), Tropical wetlands: seasonal hydrologic pulsing, carbon sequestration, and methane emissions, *Wetl. Ecol. Manage.*, Vol. 18, 573 – 586.
- Montzka, S. A., M. Krol, E. Dlugokencky, B. Hall, P. Jöckel, J. Lelieveld (2011), Small Interannual Variability of Global Atmospheric Hydroxyl, *Science*, Vol. 331.
- Moore, T. R., A. Heyes, and N. T. Roulet (1994), Methane emissions from the Southern Hudson Bay lowland, *J. Geophys. Res.*, Vol. 90, 1455-1467
- Moore, T. R., and R. Knowles (1989), The influence of water table levels on methane and carbon dioxide emissions from peatland soils, *Can. J. Soil Sc.*, Vol. 69 (1), 33-38.
- Morimoto, S., S. Aoki, T. Nakazawa, and T. Yamanouchi (2006), Temporal variations of the carbon isotope ratio of atmospheric methane observed at Ny Ålesund, Svalbard from 1996 to 2004, *Geophys. Res. Lett.*, Vol. 33, L01807
- Neef, L., M. van Weele, and P. van Velthoven (2010), Optimal estimation of the present – day global methane budget, *Global Biogeochem. Cy.*, Vol. 24, GB4024.
- Nisbet, R. E. R., R. Fisher, R. H. Nimmo, D. S. Shindell, P. M. Crill, A. V. Gallego-Sala, E. R. C. Hornibrook, E. López-Juez, D. Lowry, P. B. R. Nisbet, E. F. Shuckburgh, S. Sriskantharajah, C. J. Howe, and E. G. Nisbet (2009), Emission of methane from plants, *Proceedings of The Royal Society* 276, 1347-1354.
- O'Brian A. L. (1988), Evaluating the cumulative effects of alteration on New England wetlands, *Environ. Manag.*, Vol. 12, No 5.
- Olivier, J. G. J., J. A. Van Aardenne, F. J. Dentener, V. Pagliasi, L. N. Ganyeveld, and J. A. Peters (2005), Recent trends in global greenhouse gas emissions, regional trends 1970-2000 and spatial distribution of key sources in 2000, *Environ. Sc.*, Vol. 2, special issue 2-3
- Otto, D., D. Rasse, J. Kaplan, P. Warrant, and L. François (2002), Biospheric carbon stocks reconstructed at the Last Glacial Maximum: comparison between general circulation models using prescribed and sea surface temperatures, *Global Planet change*, Vol. 33, 117-138.
- Papa, F., C. Prigent, W. B. Rossow, B. Legresy, and F. Remy (2006), Inundated wetland dynamics over boreal regions from remote sensing: the use of Topex – Poseidon dual – frequency radar altimeter observations, *Int. J. Remote Sens.*, Vol. 27, No. 21, 4847 – 4866.
- Patra P. K., M. Takigawa, K. Ishijima, B. Choi, D. Cunnold, E. J. Dlugokencky, P. Fraser, A. J. Gomez-Pelaez, T. Goo, J. Kim, P. Krummel, R. Langenfelds, F. Meinhardt, H. Mukai, S. O'Doherty, R. G. Prinn, P. Simmonds, P. Steele, Y. Tohjima, K. Tsuboi, K. Uhse, R. Weiss, and D. Worthly (2009), Growth rate, seasonal, synoptic, diurnal

- variations and budget of methane in lower atmosphere, *J. Met. Soc. Japan*, Vol. 87, No.4.
- Pétron G., G. Frost, B. R. Miller, A. I. Hirsch, S. A. Montzka, A. Karrion, M. Trainer, C. Sweeney, A. E. Andrews, L. Miller, J. Kofler, A. Bar-Ilan, E. J. . Conway, P. Novelli, K. Masarie, B. Hall, D. Guenther, D. Kitzis, J. Miller, D. Welsh, D. Wolfe, W. Neff, and P. Tans (2012), Hydrocarbon emissions characterization in the Colorado Front Range: A pilot study, *J. Geophys. Res.*, Vol. 117, D04304.
- Phelps, A. R., K. M. Peterson, and M. O. Jeffries (1998), Methane efflux from high-latitude lakes during spring ice melt, *J. Geophys. Res.*, Vol. 103, NO. D22, 29029-29036.
- Platt, U., W. Allan, and D. Lowe (2004), Hemispheric Average Cl atom concentration from $^{13}\text{C}/^{12}\text{C}$ ratios from atmospheric methane, *Atmos. Chem. Phys.*, Vol. 4, 2393-2399.
- Prigent, C., E. Matthews, F. Aires, W. B. Rossow (2001), Remote sensing of global wetland dynamics with multiple satellite data sets, *Geophys. Res. Lett.*, Vol. 28, No. 24, 4631 – 4634.
- Prigent, C., F. Papa, F. Aires, W. B. Rossow, and E. Matthews (2007), Global inundation dynamics inferred from multiple satellite observations, 1993 – 2000, *J. Geophys. Res.*, Vol. 112, D12107.
- Prinn, R. G., J. Huang, R. F. Weiss, D. M. Cunnold, P. J. Fraser, P. G. Simmonds, A. McCulloch, C. Harth, S. Reimann, P. Salameh, S. O'Doherty, R. H. J. Wang, L. W. Porter, B. R. Miller, and P. B. Krummel (2005), Evidence for variability of atmospheric hydroxyl radicals over the past quarter century, *Geophys. Res. Lett.*, Vol. 32, L07809.
- Prinn, R. G., R. F. Weiss, B. R. Miller, J. Huang, F. N. Alyea, D. M. Cunnold, P. J. Fraser, D. E. Hartley, P. G. Simmonds (1995), Atmospheric Trends and Lifetime of CH_3CCl_3 and Global OH Concentrations, *Science*, Vol. 269.
- Quay, P. J., S. L. King, J. M. Landsdown, and D. O. Wilbur (1988), Isotopic combination of methane released from wetlands: implications for the increase in atmospheric methane, *Global Biogeochem. Cy.*, Vol. 2, NO 4, 385-397.
- Rees, T., M. Burrell, T. G. Entwistle, J. B. W. Hammond, D. Kirk, and N. J. K. Kruger (1998), Effects of low temperature on the respiratory metabolism of carbohydrates by plants, In: *Plants and Temperature* (eds. S. P. Long, F. J. Woodward, Vol. 32), 377-393, *Society for Experimental Biology, Cambridge*
- Reshetnikov, A. I., N. N. Paramonova, and A. A. Shahskov (2000), An evaluation of historical methane emissions from Soviet gas industry, *J. Geophys. Res.*, Vol. 105(D3), 3517-3529.

- Rigby, M., R. G. Prinn, P. J. Fraser, P. G. Simmonds, R. L. Langenfelds, J. Huang, D. M. Cunnold, L. P. Steele, P. B. Krummel, R. F. Weiss, S. O'Doherty, P. K. Salameh, H. J. Wang, C. M. Harth, J. Mühle, and L. W. Porter (2008), Renewed growth of atmospheric methane, *Geophys. Res. Lett.*, Vol. 35, L22805.
- Ringeval B., N. de Noblet-Ducoudre, P. Ciais, P. Bousquet, C. Prigent, F. Papa, and W. B. Rossow (2010), An attempt to quantify the impact of changes in wetland extent on methane emissions on the seasonal and interannual time scales, *Global Biogeochem. Cy.*, Vol. 24, GB2003.
- Rinne, J., T. Riutta, M. Pihlatie, M. Aurela, S. Haapanala, J. Tuovinen, E. Tuittila, and T. Vesala (2007), Annual cycle of methane emission from a boreal fen measured by the eddy covariance technique, *Tellus*, Vol. 59B, 449-457.
- Robert, A. J.: A semi-Lagrangian and semi-implicit numerical integration scheme for the primitive meteorological equations (1982), *J. Met. Soc. Japan*, Vol. 60, 319-325.
- Roeckner, E., Bäuml, G., Bonaventura, L., Brokopf, R., Esch, M., Giorgetta, M., Hagemann, S., Kirchner, I., Kornblüeh, L., Manzini, E., Rhodin, A., Schlese, U., Schulzweida, U., and Tompkins, A.: The atmospheric general circulation model ECHAM5, part I: Model description, *Max Planck Institute for Meteorology, Report No. 349*, 2003.
- Ruddiman, W. F., and J. S. Thomson (2001), The case for human cause of increased atmospheric CH₄ over the last 5000 years, *Quatern. Sci. Rev.*, Vol. 20, 1769-1777.
- Sanderson, M. G., (2001), Global distribution of freshwater wetlands for use in STOCHEM. Technical note 32 (HTCN 32), *Hadley Center for Climate Prediction and Research, Met. office Barcknell, UK*.
- Sarnthein, M., R. Gersonde, S. Niebecker, U. Pflaumann, R. Spielhagen, J. Thiede, G. Wefer, and M. Weinelt (2003), Overview of Glacial Atlantic Ocean Mapping (GLAMAP 2000), *Paleoceanography*, Vol. 18, 1030, 6pp.
- Sass, R. L., F. M. Fisher Jr., A. Ding, and Y. Huang (1999), *J. Geophys. Res.*, Vol. 104, NO. D21, 26943-26951.
- Scheele, T., G. B. Faluvegi, G. A. Schmidt (2002), Global anthropogenic methane emissions, In: Van Ham et al., (ed.), *Non-CO₂ greenhouse gases- Scientific understanding, control options and policy aspects*, Millpress, Rotterdam
- Schultz, M. G., A. Heil, J. J. Hoelzemann, A. Spessa, K. Thonicke, J. Hoelzemann, A. Spessa, K. Thonicke, J. G. Goldammer, A. C. Held, J. M. C. Pereira, and M. van der Bolt (2008), Global wildland fire emissions from 1960 to 2000, *Global Biogeochem. Cy.*, Vol. 22, No. GB. 2002.

- Segers, R., and P.A. Leffelaar (2001), Modelling methane fluxes in wetlands with gas transporting roots. 1. single root scale, *J. Geophys. Res.*, Vol. 106, 3511–3528.
- Shindell, D. T., B. P. Walter, and G. Faluvegi (2004), Impact of climate change on methane emissions from wetlands, *Geophys. Res. Lett.*, Vol. 31, L21202.
- Simmons, A. J and Burridge, D. M.: An energy and angular momentum conserving vertical finite difference scheme and hybrid vertical coordinates (1981), *Mon. Wea. Rev.*, Vol. 109, 758–766.
- Singarayer J. S., P. J. Valdes, P. Friedlingstein, S. Nelson, and D. J. Beerling (2011), Late Holocene methane rise caused by orbitally controlled increase in tropical sources, *Nature*, Vol. 470.
- Sippel, S. J., S. K. Hamilton, J. M. Melack, and B. J. Choudhury (1994), Determination of inundation area in the Amazon River Floodplain Using the SMMR 37 GHz Polarization Difference, *Remote Sens. Environ.*, Vol. 48, 70 – 76.
- Sippel, S. J., S. K. Hamilton, J. M. Melack, and E. M. M. Novo (1998), Passive microwave observations of inundation area and the area/stage relation in the Amazon River floodplain, *Int. J. of Remote Sens.*, Vol. 19, No. 16, 3055 – 3074.
- Sphani, R., J. Chappellaz, T. F. Stocker, L. Loulergue, G. Hausammann, K. Kawamura, J. Flückiger, J. Schwander, D. Raynaud, V. Masson-Delmotte, and J. Jouzel (2005), Atmospheric Methane and Nitrous Oxide of the Late Pleistocene from Antarctic Ice Cores, *Science*, Vol. 310, 1317
- Stauffer, B., E. Lochboronner, H. Oeschger and J. Schwander (1988), Methane concentration in the glacial atmosphere was only half of the preindustrial Holocene, *Nature*, Vol. 332, 812-814.
- Stevenson, D.S., F.J. Dentener, M.G. Schultz, K. Ellingsen, T.P.C. van Noije, O. Wild, G. Zeng, M. Amann, C.S. Atherton, N. Bell, D.J. Bergmann, I. Bey, T. Butler, J. Cofala, W.J. Collins, R.G. Derwent, R.M. Doherty, J. Drevet, H.J. Eskes, A.M. Fiore, M. Gauss, D.A. Hauglustaine, L.W. Horowitz, I.S.A. Isaksen, M.C. Krol, J.-F. Lamarque, M.G. Lawrence, V. Montanaro, J.-F. Müller, G. Pitari, M.J. Prather, J.A. Pyle, S. Rast, J.M. Rodriguez, M.G. Sanderson, N.H. Savage, D.T. Shindell, S.E. Strahan, K. Sudo, S. Szopa (2006), Multi-model ensemble simulations of present-day and near-future tropospheric ozone, *J. Geophys. Res.*, Vol. 111, D08301, doi:10.1029/2005JD006338.
- Stier, P., Feichter, J., Kinne, S., Kloster, S., Vignati, E., Wilson, J., Ganzeveld, L., Tegen, I., Werner, M., Balkanski, Y., Schulz, M., Boucher, O., Minikin, A., and Petzold, A.: The aerosol climate model ECHAM5-HAM, *Atmos. Chem. Phys.*, Vol. 5, 1125–1156, 2005.
- Stillwell-Soller, L. M., L. F. Klinger, D. Pollard, and S. L. Thompson (1995), The Global Distribution of freshwater Wetlands. *NCAR Technical Note TN-416+STR*, National Center for Atmospheric Research, Boulder, CO.

- Subak, S. (1994) Methane from the House of Tudor and the Ming Dynasty, *Chemosphere*, Vol. 29, 843-854.
- Suyker, A. E., S. B. Verma, and R. J. Clement (1996), Methane flux in a boreal fen: Season – long measurement eddy correlation, *J. Geophys. Res.*, Vol. 101, No. D22, 28,637 – 28,647.
- Tansey, K., Grégoire, J. M., Stroppiana, D., Sousa, A., Silva, J.M.N., Pereira, J.M.C., Boschetti, L., Maggi, M., Brivio, P.A., Fraser, R., Flasse, S., Ershov, D., Binaghi, E., Graetz, D. and Peduzzi, P. (2004). *J. Geophys. Res. – Atmospheres*, Vol. 109, D14S03, doi:10.1029/2003JD003598
- Taraborelli, D., M. G. Lawrence, J. N. Crowley, T. J. Dillon, S. Gromov, C. B. M. Groß, L. Vereecken, and J. Leileveld (2012), Hydroxyl radical buffered by isoprene oxidation over tropical forest, *Nature Geoscience*, Vol. 5, DOI:10.1038/NGE1405.
- Valdes P. J., D. J. Beerling, and C. E. Johnson (2005), The ice age methane budget, *Geophys. Res. Lett.*, Vol. 32, L02704.
- Van der Werf, G. R., J. T. Randerson, G. C. Collatz, and L. Gigilo (2003), Carbon emissions from fires in tropical and subtropical ecosystems, *Glob. Change Biol.*, Vol. 9(4), 547-562.
- Van der Werf, G. R., J. T. Randerson, L. Gigilo, G. C. Collatz, P. S. Kasibhatla, and A. F. Arellano, Jr. (2006), *Atmos. Chem. Phys.*, Vol. 6, 3423-3441.
- Walter, B. P., M. Heimann (2000), A process-based, climate-sensitive model to derive methane emissions from natural wetlands: Application to five wetland sites, sensitivity to model parameters, and climate, *Global Biogeochem. Cy.*, Vol. 14, No. 3, 745 – 765.
- Walter, B. P., M. Heimann, E. Matthews (2001), Modeling modern methane emissions from natural wetlands 1. Model description and results, *J. Geophys. Res.*, Vol. 106, No. D24, 34,189 – 34,206.
- Wang, J. S., J. A. Logan, and M. B. McElroy (2004), A 3-D model analysis of the slowdown and interannual variability in the methane growth rate from 1988 to 1997, *Global Biogeochem. Cy.*, Vol. 18, GB3011.
- Wang, M. X., A. Dai, X. Shangguan, L. Ren, R. Shen, H. Schultz, W. Seiler, R. A. rasmussen, and M. A. Khalil (1994), Sources of methane in China, in CH₄ and N₂O: Global Emissions and Controls From Rice fields and Other Agricultural and Industrial Sources, edited by K. Minami, A., A. Mosier, and R. Sass, 9-26, *Natl. Inst of Agro Environ. Sci., Tsukuba, Japan*.
- Wang, Y., and D. Jacob (1998), Anthropogenic forcing on tropospheric ozone and OH since pre-industrial times, *J. Geophys. Res.*, Vol. 103, 3399-3417.

- Warrant P., L. François, D. Strivay, and J. C. Gérard: CARAIB: A global model of terrestrial biological productivity, *Global Biogeochem. Cy.*, Vol. 8, 255-270.
- Warwick, N. J., S. Bekki, K. S. Law, E. G. Nisbet, and J. A. Pyle (2002), The impact of meteorology on the interannual growth rate of atmospheric methane, *Geophys. Res. Lett.*, Vol. 29, No. 20, 1947.
- Wassman, R., and U. Thein (1996), Spatial and seasonal variation of methane emission from an Amazon flood-plain lake. *Mitteilungen der International Vereinigung für Theoretische und Angewandte Limnologie*, Vol. 25, 179-185.
- Weber S. L., A. J. Drury, W. H. J. Toonen, and M. van Weele (2010), Wetland methane emissions during the Last Glacial Maximum estimated from PMIP2 simulations: Climate, vegetation, and geographic controls, *J. Geophys. Res.*, Vol. 115, D06111.
- Whalen S., and W. Reeburg (1996), Moisture and temperature sensitivity of CH₄ oxidation in boreal soils, *Soil Biology and Chemistry*, Vol. 28, 1271-1281.
- Whalen S., W. Reeburg, and W. Barber (1992), Oxidation of methane in boreal forest soils: a comparison of seven measures. *Biogeochemistry*, Vol. 16, 181-211.
- Whalen, S. C., W. S. Reeburgh, and K. A. Sandbeck (1990), Rapid oxidation in a Landfill Cover Soil, *Appl. Environ. Microbio.*, Vol. 61, 3405-3411.
- Wilson, J. O., P. M. Crill, K. B. Bartlett, D. I. Sebacher, R. C. Harriss, and R. L. Sass (1989), Seasonal variations of methane emissions from a temperate swamp, *Biogeochemistry*, Vol. 8, 55 – 71.
- Windsor, J., T. R. Moore, and N. T. Roulet (1992), episodic fluxes of methane from subarctic fens, *Can. J. Soil Sci.*, Vol. 72, 441-452.
- Worthy D. E. J., Elton Chan, M. Ishizawa, D. Chan, C. Poss, E. J. Dlugokencky, S. Maksyutov, and I. Levin (2009), Decreasing anthropogenic methane emissions in Europe and Siberia inferred from continuous carbon dioxide and methane observations at Alert, Canada, *J. Geophys. Res.*, Vol. 114, D10301.
- Wuebbles D. J., K. Hayhoe (2002), Atmospheric methane and global change, *Earth Sci. Rev.*, Vol. 57, 177-210.

Acknowledgments

This work is done at Institute for Energy and Climate Science (IEK-8), Forschungszentrum Jülich, Germany from May 2009 to October 2012 under the supervision of Prof. Dr. Andreas Wahner.

I would like to express my sincere gratitude to Prof. Wahner for giving me the opportunity to work at Forschungszentrum Jülich.

I am thankful to Prof. Dr. Michael Kerschgens from University of Cologne on being the second referee of this work.

I am deeply grateful to PD. Dr. Martin Schultz for his supervision throughout this study. I received an excellent guidance from him to build the framework of this study and to set up the pathway in order to achieve its objectives. His knowledge and experience in the field of meteorology brought immense contribution in this work.

I am deeply grateful to Dr. Louis François from University of Liège to lend his support in terms of providing the CARAIB data which were used extensively in the simulation study both for present and past climate.

I also find this opportunity to express my gratitude to Dr. Peter Bergamaschi from JRC, Ispra for the methane emission data, which were indispensable for the model study.

I also thank Dr. Thomas Laepple and Xu Zhang from AWI, Bremerhaven and Dr. Uwe Mikolajewicz from MPI, Hamburg for sharing data on LGM boundary conditions which were essential to set up the model run.

From my working group at Jülich, I would like to thank my colleagues for their collective and individual support throughout this work. I am thankful to Dr. Olaf Stein for those healthy discussions anytime over various problems encountered in this study. I also convey my sincere thanks to my colleagues Sabine Schröder and Snehal Waychal for their consistent support particularly to solve the technical issues related to the thesis work.

I thank my colleagues Dr. Saroj Kumar Sahu and Olga Lyapina for their valuable comments which were pretty useful. I also express my gratitude to my former colleagues Dr. Angelika Heil, Dr. Corenelia Richter and Dr. Anke Schickling for their valuable inputs in this study.

I am indebted to the team of Jülich Supercomputing Center (JSC) for permitting me to carry out simulation on platform of JUMP and JUROPA and helping with the technical assistance.

Last but not the least I would like to thank my family and for their consistent support and word of encouragement which were essential to carry out the PhD work.

Erklärung

Ich versichere, dass ich die von mir vorgelegte Dissertation selbstständig angefertigt, die benutzten Quellen und Hilfsmittel vollständig angegeben und die Stellen der Arbeit – einschließlich Tabellen, Karten und Abbildungen –, die anderen Werken im Wortlaut oder dem Sinn nach entnommen sind, in jedem Einzelfall als Entlehnung kenntlich gemacht haben; dass diese Dissertation noch keiner anderen Fakultät oder Universität zur Prüfung vorgelegen hat; dass sie – abgesehen von unten angegebenen Teilpublikationen – noch nicht veröffentlicht worden ist sowie, dass ich eine solche Veröffentlichung vor Abschluss des Promotionsverfahrens nicht vornehmen werde.

Die Bestimmungen dieser Promotionsordnung sind mir bekannt. Die von mir vorgelegte Dissertation ist von Prof. Dr. Andreas Wahner betreut worden.

Köln, 22.10.2012

Abhijit Basu

Lebenslauf

Persönliche Angaben

Name	Abhijit Basu
Geburtsdatum	31. Oktober 1982
Geburtsort	Kalkutta / Indien
Familienstand	verheiratet
Staatsangehörigkeit	indisch

Ausbildung

08/1988-02/1999	R.K. Mission Secondary School in Kalkutta
06/1999-04/2001	Sailendra Sircar Govt. Spon. High School in Kalkutta
08/2001-04/2004	Bachelor of Sciences in Physik (Hauptfach), Chemie und Mathematik, Scottish Church College, University of Calcutta
07/2004-08/2006	Master of Sciences in Atmospheric Sciences, University of Calcutta Special paper in Satellite meteorology Thema der Master-Arbeit: "A soft computing approach to view the relative contribution of some surface parameters in the occurrence of Severe Local Storms"
02/2007-12/2008	Master of Technology, Remote Sensing and GIS, Indian Institute of Remote Sensing (Department of Atmospheric and Marine Sciences), Department of Space, Govt. of India Thema der Master-Arbeit: "Understanding and modelling the atmospheric Carbon dioxide transport and estimation of CO ₂ concentration over Indian Sub-continent"
03/2009-5/2009	Probezeit als Wissenschaftler am Institut für Energie- und Klimaforschung (IEK-8: Troposphäre), Forschungszentrum Jülich
seit 06/2009	Promotionsstudium am Institut für Geophysik und Meteorologie der Universität Köln und am Institut für Energie und Klimaforschung (IEK- 8: Troposphäre), Forschungszentrum Jülich

Band / Volume 154

Coupled hydrogeophysical inversion for soil hydraulic property estimation from time-lapse geophysical data

M. Cho Miltin (2012), xi, 79 pp.

ISBN: 978-3-89336-823-5

Band / Volume 155

Tiefentschwefelung von Fluggasturbinenkraftstoffen für die Anwendung in mobilen Brennstoffzellensystemen

Y. Wang (2012), 205 pp.

ISBN: 978-3-89336-827-3

Band / Volume 156

Self-consistent modeling of plasma response to impurity spreading from intense localized source

M. Koltunov (2012), V, 113 pp.

ISBN: 978-3-89336-828-0

Band / Volume 157

Phosphorsäureverteilung in Membran-Elektroden-Einheiten dynamisch betriebener Hochtemperatur-Polymerelektrolyt-Brennstoffzellen

W. Maier (2012), VI, 105 pp.

ISBN: 978-3-89336-830-3

Band / Volume 158

Modellierung und Simulation von Hochtemperatur-Polymerelektrolyt-Brennstoffzellen

M. Kvesic (2012), ix, 156 pp.

ISBN: 978-3-89336-835-8

Band / Volume 159

Oxidation Mechanisms of Materials for Heat Exchanging Components in CO₂/H₂O-containing Gases Relevant to Oxy-fuel Environments

T. Olszewski (2012), 200 pp.

ISBN: 978-3-89336-837-2

Band / Volume 160

Ice Crystal Measurements with the New Particle Spectrometer NIXE-CAPS

J. Meyer (2013), ii, 132 pp.

ISBN: 978-3-89336-840-2

Band / Volume 161

Thermal Shock Behaviour of Different Tungsten Grades under Varying Conditions

O. M. Wirtz (2013), XIV, 130 pp.

ISBN: 978-3-89336-842-6

Band / Volume 162

**Effects of ^{137}Cs and ^{90}Sr on structure and functional aspects
of the microflora in agricultural used soils**

B. Niedrée (2013), XII, 92 pp.

ISBN: 978-3-89336-843-3

Band / Volume 163

Lidar observations of natural and volcanic-ash-induced cirrus clouds

C. Rolf (2013), IX, 124 pp.

ISBN: 978-3-89336-847-1

Band / Volume 164

**CO₂-Abscheidung, -Speicherung und -Nutzung:
Technische, wirtschaftliche, umweltseitige und gesellschaftliche Perspektive
Advances in Systems Analysis 2**

W. Kuckshinrichs; J.-F. Hake (Eds.) (2012), iv, 354 pp.

ISBN: 978-3-89336-850-1

Band / Volume 165

**Interest Mediation and Policy Formulation in the European Union
Influence of Transnational Technology-Oriented Agreements on European Policy
in the Field of Carbon Capture and Storage
Advances in Systems Analysis 3**

O. Schenk (2013), XIII, 253 pp.

ISBN: 978-3-89336-852-5

Band / Volume 166

**Versagensverhalten plasmagespritzter Mg-Al-Spinell-Schichten
unter Thermozyklierung**

S. M. Ebert (2013), X, 173 pp.

ISBN: 978-3-89336-853-2

Band / Volume 167

**Coupled modeling of water, vapor and heat in unsaturated soils -
Field applications and numerical studies**

C. Steenpaß (2013), X, 123 pp.

ISBN: 978-3-89336-854-9

Band / Volume 168

**An analysis of the global atmospheric methane budget under different
climates**

A. Basu (2013), v, 110 pp.

ISBN: 978-3-89336-859-4

Energie & Umwelt / Energy & Environment
Band / Volume 168
ISBN 978-3-89336-859-4

